ADAPTATION AND THE MORTALITY EFFECTS OF TEMPERATURE ACROSS
U.S. CLIMATE REGIONS

Garth Heutel
Nolan H. Miller
David Molitor

Adaptation and the Mortality Effects of Temperature Across U.S. Climate Regions
Garth Heutel, Nolan H. Miller, and David Molitor
NBER Working Paper No. 23271
March 2017, Revised January 2020
JEL No. I18,J14,Q54

ABSTRACT

We estimate how the mortality effects of temperature vary across U.S. climate regions to assess local and national damages from projected climate change. Using 22 years of Medicare data, we find that both cold and hot days increase mortality. However, hot days are less deadly in warm places while cold days are less deadly in cool places. Incorporating this heterogeneity into end-of-century climate change assessments reverses the conventional wisdom on climate damage incidence: cold places bear more, not less, of the mortality burden. Allowing places to adapt to their future climate substantially reduces the estimated mortality effects of climate change.

Garth Heutel
436 Andrew Young School
Department of Economics
Georgia State University
PO Box 3992
Atlanta, GA 30302-3992
and NBER
gheutel@gsu.edu

Nolan H. Miller
College of Business
University of Illinois
4033 BIF
515 East Gregory Drive
Champaign, IL 61820
and NBER
nmiller@illinois.edu

David Molitor
University of Illinois at Urbana-Champaign
340 Wohlers Hall
1206 S. Sixth Street
Champaign, IL 61820
and NBER
dmolitor@illinois.edu

1   Introduction

The prospect of rising global temperatures over the 21st century has focused attention on understanding how climate change affects human well-being and whether adaptation or mitigation strategies can offset its harmful effects (IPCC, 2014). One common approach to estimating climate change effects is to first estimate economic damages due to weather and then calculate climate damages using shifts in the future weather distribution predicted by climate models (Deschênes and Greenstone, 2011). Applications of this approach have generally assumed that the relationship between weather and mortality is uniform across regions and is constant over time. For example, Hsiang et al. (2017) estimate that excess mortality will account for about 70% of end-of-century (2080–2099) climate damages in the United States and that northern, cooler regions will generally bear lower mortality costs from climate change than warmer regions. However, both the overall magnitude and geographic distribution of climate damages could deviate substantially from these predictions if the mortality effects of weather vary geographically or if places adapt to their future climate.

In this paper, we estimate how the mortality effects of temperature vary across U.S. climate regions and use these estimates to predict local and national end-of-century climate change impacts on U.S. elderly mortality. We assess climate change impacts for three cases: assuming homogeneous effects of temperature across regions, incorporating heterogeneity in a region's current temperature-mortality relationship, and allowing for both current heterogeneity and future adaptation. Our analysis leverages Medicare administrative data on dates of death and ZIP codes of residence for all elderly U.S. beneficiaries from 1992–2013, daily weather monitor readings, and end-of-century climate change predictions from 21 climate models and two different emissions scenarios.

Our analysis proceeds in two parts. In the first part, we conduct a nonparametric analysis aimed at establishing the extent to which mortality effects of temperature vary across climate regions. While both hot and cold days increase mortality, on average, relative to a moderate day, we find that hot days are much deadlier in cool regions than in warm ones. The reverse is true for cold days. This heterogeneity implies that, absent future adaptation, a warming climate will increase mortality more in cool places—and less in warm places—than would be implied by homogeneous temperature effects. In addition, these results suggest that attempts to account for adaptation to hot weather under a warming climate must also account for the potential for regions to simultaneously de-adapt to cold weather.

In the second part, we assess the mortality effects of projected end-of-century climate change. Informed by our heterogeneity analysis, we first estimate the mortality effects of temperature as a smooth, semi-parametric function of temperature and local (ZIP code

level) climate. We then calculate climate damages for each ZIP code by combining temperature effects with projected shifts in the future weather distribution for each ZIP code. This approach allows us to model both heterogeneity in the current temperature-mortality relationship based on a region's historical climate and the potential for the region to adapt to its future climate.

We find that accounting for heterogeneity and adaptation substantially influences the sign, magnitude, and geographic distribution of predicted climate damages relative to a conventional approach that assumes homogeneous current temperature effects and no future adaptation. Using the conventional approach, we predict an overall increase in elderly mortality of 0.76%, with warm regions bearing larger burdens and cool regions benefiting from mortality reductions, similar to conclusions by Houser et al. (2014) and Hsiang et al. (2017). However, accounting for heterogeneous current temperature effects implies a much larger aggregate mortality increase of 2.15% and reverses the distribution of predicted climate damages: cold places bear more, not less, of the mortality burden.

Further allowing places to adapt to their future climate yields mortality effects of climate change that are systematically lower than estimates that do not allow for adaptation. When we account for both current heterogeneity and future adaptation, we estimate an overall *decrease* in U.S. elderly mortality of approximately 0.53% by the end of the century, compared to the overall mortality increase of 2.15% for the case of heterogeneous effects with no adaptation. This finding is best interpreted as quantifying the potential scope for adaptation to future climate change using currently available technologies that regions have found worthwhile to adopt given historical costs and their current climates. Because we model neither the future cost of adaptation nor the nonmortality effects of climate change on elderly welfare, our findings do not imply that climate change will necessarily improve elderly well-being.

Our paper contributes to a growing literature that explores adaptation to climate change.[1] Methodologically, the studies most closely related to ours are Butler and Huybers (2013) and Auffhammer (2017), which use a similar approach to consider regional adaptation in maize production and in energy use, respectively. In contemporaneous work, Portnykh (2017) considers weather, adaptation, and mortality using Russian data. Our paper also contributes to studies of how the mortality effects of temperature vary across climate regions. For example, Curriero et al. (2002) and Barreca et al. (2016) find that cold days tend to have larger effects in southern climates, while hot days tend to have larger effects in northern climates. Barreca et al. (2015) more thoroughly examine how the mortality impacts of hot

---

[1]Kahn (2016) and Massetti and Mendelsohn (2018) review the climate adaptation literature. Deschênes (2014) reviews the empirical literature on temperature, human health, and adaptation.

days vary across U.S. states according to the frequency at which they occur.

Our work expands on these studies in three primary ways. First, we use more spatially and temporally granular data spanning the United States to characterize graphically, and in a statistically precise way, how the entire temperature-mortality relationship varies with local climate. This is important because climate change can affect the likelihood of both hot and cold days, varying by region. Second, we combine climate-specific temperature effects with location-specific climate change projections to predict end-of-century climate damages both locally and in aggregate. Third, we predict the scope for adaptation to climate change using cross-sectional heterogeneity in the observed temperature-mortality relationship, simultaneously accounting for adaptation to heat and possible de-adaptation to the cold.

The remainder of this paper proceeds as follows. Section 2 describes our data. In section 3, we estimate climate-specific temperature-mortality relationships. Section 4 makes predictions of long-run climate change-induced mortality, with and without climate-based regional heterogeneity and with and without adaptation. Section 5 concludes.

2   Data

2.1   Data Description

Our analysis leverages a novel combination of three primary data sources: daily weather monitor readings from the National Oceanic and Atmospheric Administration's (NOAA) Global Historical Climate Network (GHCN), elderly mortality and place of residence from Medicare administrative data, and climate projections from the NASA Earth Exchange Global Daily Downscaled Projections (NEX-GDDP). We briefly describe the weather and mortality data and variable construction in this section. Section 4.1 describes the climate model projections. Appendix section A.1 provides more detailed data descriptions.

The primary geographic units for our analysis are ZIP codes, as defined by the 2010 U.S. Census Bureau's ZIP Code Tabulation Areas (ZCTAs). ZCTAs aggregate census blocks to form real representations of United States Postal Service (USPS) ZIP Code mail delivery routes. For most areas, the ZCTA code is the same as the USPS ZIP Code.

We obtain daily minimum and maximum temperatures from NOAA's GHCN database, which provides climate summaries for weather stations across the 50 U.S. states, the District of Columbia, and Puerto Rico. For each ZIP code, we construct daily high and low temperatures as the inverse distance-weighted average of all available maximum and minimum temperatures, respectively, for monitors within 20 miles of the ZIP code centroid, following the monitor aggregation method used by Currie and Neidell (2005) and Beatty

and Shimshack (2014). The daily average temperature is defined as the midpoint of the daily high and low temperatures.[2]

We categorize ZIP codes into climate regions based on their cooling degree days (CDD), derived from NOAA's 1981–2010 Climate Normals for U.S. weather stations. CDD are based on daily average temperatures and are designed to reflect the energy needed to cool a building to a base temperature, typically 65°F. For example, one day with an average temperature of 75°F represents 10 CDD, while a day with temperatures below the base temperature represents 0 CDD. A weather station's CDD Normal is a three-decade average of its annual CDD, which is the sum of daily CDD values across all days in the year. The CDD Normal for a ZIP code is the inverse distance-weighted average of CDD Normals at the nearest weather station and any other stations within a 20-mile radius of the ZIP code centroid.

Finally, we measure mortality using Medicare enrollment files from 1992–2013. These files provide demographic data on all individuals eligible for Medicare in each year, including date of birth, date of death, and ZIP code of residence. We restrict our sample to elderly beneficiaries aged 65–100, who represent over 97% of the U.S. elderly resident population (appendix figure B.1). We define daily mortality for a ZIP code as those who die within a given time period (e.g., within three days of the index date) as a fraction of all beneficiaries residing in the ZIP code who were alive and eligible for Medicare as of the index date.

2.2 Summary Statistics

The primary sample for our analysis contains 32,860 ZIP codes, yielding over 250 million ZIP-code-day observations over the sample period (1992–2013). Appendix figure B.2 shows how climate varies across the sample. The Medicare population-weighted average ZIP code CDD Normal is 1,404. The coolest third of ZIP codes have fewer than 787 CDD, with some parts of Alaska and Colorado having 0 CDD, as the average temperature never exceeds 65°F. The warmest third of ZIP codes have at least 1,442 CDD, with some very hot ZIP codes in Arizona, California, Florida, and Puerto Rico exceeding 4,500 CDD.

Figure 1 summarizes the distribution of realized temperature over the sample across each of 19 temperature bins ranging in 5°F increments from < 10°F to > 95°F. The gray-shaded region presents the distribution of daily average temperature for the United States as a whole, while the blue, gold (dashed), and orange curves present respective distributions for the coolest, middle, and warmest thirds of U.S. ZIP codes.

---

[2]Another source of daily weather data comes from the PRISM Climate Group, which produces spatially interpolated data at a 4km resolution. Because PRISM data are only available for the conterminous United States, we use the GHCN weather data for our main analysis. We also construct daily ZIP code weather based on PRISM data (appendix section A.1) and show in appendix section A.2 that results based on PRISM weather data are qualitatively similar to those based on GHCN data.

Appendix tables B.1a–B.1b summarize daily mortality by temperature bin for each of the three climate terciles and for the United States as a whole, respectively. Average three-day mortality was 39.4 deaths per 100,000 beneficiaries, corresponding to an annual mortality rate of 4.8%. However, mortality was systematically lower on warmer ZIP days, with the lowest three-day mortality rate of 35 deaths per 100,000 occurring after days with average temperatures above 95°F. A naïve interpretation of this pattern is that replacing cool days with very hot days reduces mortality. Yet this conclusion could be flawed either because hot days tend to occur during the summer, confounding the temperature effect with seasonality, or because the population residing in regions where hot days occur most often differs systematically from cooler regions. The richness of our data allows us to address these potential confounders by controlling flexibly for both location and seasonality.

3   Heterogeneous Mortality Effects of Temperature

In this section, we examine the extent to which the mortality effects of temperature vary across climate regions. For this analysis, we define climate regions as the coolest, middle, and warmest population-weighted third of ZIP codes based on CDD Normals. We then nonparametrically estimate the temperature-mortality relationship for each climate tercile.

3.1   Empirical Strategy

We use year-over-year variation in daily temperature to identify the causal effect of temperature on mortality, inspired by the approach of Deschênes and Greenstone (2011). Our analysis uses daily observations of mortality and temperature at the ZIP code level. Our primary outcome of interest, $mortality_{zd}$, is the number of deaths per 100,000 beneficiaries in ZIP code z within three days after index day d.[3] Our estimating equation is

$$
\begin{aligned}
mortality_{zd} = & \sum_{b \in B \setminus \{65-70\}} \beta_b^{cool} tempbin_{zd}^b \times 1\left(ZIP\ z\ in\ coolest\ third\ of\ regions\right) \\
& + \sum_{b \in B \setminus \{65-70\}} \beta_b^{mid} tempbin_{zd}^b \times 1\left(ZIP\ z\ in\ middle\ third\ of\ regions\right) \\
& + \sum_{b \in B \setminus \{65-70\}} \beta_b^{hot} tempbin_{zd}^b \times 1\left(ZIP\ z\ in\ warmest\ third\ of\ regions\right) \\
& + ZipDay_{zd} + L_{zd} + StYr_{zd} + \varepsilon_{zd}.
\end{aligned}
\tag{1}
$$

---

[3]Using a post-event window captures possible lags in mortality effects and near-term mortality displacement (harvesting). Appendix figure B.4 shows results for mortality windows of up to 28 days after the index day. We do not observe harvesting at either very hot or very cold temperatures when extending the mortality window beyond three days, and therefore we focus our primary analysis on three-day mortality.

The primary independent variables of interest in equation 1 are temperature indicators $tempbin_{zd}^b$ defined by which of the 19 temperature bins $b \in B = \{< 10, 10 - 15, \ldots, 90 - 95, > 95\}$ the average temperature in ZIP code z falls in on day d. The temperature bins are then interacted with indicators for the climate tercile containing the ZIP code. This specification allows for arbitrary nonlinearities in the relationship between temperature and mortality and further allows this relationship to vary arbitrarily by climate region.

Because equation 1 includes ZIP code fixed effects, the coefficients on the set of temperature indicators for each climate region are only identified up to a common constant (i.e., a vertical shift in the temperature-mortality relationship). This corresponds to arbitrarily omitting one temperature bin in the regression, which we choose to be the 65°F–70°F bin. As a result, the coefficients β_b^c describe the mortality effect in climate region c of replacing a day with an average temperature in bin b with a 65°F–70°F day. Identification up to a common constant also implies that all statements we make about heterogeneous treatment effects reflect differences in the curvature of the temperature-mortality relationship, not differences in mortality levels across regions.

We identify the effects of temperature on mortality by isolating year-over-year variation in temperature and mortality, controlling for both geography and seasonality using fixed effects $ZipDay_{zd}$ for each ZIP code and day of year combination. This control strategy accounts for seasonal mortality patterns that may vary by ZIP code, such as elevated winter mortality and reduced summer mortality. To account for serial correlation in daily temperature and potentially lagged mortality effects, L_{zd} includes three fully interacted sets of 5-degree average temperature bins for the preceding two and six days and the subsequent two days, which are further allowed to vary by climate tercile. Finally, we include state-by-year fixed effects, $StYr_{zd}$, to control for arbitrary annual shocks that may vary by state, such as changes to Medicare or Medicaid policy. All regressions are weighted by the ZIP code's Medicare population. We two-way cluster standard errors at the county and state-date levels to allow for arbitrary correlations within groups of nearby ZIP codes over time and across all ZIP codes in the state at a particular point in time.

3.2 Results

Figure 2a depicts results from estimating equation 1 with three-day mortality as the outcome. Markers with whisker lines plot the nonparametric temperature bin estimates and associated 95% confidence intervals. Nonparametric estimates are shown only for the coolest and warmest climate terciles and for binned temperatures that occur with a frequency of at least one day per decade in the climate region. Solid lines plot estimates from a semi-parametric

version of equation 1, where temperature bin indicators are replaced by a 5th-degree polynomial in the temperature bin. The semi-parametric and nonparametric estimates agree closely for temperatures occurring at least one day per decade. Shaded regions, representing 95% confidence intervals on the semi-parametric estimates, are shown for the coolest and warmest terciles. For comparison, figure 2b shows the results of estimating equation 1 under the assumption of homogeneous temperature effects.[4]

Figure 2a reveals substantial heterogeneity in temperature effects by climate tercile. In the warmest third of ZIP codes, depicted in orange, mortality effects are lowest on days with average temperatures of 75°F–80°F. For the coolest third of ZIP codes, depicted in blue, mortality is minimized on days with temperatures of 60°F–65°F. As temperatures increase above 75°F, the colder regions feature a stark increase in mortality, while warmer regions exhibit much more modest effects. For example, an 85°F–90°F day increases the mortality rate in the coldest decile by 1.8 deaths per 100,000 but has nearly no effect (0.15 additional deaths per 100,000) in the warmest decile. On the other hand, mortality increases 2.6–4.8 times more on days at or below freezing in the warmest region than in the coolest one.

Figure 2a suggests that regions are both relatively good at dealing with temperatures they experience frequently and are relatively bad at dealing with temperatures they experience infrequently. Comparing the temperature-mortality relationships in figure 2a with the temperature frequency plots in figure 1 reveals that for days with temperature greater than 65°F, which occur with greater frequency relative to a 65°F day in the warmest region than the coolest, mortality effects are larger in the warmest region than in the coolest. The opposite is true for days below 65°F. Although the reference category of 65°F is a choice, it is also true that the curve for the warmest tercile is flatter than the curve for the coolest tercile for days above 65°F and is steeper for days below 65°F.

Comparing the climate-specific heterogeneous effects in figure 2a with the homogeneous effects in figure 2b illustrates how properly accounting for temperature effect heterogeneity can affect the projected impact of climate change. The homogeneous effects curve lies between the curves for the warmest and coolest regions, implying that using homogeneous effects understates the mortality effects of hot days in cool regions and overstates them in warm ones. The opposite is true for cold days. So while the homogeneous effects estimates imply that replacing a cold 25°F–30°F day with a hot 85°F–90°F day has little effect on mortality in any region, this replacement actually increases mortality by 1.49 deaths per 100,000 in the coolest tercile and reduces mortality in the warmest tercile decrease by 0.75

---

[4]Appendix tables B.1a and B.1b give numerical values of the nonparametric and semi-parametric estimates for all temperature bins in figures 2a and 2b, respectively. The tables also report standard errors under our preferred approach to clustering and for clustering at the county or state level.

deaths per 100,000. In addition, the homogeneous effects are not a simple average of the heterogeneous effects but instead lie closer to the cooler regions' curve for cold temperatures and closer to the warmer regions' curve for hot temperatures. Thus, the homogeneous effects do not reflect the national average effects of temperature.

As further illustration of the importance of allowing for heterogeneous temperature effects when assessing climate change effects, figure 3 presents predicted mortality impacts of replacing the climate of each tercile by the climate of one of the other terciles. When homogeneous effects are assumed (blue bars), warming is always associated with decreased mortality. However, taking into account current climate-specific heterogeneity (green bars), a qualitatively different pattern emerges. Under heterogeneous effects, we see that warming the coolest tercile's temperature distribution to that of either the middle or warmest tercile, or warming the middle tercile's temperature distribution to that of the warmest tercile, increases mortality, the opposite of what occurred in the homogeneous effects case. Further, for each of the current climate terciles, a change in a region's temperature increases mortality whether that change involves warming or cooling. Thus the heterogeneity we observe is not simply due to some regions being better at dealing with all temperatures than other regions. Rather, whatever factors determine a region's temperature-mortality curve, they tend to perform particularly well given the region's actual climate relative to other climates.

3.3   Regional Heterogeneity as Adaptation

Regional heterogeneity in the temperature-mortality relationship could arise due to regional adaptation, whether technological, behavioral, and/or biological in nature, or due to regional differences in characteristics that are correlated with current climate but do not result from human choices or physiology. This distinction is important for interpretation because if regional differences are caused by factors that are immutable, then even though Chicago in the future may face the climate that Dallas does now, we should not expect the Chicago of the future to be as good at dealing with heat as Dallas currently is. Thus, understanding the extent to which *current* heterogeneity is due to adaptation is important for understanding the extent to which *future* adaptation may mitigate the impact of climate change.

The nonlinear pattern of temperature effect heterogeneity that we document with respect to baseline climate is informative of the underlying mechanisms driving this heterogeneity. For example, the effects of hot days are smaller but the effects of cold days are larger in warm regions than in cooler ones. This pattern is not readily explained by factors that reduce sensitivity to both cold and hot days. In particular, the treatment effect heterogeneity we document seems unlikely to reflect regional differences in wealth or underlying health

8

endowments since these differences plausibly reduce sensitivity to both hot and cold weather. By contrast, this nonlinear pattern is consistent with a wide variety of adaptation behaviors.

There are numerous ways in which people and communities may adapt to their climate, such as through biological acclimatization, migration to different regions based on health, infrastructure investments, or architectural design. In appendix section A.4, we provide evidence that air conditioning (AC) adoption is strongly associated with differences in heat-related mortality across regions but not with cold-related mortality. Since AC adoption can be correlated with many other adaptive behaviors that also reduce the mortality effects of heat (e.g., designing buildings to optimize thermal performance), our estimates should not be interpreted as identifying the causal effect of AC. Nevertheless, the AC results provide additional, albeit suggestive, evidence that adaptive behaviors can explain the regional heterogeneity we document.

Our finding that places seem well-adapted to their current climate suggests it is reasonable to expect that regions could continue to find it worthwhile to adapt to a changing climate. It is important to note, however, that this statement concerns the observed degree of historical adaptation to the current range of climates given current technology. The degree to which places continue to adapt to climate change will depend on the future cost of available adaptation technologies and on the ability of currently hot places to adapt to climates much hotter than any U.S. regions currently experience.

4   Climate Change-Induced Mortality and Adaptation

In this section, we develop estimates of the end-of-century mortality impact of climate change accounting for heterogeneity and adaptation. To fix ideas, let $m_z^p(t)$ denote the mortality effect in ZIP code z and period p of a day with average temperature in bin t. We will consider both the current and future periods by $p = current$ and $p = future$, respectively. Let $g_z^p(t)$ be the number of days per year in which the temperature falls in bin t in period p. Current annual mortality (CAM_z) is therefore

$$CAM_z = \sum_t m_z^{current}(t) g_z^{current}(t).$$

We are interested in the change in excess mortality due to climate change. Let $m_z^{future}(t)$ denote the future mortality effect of temperature bin t in location z. In this case, the change in excess mortality would incorporate both the change in the temperature distribution and

the change in the temperature-mortality relationship:

$$FAM_z - CAM_z = \sum_t m_z^{future}(t)g_z^{future}(t) - \sum_t m_z^{current}(t)g_z^{current}(t). \qquad (2)$$

4.1 Empirical Implementation

Computing the estimated change in excess mortality involves the four functions on the right hand side of equation 2: current and future temperature distributions and current and future temperature-mortality relationships. The current temperature distribution is that observed for the ZIP code in the sample from 1992–2013. Our predictions of future temperature distributions are based on ZIP-code-specific projected changes in the daily temperature distribution between the current period (1992–2013) and the end of the century (2080–2099).

We derive projected changes in temperature for each of the 21 climate models for which daily scenarios are produced and distributed as part of the NEX-GDDP dataset. The NEX-GDDP data include daily minimum and maximum temperature predictions on a 25km by 25km grid (0.25-degree spatial resolution). We focus on climate model projections made under the Representative Concentration Pathway (RCP) 8.5 "business as usual" scenario, where emissions continue to rise throughout the 21st century (Meinshausen et al., 2011). Finally, we aggregate the gridded model projections to the ZIP code level using inverse distance weighting of all climate model grid points within 20 miles of the ZIP code centroid.[5]

To create a consensus projection from the 21 models, we average over all of the models using the weights employed by the Fourth National Climate Assessment (Sanderson, Knutti and Caldwell, 2015; Sanderson and Wehner, 2017). These weights, shown in column 1 of appendix table B.2a, positively value model predictive skill but penalize codependency between models. We refer to the weighted average model as the meta-model and the weighted average predicted temperature distribution as the meta-distribution.

The meta-model projects that average annual temperatures in the United States will rise by 8°F by the end of the century under the RCP 8.5 emissions scenario. Appendix figure B.6 maps the projected changes in temperature and CDD. Although predicted warming tends to be higher in areas that are currently cooler, comparing appendix figures B.2 and B.6 shows that there is significant variation in predicted warming even among regions that currently have quite similar climates.[6]

With sufficient observations for each ZIP code, we could estimate the temperature-mortality relationship nonparametrically for each ZIP code using equation 1 in the same way

---

[5]See Auffhammer et al. (2013) for a discussion of the use of climate models in economic analysis.

[6]The techniques we use apply equally well to the output of any of the 21 individual climate models. We show the results of doing this in section 4.4.

that we estimated it nonparametrically at the climate tercile level. In practice, however, there are not enough observations for each ZIP code to estimate this relationship precisely. Instead, we estimate the daily temperature-mortality relationship as a semi-parametric, smooth function $f(t, CDD)$ that depends on both daily average temperature and climate, as captured by the ZIP code's CDD Normal.

The regression equation used to estimate this semi-parametric function of temperature and climate is identical to equation 1 except the temperature and climate indicators are replaced by this smooth function $f(t, CDD)$ of temperature and climate, yielding the estimating equation:

$$mortality_{zd} = f(t_{zd}, CDD_z) + ZipDay_{zd} + L_{zd} + StYr_{zd} + \varepsilon_{zd}. \tag{3}$$

We define $f(t, CDD)$ to be a linear spline in temperature with knot points at 10-degree increments from 30°F to 90°F, which is then fully interacted with a spline in log CDD with knot points at the 33rd and 66th percentiles of the current distribution of ZIP-code-level CDD normals (the same cutoff points used to define the climate terciles). Specifically, if F_{CDD} is the cumulative distribution function of the current CDD Normal distribution, then

$$f(t, CDD) = s(t, \beta) + \sum_{p=0}^{2} \max\left(\log CDD - \log F_{CDD}^{-1}(0.33p), 0\right) \times s(t, \beta^p),$$

where

$$s(t, \beta) = \beta_0 t + \sum_{k=3}^{9} \beta_k \max(t - 10k, 0).$$

Since $f(t, CDD)$ is identified up to a constant, we always evaluate it relative to a reference temperature of 65°F. We compare the parametric estimates from equation 3 to the nonparametric temperature bin results from equation 1, and we reestimate equation 1 but with fitted, three-day mortality values $\hat{mortality}_{zd} = \hat{f}(t, CDD)$ as the outcome and controlling only for temperature bin indicators. As shown in appendix figure B.7, the parametric estimates broadly align with the nonparametric estimates in each climate tercile.

Appendix figure B.8 further illustrates the parametric estimates from equation 3 by plotting the fitted temperature-mortality relationship $\hat{f}(t, CDD)$ for two cold ZIP codes (Fargo, ND, and Minneapolis, MN), one moderate ZIP code (Chicago, IL), and two hot ZIP codes (Dallas, TX, and Miami, FL), evaluated at each ZIP code's current CDD Normal. As with the nonparametric tercile-based regressions presented in figure 2a, cold places suffer the most from hot days, while hot places suffer the most from cold days. This figure also

11

previews how we will model adaptation to future climate. The climate models we use project Chicago's end-of-century CDD to be 2,327, which is very close to Dallas's current climate with 2,668 CDD. When we consider adaptation, we will use the temperature-mortality curve for a region with 2,327 CDD—essentially that of current-Dallas—to proxy for future-Chicago, assuming the region fully adapts to its new climate.

Finally, we can relate the estimate of $f(t, CDD)$ to the mortality effect $m_z^p(t)$ of a day with average temperature t in ZIP code z in period p, introduced in our general framework above. If $M65_z^p$ represents mortality on a 65°F day in ZIP code z and period p, then

$$m_z^p(t) = M65_z^p + f(t, CDD_z^p).$$

4.2 Adaptation Predictions

We estimate the change in mortality between the current period (1992–2013) and the end of the century (2080–2099) using the meta-predictions of climate change under the RCP 8.5 emissions scenario. To investigate the importance of accounting for regional heterogeneity and adaptation, we construct these estimates under three different sets of assumptions about how the mortality effects of temperature vary spatially and over time.

4.2.1 Homogeneous Current Effects with No Future Adaptation

Our first set of predictions relies on two simplifications commonly made when predicting the mortality effects of climate change. The first simplification is to use a homogeneous mortality estimate, $m^{period}(t)$, rather than region-specific estimates, $m_z^{period}(t)$. The second is to estimate health damages under an assumption of no adaptation (i.e., to define $m_z^{future}(t)$ to be equal to $m_z^{current}(t)$). We implement this empirically by estimating a version of equation 3 where we drop all terms in $f(t, CDD)$ that depend on CDD to get a single temperature-mortality relationship $m(t)^{current} = M65 + f(t)$. We then use that relationship for all ZIP codes in both current and future periods. Note that while we use the same mortality function $f(t)$ for all regions, each ZIP code's mortality change is computed with respect to its own projected future temperature distribution. We call this the case of *homogeneous current effects with no future adaptation.*

4.2.2 Current Climate Heterogeneity with No Future Adaptation

Our second set of predictions allows each ZIP code to have its own temperature-mortality relationship, $m_z^{current}(t)$, by estimating equation 3 where $f(t, CDD)$ is permitted to depend on the ZIP code's current CDD Normal. Thus, any two ZIP codes with the same current CDD

Normals will have the same estimated temperature-mortality curve. Using this mortality relationship to capture both current and future conditions, we continue to assume there is no adaptation. We call this the case of *current climate heterogeneity with no future adaptation.*

4.2.3 Current Climate Heterogeneity with Future Adaptation

In our third set of predictions, we account for both climate-specific heterogeneity in the temperature-mortality relationship and adaptation over time. We operationalize this by evaluating the future mortality effects of temperature, $f(t, CDD)$, in ZIP code z under the projected future climate (CDD) in that ZIP code. Intuitively, this approach assumes that if Chicago's climate changes so that its end-of-century CDD is equal to Dallas's current CDD, then Chicago's end-of-century temperature-mortality relationship will be the same as Dallas's is today, up to a constant.

Since under our approach to adaptation, the current and future temperature-mortality relationships are allowed to differ, the constant terms in $m_z^{current}(t)$ and $m_z^{future}(t)$, which are not identified empirically, do not drop out of the calculation of climate change mortality effects (equation 2). For our computations, we assume that mortality on a 65°F day does not change over time (i.e., $M65_z^{current} = M65_z^{future}$). Our justification for this assumption is that when the average temperature is near 65°F, individuals typically do not choose to heat or cool their homes. This assumption is appropriate if regional differences in mortality on 65°F days, after adjusting for seasonal and other fixed effects, reflect baseline differences in mortality across ZIP codes that are not affected by differences in climate. We call this the *current climate heterogeneity with future adaptation case.*

Our approach to modeling adaptation assumes that adaptation is complete in the sense that if future-Chicago has Dallas's current climate, future-Chicago will respond to temperature like Dallas does today. This need not be the case if the cost of adaptation changes or if some characteristics of current-Chicago are immutable. In addition, our approach assumes that a region's past adaptation to its current climate has no long-lasting effects in the sense that if Chicago has Dallas's climate in the future, after it adapts it will be no better at dealing with cold temperatures than Dallas is now, even though Chicago currently has a significant advantage over Dallas in this area.[7] Finally, this approach ignores the possibility of technological progress, which may moderate the temperature-mortality relationship beyond what we capture.

---

[7]These concerns could be incorporated into our approach by either basing future-Chicago's temperature-mortality relationship on a weighted average of current-Chicago and current-Dallas, with the relative weight placed on regions that currently have Chicago's future climate capturing the extent of adaptation, or by placing separate weights on the two areas for temperatures above and below 65°F.

4.2.4 Example: Chicago

Figure 4 depicts the relevant pieces of equation 2 for computing the projected end-of-century change in mortality for Chicago. Chicago's current and future temperature distributions are depicted by the blue and orange shaded regions, respectively. To compute the mortality effect with homogeneous effects and no adaptation, we use the dashed homogeneous temperature-mortality relationship in both the current and future periods. For the current climate heterogeneity with no future adaptation case, expected mortality is computed using Chicago's current temperature-mortality relationship in both periods. Finally, to allow for current climate heterogeneity and future adaptation, we compute current mortality using Chicago's current temperature-mortality curve and its current temperature distribution (both shown in blue), and we compute future mortality using Chicago's future curve its future temperature distribution (both shown in orange).

4.3 End-of-Century Mortality Prediction Results

Figure 5 presents the results from assessing annual mortality effects of end-of-century climate change as predicted by the meta-model under the RCP 8.5 emissions scenario. Panel A depicts results under the conventional approach of assuming homogeneous current effects and no adaptation. Each box and whisker plot summarizes percentage changes in predicted annual mortality by the end of the century (2080–2099, vertical axis) for ZIP codes whose current climate falls in the bin depicted on the horizontal axis. Boxes stretch from the 25th percentile (lower hinge) to the 75th percentile (upper hinge) of mortality effects. The median is plotted as a line across the box, and whiskers stretch from the 5th–95th percentiles. In this case, mortality effects increase with CDD up to around 2,000 CDD, which is well into the warmest climate tercile (which begins at 1,442 CDD), and then flatten out as CDD continue to increase. These findings are further summarized by column 5 of table 1, who shows the aggregate percentage mortality change for each of the climate terciles and for the United States as a whole.[8] The average mortality effects increase in magnitude from the coolest to the warmest third of ZIP codes, with a 0.76% increase in mortality overall. This pattern agrees with the conventional wisdom that the effects of climate change will be largest in regions that are currently hot.

The results change markedly once heterogeneity, with respect to current climate, is incorporated into the climate assessment. Panel B of figure 5 illustrates the heterogeneous current climate effects and the no-adaptation case. Here, the pattern is reversed relative

---

[8]Appendix tables B.2a–B.2d show the analog of table 1 for the unweighted meta-model and for each of the individual climate models.

to the conventional approach, with the mortality effect being flat up to 1,500 CDD (which includes the coolest and middle ZIP code terciles), and then declining as CDD continue to rise. The large average increases in mortality in cool and moderate ZIP codes result from two factors in combination: these regions are currently poorly adapted to very hot days, but climate models project increased exposure to such days in the future.[9]

Aggregate results for the case of heterogeneous effects by climate with no future adaptation are presented in column 6 of table 1. Mortality increases are larger in the coolest third of ZIP codes (2.25%) than in the warmest (1.33%). The mortality increase in the middle (2.89%) tercile is slightly larger than in the coolest, as these ZIP codes expect, on average, to experience more very hot days in the future than the coolest ones. Overall, our analysis predicts an increase in mortality across all U.S. ZIP codes of 2.15%, almost three times larger than is implied by homogeneous effects (0.76%). To put this number in perspective, this increase is roughly equivalent to the share of U.S. elderly deaths in 2013 due to chronic kidney disease (2.1%), accidents (2.4%), or influenza (2.5%) and around 10% of the share of elderly deaths due to cancer (21.4%).[10]

Panel C of figure 5 presents results under heterogeneous current climate effects with future adaptation. Three features emerge. First, net of adaptation, climate change is expected to be worse in the coolest regions than in the warmest ones. Second, incorporating adaptation to future climate yields mortality effects of climate change that are systematically lower than the no-adaptation estimates in panel B. Third, the predicted mortality change under adaptation is negative for regions with a current climate of 1,000 CDD (e.g., current-Chicago) and up. Column 7 of table 1 summarizes these findings at a more aggregate level. For each climate tercile and the United States overall, the mortality effect with future adaptation is smaller than without (column 6); i.e., adaptation reduces the assessed mortality effects of climate change. In each case, the magnitude of these differences is large, with the mortality effect shrinking by over 60% for the coolest third of ZIPs and actually becoming negative for the two other terciles and for the United States overall.

These findings indicate that climate change could reduce elderly mortality in the United

---

[9]As indicated by the height of the box and whisker plots, effects in panel B are also more dispersed than those in panel A, especially among cooler regions. This difference arises for two reasons. First, ZIP codes with the same climate today can have different predicted future climates, including different fractions of very hot days. Second, because cooler regions are particularly bad at dealing with very hot days (i.e., the temperature-mortality curve is very steep for hot days), as in figure 2a, small variations in the proportion of very hot days can induce very different mortality predictions.

[10]Centers for Disease Control and Prevention, National Center for Health Statistics. Underlying Cause of Death 1999-2017 on CDC WONDER Online Database, released December 2018. Data are from the Multiple Cause of Death Files, 1999–2017, as compiled from data provided by the 57 vital statistics jurisdictions through the Vital Statistics Cooperative Program. Accessed at http://wonder.cdc.gov/ucd-icd10.html on August 5, 2019, 7:41:38 p.m.

States if places adapt to the future climates the way places are adapted to their current climates. That currently hot regions appear better adapted to heat than cooler places suggests that the benefits of adaptation exceed the cost within the domain of current climates. At the same time, there remains uncertainty about which adaptation technologies will be available in the future, how much they will cost to use, and how effective they will be at mitigating the effects of climates that are much hotter than any currently being experienced in the United States.

One aspect of adaptation where these concerns are particularly salient is migration. If the adaptation to hot temperatures we currently observe is driven by migration based on current climates, with individuals who are particularly vulnerable to heat moving to cooler climates, then their ability to continue to migrate in this way in the future depends on the continued availability of similarly desirable locations with cool climates in the future.

Even if climate change reduces mortality, it is important to note that this does not necessarily imply an improvement in elderly welfare. If adaptation to heat involves staying indoors and running the AC, then a decrease in utility from outdoor activities may offset some or all of the mortality benefit of adaptation relative to the current situation. In addition, warmer global temperatures may lead to changes in sea levels, agriculture, vector-borne disease prevalence, and other factors that may directly reduce human well-being.

4.4   Alternative Climate Projections

Our primary climate assessment results use climate change projections from the weighted meta-model under the RCP 8.5 emissions scenario. In appendix A.3, we show results for the RCP 4.5 emissions scenario, a mid-range projection under which emissions peak around 2,040 and then decline. Mortality effects under the RCP 4.5 scenario are qualitatively similar to, but more muted than, the effects under the RCP 8.5 scenario.

Appendix figures B.9b–B.9w and appendix tables B.2a–B.2d present separate prediction results for each of the 21 individual climate change models and an unweighted version of the meta-model. These results are broadly consistent with those of our main projections. Because the NEX-GDDP dataset contains a single realization of daily temperatures for each model, we are unable to consider uncertainty within a particular model that could arise due to uncertainty about appropriate choices of parameter values or realizations of stochastic quantities. However, the individual models predict end-of-century changes in average temperature ranging from about 5°F to 11.5°F. Comparing effects for the individual models provides insight into the range of possible outcomes in models that exhibit a relatively high or low degree of warming.

4.5 Geography of the Mortality Effects of Climate Change

Figure 6 maps the estimated mortality impact of end-of-century climate change under the three cases that we simulate, aggregated by county to facilitate comparison with prior studies. Panel A, which assumes homogeneous temperature effects, shows that the areas that are currently the hottest, the Deep South and Desert Southwest, will tend to suffer the largest mortality increases. Many of the coldest parts of the country, in the Northeast, Upper Midwest, and Northwest, are predicted to see a decrease in mortality due to the decrease in very cold days resulting from climate change. This geographic pattern mirrors the all-age mortality result of Hsiang et al. (2017) (see figure 2 of that paper), which also assumes homogeneous effects and no future adaptation.

Panel B of figure 6, which maps mortality predictions allowing for current climate heterogeneity but not future adaptation, reverses the geographic distribution of climate damages relative to assuming homogeneous temperature effects. Here, the mortality impacts are the smallest in the warmest regions of the country. The largest effects are expected to be felt in a swath across the Midwest and Central Plains, which expect a large increase in hot days and are currently poorly adapted to dealing with heat.

Panel C of figure 6 maps mortality predictions that incorporate both current heterogeneity and future adaptation to climate change. Here we see that adaptation has the potential to significantly moderate the impact of warming over much of the country, with the yellow and green areas exhibiting small positive to negative mortality effects. In isolation, these negative effects do not necessarily imply a benefit due to adaptation itself since some regions are projected to benefit from climate change even without additional adaptation in the future (panel B). However, many of the areas that are medium or dark green in panel C are also dark orange or red in panel B, indicating a large adaptation benefit. These regions would be expected to have the largest per-capita willingness to pay for adaptation to climate change.

5 Conclusion

This paper demonstrates the importance of accounting for regional heterogeneity and adaptation in predicting the impact of climate change on U.S. elderly mortality. Incorporating heterogeneous mortality effects of temperature into a climate change assessment substantially increases the estimated mortality impact of warming and changes which regions are likely to suffer the most. Allowing for adaptation yields estimated mortality impacts of climate change that are much lower than those calculated without adaptation and possibly even negative. Although we do not consider the future cost of adaptation, our results show

that regions have chosen to engage in adaptation that significantly reduces elderly mortality given currently available technologies and current/historical costs, suggesting that there is significant ability to moderate the mortality impact of future warming even using technologies that are readily available today. The potential for future technological change to reduce the costs of adaptation may lower the mortality effect of climate change even further.

Our paper has focused on the mortality effects of climate change among the U.S. elderly. While the elderly are a relatively vulnerable group, the United States is a wealthy and geographically diverse country where the opportunity to adapt to climate change may be particularly high. Effects of climate change could differ for other populations, especially those in poorer or more geographically constrained countries (e.g., Bangladesh) with less opportunity to adapt to future climate change. Although we do not consider the non-elderly, other countries, or nonmortality outcomes, the methods we employ could be applied to estimating climate-change impacts in these environments as well.

Finally, it is important to recognize that our estimates of heterogeneity and adaptation are based on current experience and that our climate change assessments extrapolate from this experience to a future as simulated by climate models. However, the climate of the future may move outside of our present experience or even beyond what is projected by climate models. Because of this, there remains significant uncertainty about the future damages from climate change and the likelihood of large-scale, potentially catastrophic changes that is not fully incorporated into our model and could not be without quantifying these risks through additional assumptions. This uncertainty could easily dominate the statistical uncertainty expressed in the standard errors of our estimates. As Martin Weitzman wrote in this journal when deriving his "Dismal Theorem" and arguing in favor of a precautionary principle with respect to climate policy (Weitzman, 2009), "it is not possible to learn enough about the frequency of extreme tail events from finite samples alone to make [utility-based welfare calculations] independent of artificially imposed bounds on the extent of possibly ruinous disasters. ... Climate-change economics generally—and the fatness of climate-sensitivity tails specifically—are prototype examples of this principle, because we are trying to extrapolate inductive knowledge far outside the range of limited past experience."

References

Auffhammer, Maximilian. 2017. "Climate Adaptive Response Estimation: Short and Long Run Impacts of Climate Change on Residential Electricity and Natural Gas Consumption Using Big Data." *Mimeo, Department of Agricultural and Resource Economics, University of California at Berkeley.*

Auffhammer, Maximilian, Solomon M. Hsiang, Wolfram Schlenker, and Adam Sobel. 2013. "Using Weather Data and Climate Model Output in Economic Analyses of Climate Change." *Review of Environmental Economics and Policy*, 7(2): 181–198.

Barreca, Alan, Karen Clay, Olivier Deschênes, Michael Greenstone, and Joseph S Shapiro. 2015. "Convergence in adaptation to climate change: evidence from high temperatures and mortality, 1900–2004." *The American Economic Review*, 105(5): 247–251.

Barreca, Alan, Karen Clay, Olivier Deschênes, Michael Greenstone, and Joseph S. Shapiro. 2016. "Adapting to Climate Change: The Remarkable Decline in the US Temperature-Mortality Relationship over the Twentieth Century." *Journal of Political Economy*, 124(1): 105–159.

Beatty, Timothy K. M., and Jay P. Shimshack. 2014. "Air pollution and children's respiratory health: A cohort analysis." *Journal of Environmental Economics and Management*, 67(1): 39–57.

Butler, Ethan, and Peter Huybers. 2013. "Adaptation of US maize to temperature variations." *Nature Climate change*, 3: 68–72.

Currie, Janet, and Matthew Neidell. 2005. "Air Pollution and Infant Health: What Can We Learn from California's Recent Experience?" *The Quarterly Journal of Economics*, 120(3): 1003–1030.

Curriero, Frank C., Karlyn S. Heiner, Jonathan M. Samet, Scott L. Zeger, Lisa Strug, and Jonathan A. Patz. 2002. "Temperature and Mortality in 11 Cities of the Eastern United States." *American Journal of Epidemiology*, 155(1): 80–87.

Deschênes, Olivier. 2014. "Temperature, human health, and adaptation: A review of the empirical literature." *Energy Economics*, 46: 606–619.

Deschênes, Olivier, and Michael Greenstone. 2011. "Climate Change, Mortality, and Adaptation: Evidence from Annual Fluctuations in Weather in the US." *American Economic Journal: Applied Economics*, 3(4): 152–185.

Houser, Trevor, Robert Kopp, Solomon M Hsiang, Michael Delgado, Amir Jina, Kate Larsen, Michael Mastrandrea, Shashank Mohan, Robert Muir-Wood, DJ Rasmussen, et al. 2014. "American Climate Prospectus: Economic Risks in the United States." *Rhodium Group*.

Hsiang, Solomon, Robert Kopp, Amir Jina, James Rising, Michael Delgado, Shashank Mohan, D. J. Rasmussen, Robert Muir-Wood, Paul Wilson, Michael Oppenheimer, Kate Larsen, and Trevor Houser. 2017. "Estimating economic damage from climate change in the United States." *Science*, 356(6345): 1362–1369.

IPCC. 2014. "IPCC, 2014: Climate Change 2014: Synthesis Report." *Contribution of Working Groups I II and III to the Fifth Assessment Report of the intergovernmental panel on Climate Change [Core Writing Team, Pachauri, RK and Meyer, LA. (eds)]. IPCC, Geneva, Switzerland.*

Kahn, Matthew E. 2016. "The Climate Change Adaptation Literature." *Review of Environmental Economics and Policy*, 10(1): 166–178.

Massetti, Emanuele, and Robert Mendelsohn. 2018. "Measuring Climate Adaptation: Methods and Evidence." *Review of Environmental Economics and Policy*, 12(2): 324–341.

Meinshausen, Malte, S. J. Smith, K. Calvin, J. S. Daniel, M. L. T. Kainuma, J.-F.

Lamarque, K. Matsumoto, S. A. Montzka, S. C. B. Raper, K. Riahi, A. Thomson, G. J. M. Velders, and D. P. P. van Vuuren. 2011. "The RCP greenhouse gas concentrations and their extensions from 1765 to 2300." *Climatic Change*, 109(1-2): 213.

Portnykh, Margarita. 2017. "The Effect of Weather on Mortality in Russia: What if People Adapt?" *Working paper.*

Rogot, Eugene, Paul D. Sorlie, and Eric Backlund. 1992. "Air-conditioning and Mortality in Hot Weather." *American Journal of Epidemiology*, 136(1): 106–116.

Sanderson, Benjamin M, Reto Knutti, and Peter Caldwell. 2015. "A representative democracy to reduce interdependency in a multimodel ensemble." *Journal of Climate*, 28(13): 5171–5194.

Sanderson, B.M., and M.F. Wehner. 2017. "Model Weighting Strategy, Appendix B." *Climate Science Special Report: Fourth National Climate Assessment*, , ed. D.J. Wuebbles, D.W. Fahey, K.A. Hibbard, D.J. Dokken, B.C. Stewart and T.K. Maycock Vol. 1, 436–442. Washington, DC:U.S. Global Change Research Program.

Van Vuuren, Detlef P, Jae Edmonds, Mikiko Kainuma, Keywan Riahi, Allison Thomson, Kathy Hibbard, George C Hurtt, Tom Kram, Volker Krey, Jean-Francois Lamarque, et al. 2011. "The representative concentration pathways: an overview." *Climatic change*, 109(1-2): 5.

Weitzman, Martin L. 2009. "On modeling and interpreting the economics of catastrophic climate change." *The Review of Economics and Statistics*, 91(1): 1–19.

Figure 1: U.S. Daily Average Temperature Distribution
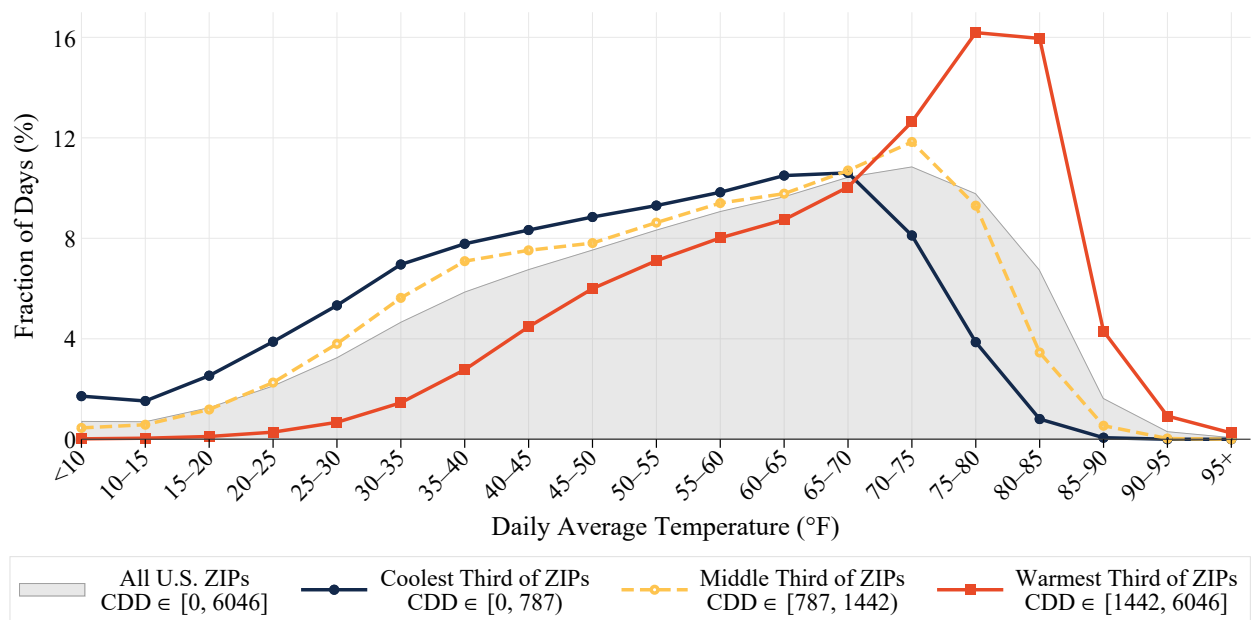
Notes: This figure summarizes the distribution of daily average temperature in the United States from 1992–2013. Distributions are reported separately for the entire United States and for the coolest, middle, and warmest population-weighted thirds of ZIP codes based on CDD Climate Normals. Daily temperature data come from the Global Historical Climatology Network land surface station database. Appendix tables B.1a–B.1b report numerical values of the points in this figure.

Figure 2: Mortality Effects of Temperature
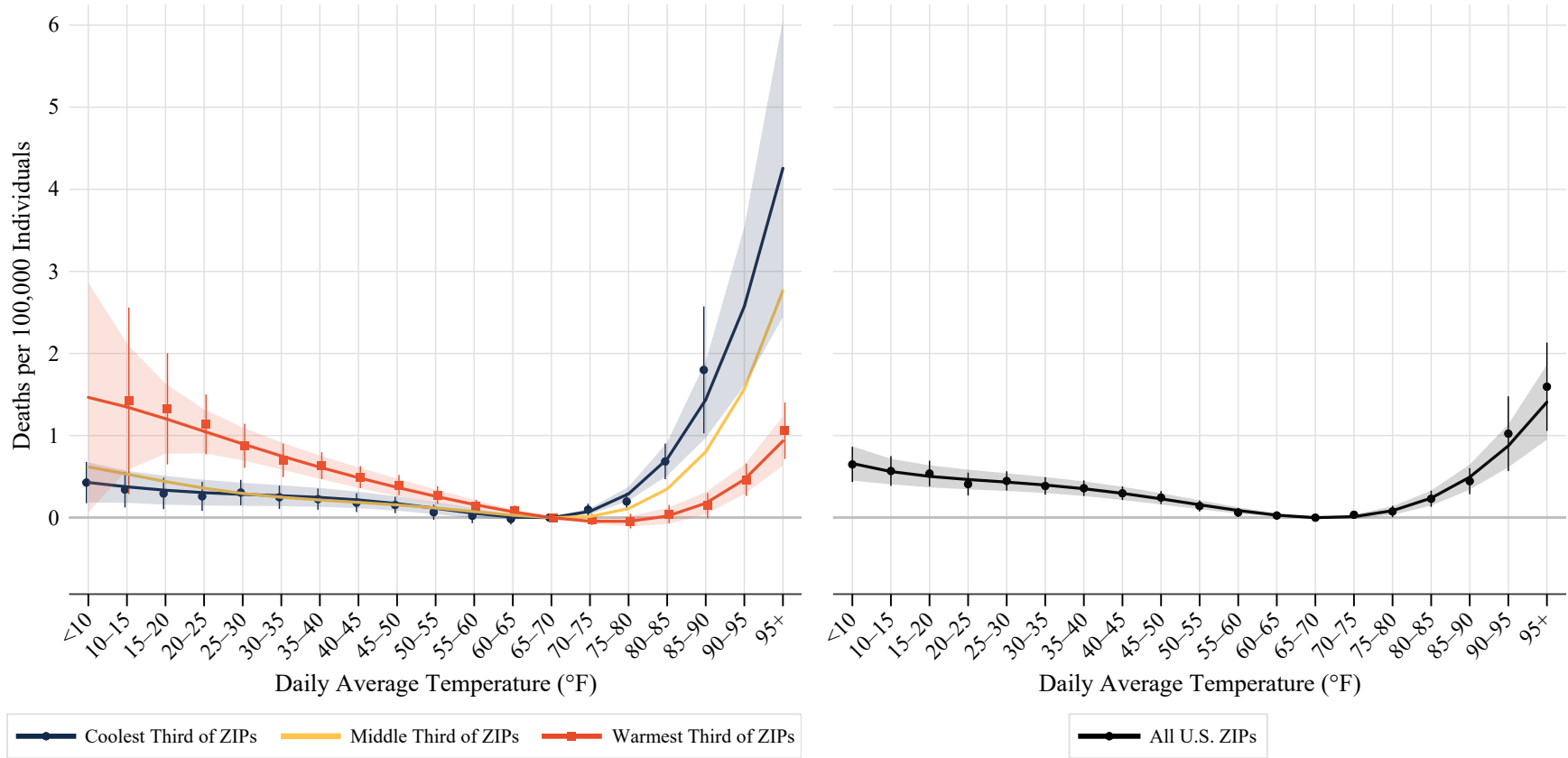
(a) Climate-Specific Temperature Effects

(b) Homogeneous Temperature Effects

Notes: This figure plots estimated three-day mortality effects of temperature. In panel A, effects are allowed to differ by the coolest, middle, or warmest third of ZIP codes as defined in figure 1. In panel B, effects are restricted to be common to all U.S. ZIP codes. Effects reflect excess mortality on a day with a given average temperature relative to a day with an average temperature of 65°F–70°F. Markers with whisker lines plot nonparametric temperature bin estimates and associated 95% confidence intervals. Markers are only shown for binned temperatures that occur with a frequency of at least one day per decade in the climate region. Solid lines and shaded regions plot semi-parametric polynomial estimates and associated 95% confidence intervals. Confidence intervals are based on two-way clustered standard errors at the county and state×date levels. Numerical values for all point estimates and standard errors are reported in appendix tables B.1a–B.1b.

Figure 3: Predicted Mortality Effects of Regional Climate Swaps
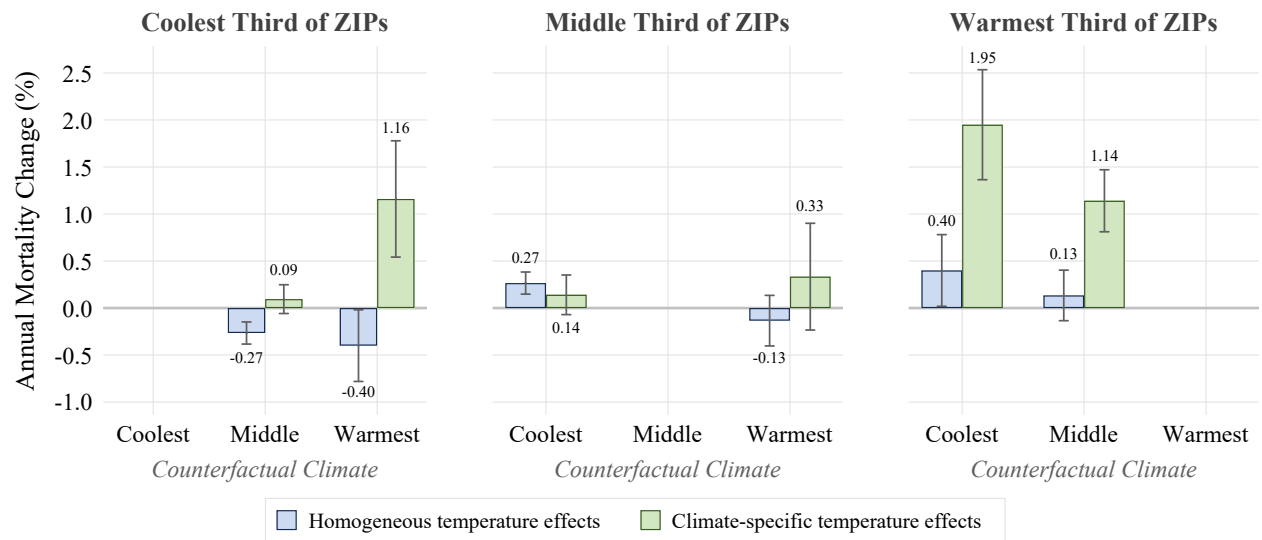
Notes: This figure summarizes mortality impacts from counterfactual scenarios in which each of these climate region's current temperature distribution is replaced by the current distribution of one of the other two climate regions, shown in figure 1.

Figure 4: Climate Change Assessment for Chicago, IL
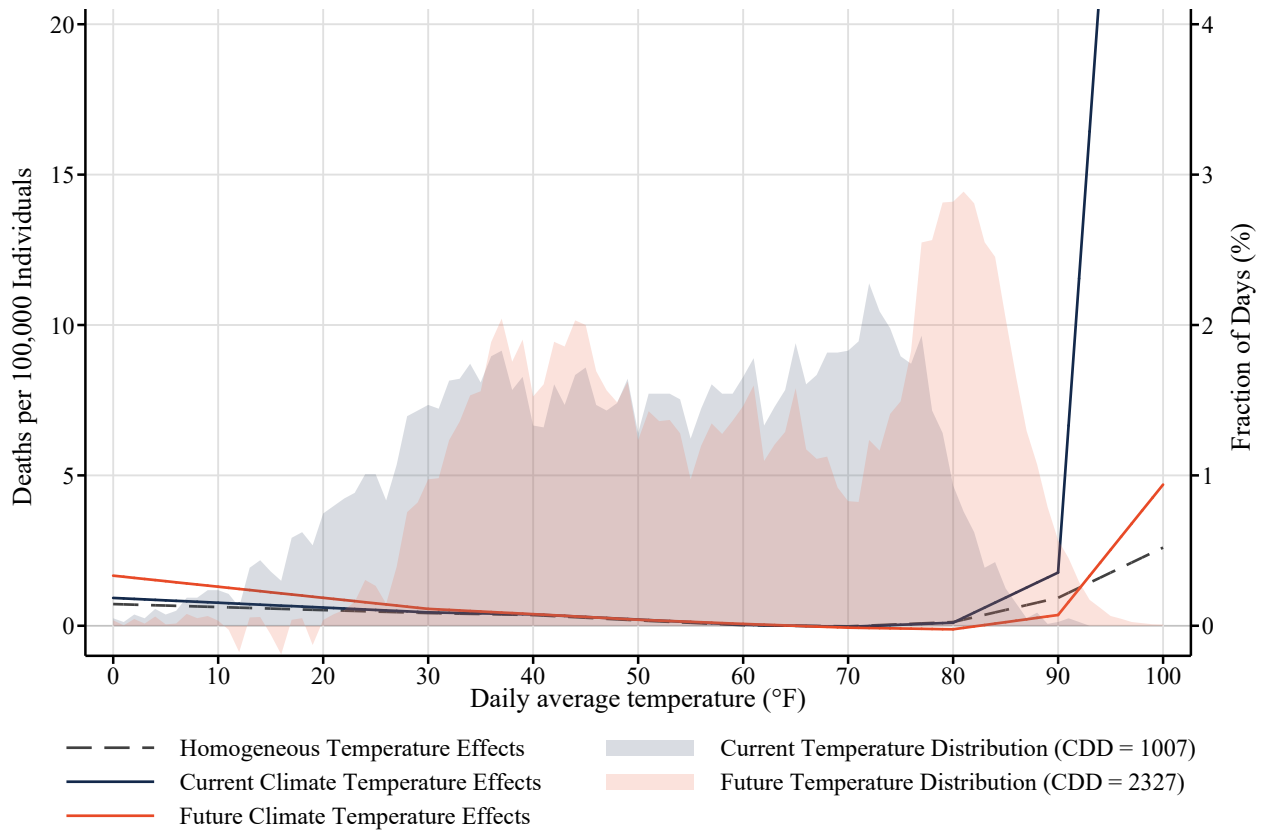
Notes: This figure depicts the components used by equation 2 to assess end-of-century (2080–2099) climate change impacts on mortality in Chicago, IL. The end-of-century temperature distribution is based on the meta-model projection for Chicago under the RCP 8.5 greenhouse gas emissions scenario.

Figure 5: End-of-Century Climate Change Mortality Effects
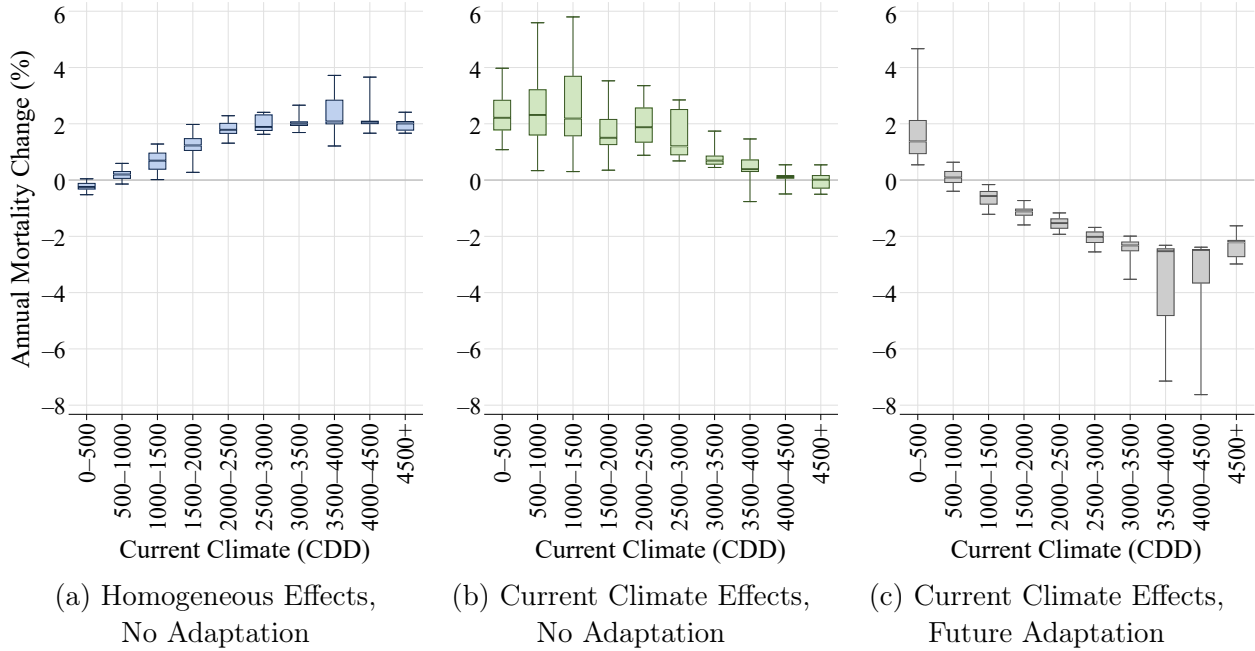
(a) Homogeneous Effects,
No Adaptation

(b) Current Climate Effects,
No Adaptation

(c) Current Climate Effects,
Future Adaptation

Notes: The figure summarizes annual mortality effects of end-of-century (2080–2099) climate change as projected by the meta-model, an average of the 21 NEX-GDDP climate models, under the RCP 8.5 emissions scenario. Effects are calculated for each ZIP code based on the ZIP code's current and future (projected) climates. Panel A reports climate effects under the assumption of homogeneous temperature effects. Panel B reports climate effects that allow for heterogeneous temperature effects based on current climate but do not allow for future adaptation. Panel C reports climate effects that incorporate both current heterogeneity and future adaptation. Box and whisker plots summarize the distribution of climate change effects across ZIP codes in each climate range. Boxes stretch from the 25th percentile (lower hinge) to the 75th percentile (upper hinge). The median is plotted as a line across the box. Whiskers stretch from the 5th percentile to the 95th percentile.

Figure 6: Geography of End-of-Century Climate Change Effects
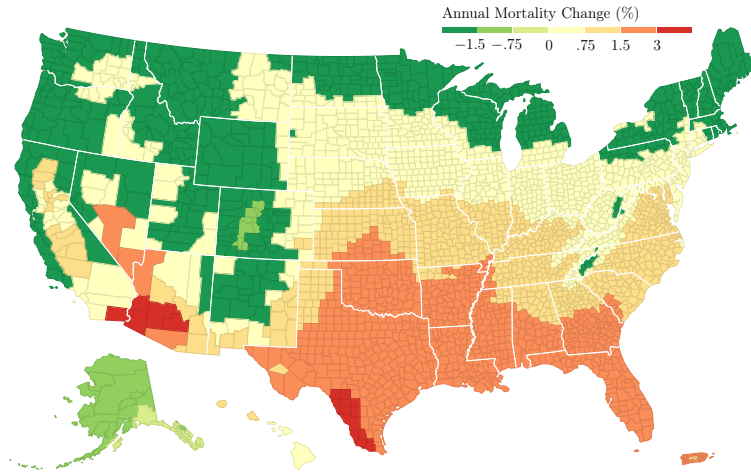
(a) Homogeneous Effects, No Future Adaptation
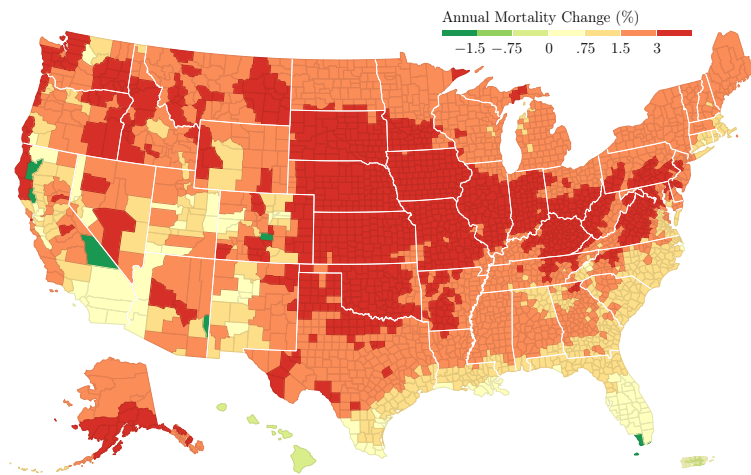
(b) Current Climate Heterogeneity, No Future Adaptation
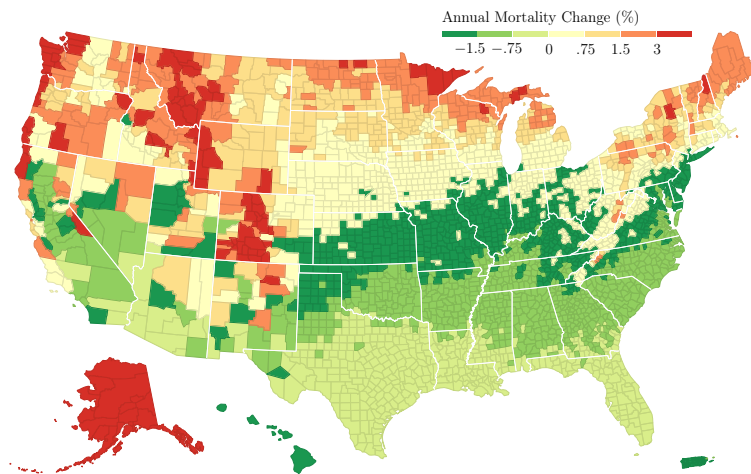
(c) Current Climate Heterogeneity, Future Adaptation

Notes: The map shows county-level aggregates of the ZIP-code-level climate change impacts on annual mortality summarized in figure 5. Panel A reports climate effects under the assumption of homogeneous temperature effects. Panel B reports climate effects that allow for heterogeneous temperature effects based on current climate but do not allow for future adaptation. Panel C reports climate effects that incorporate both current heterogeneity and future adaptation.

Table 1: End-of-Century Climate Change Effects

	(1)	(2)	(3)	(4)	(5)	(6)	(7)
					Annual Mortality Change (%)		
	Avg. Temp. (°F)		Annual CDD		Homogeneous Effects	Climate Heterogeneity	
	Current	Future	Current	Future	No Adaptation	No Adaptation	Future Adaptation
Coolest third of ZIPs	49.4	58.1	525	1,661	−0.03	2.25***	0.84**
					(0.12)	(0.50)	(0.35)
Middle third of ZIPs	55.2	63.5	1,079	2,491	0.54***	2.89***	-0.41
					(0.16)	(0.93)	(0.35)
Warmest third of ZIPs	66.5	73.6	2,600	4,397	1.75***	1.33***	−1.97***
					(0.28)	(0.31)	(0.67)
All U.S. ZIPs	57.1	65.1	1,413	2,864	0.76***	2.15***	−0.53*
					(0.18)	(0.47)	(0.32)

Notes: The table summarizes ZIP code-level climate change impacts, aggregated to climate terciles and to the United States as a whole. Columns 1–4 summarize the current climate of each region as well as the end-of-century (2080–2099) climate projected by the meta-model under the RCP 8.5 greenhouse gas emissions scenario. Columns 5–7 are based on the ZIP-code-level annual mortality effects summarized in figure 5. Column 5 reports climate effects under the assumption of homogeneous temperature effects. Column 6 reports "business as usual" climate effects that allow for heterogeneous temperature effects based on current climate but do not allow for future adaptation. Column 7 reports climate effects that incorporate both current heterogeneity and future adaptation.

Online Appendix
Adaptation and the Mortality Effects of Temperature Across U.S. Climate Regions

Garth Heutel, Georgia State University and NBER
Nolan Miller, University of Illinois and NBER
David Molitor, University of Illinois and NBER

September 2019

Appendix A: Supplementary Material

A.1 Data Description

A.1.1 Medicare Data

Our baseline sample consists of Medicare beneficiaries age 65–100 and is derived from 100% Medicare enrollment information files for years 1992–2013.[1] These annual files include an observation for each beneficiary enrolled in Medicare for at least one day in that calendar year, whether enrolled in Original Medicare (fee-for-service) or Medicare Advantage. The enrollment files report a variety of demographic and enrollment variables, including unique beneficiary identifiers that link individuals over time; monthly indicators for Medicare eligibility; state, county, and ZIP code of residence based on the mailing address for official correspondence; and date of birth, date of death, and gender.

Medicare beneficiaries include the vast majority of elderly living in the United States. Appendix figure B.1a compares the number of Medicare beneficiaries in the enrollment files to census estimates of the number of U.S. resident population who are age 65 and over. To aid comparison, we use census estimates of the resident population on July 1 each year and limit the Medicare sample to beneficiaries residing in the 50 states and the District of Columbia and who turned 65 before July 1. Over the period 1992–2013, the census estimates an average of 36.7 million elderly individuals each year, compared to 35.9 million elderly beneficiaries in Medicare. Thus, the Medicare sample covers over 97% of elderly living in the United States, a share that remains roughly constant over the sample period.

The mortality variables used in our analysis are based on dates of death recorded in the Medicare enrollment files. Medicare's death data come primarily from the Social Security Administration but are augmented based on reviews triggered by hospitalization claims indicating patient death. The annual mortality rates in the Medicare data align closely to mortality rates based on National Vital Statistics death records and census population estimates, as shown in appendix figure B.1b. While all recorded deaths in the Medicare data are validated, some death *dates* in the data are not validated and are assigned the last date in the month of death. Because much of our analysis is performed at the daily level, we drop individuals who die at any point in the year and who do not have a validated death date flag. This restriction affects fewer than 3% of the deaths in our sample.

A.1.2 Daily Temperature and Climate Normals

GHCN-Daily Our primary source for daily temperature variables is the Global Historical Climatology Network (GHCN)-Daily database, which provides weather measurements from land surface stations across the United States, including the 48 adjoining U.S. states, the District of Columbia, Alaska, Hawaii, and Puerto Rico. We calculate daily high and low GHCN temperatures for each 2010 Census ZCTA as the inverse distance-weighted average of all available daily maximum and minimum temperatures, respectively, for GHCN stations within a 20-mile radius of the ZCTA centroid. The daily average GHCN temperature for a ZCTA is calculated as the midpoint of the daily high and low GHCN temperatures.

---

[1] The Research Data Assistance Center (ResDAC) provides a helpful overview of the Medicare data files at http://www.resdac.org.

PRISM   We also calculate daily temperature using the PRISM daily dataset. PRISM data provide interpolated daily temperature values at a 4km resolution and cover only the conterminous United States (the 48 adjoining U.S. states and the District of Columbia). We calculate daily high and low PRISM temperatures for each 2010 Census ZCTA as the inverse distance-weighted average of daily maximum and minimum temperatures, respectively, for PRISM grid points within a 20-mile radius of the ZCTA centroid. The daily average PRISM temperature for a ZCTA is calculated as the midpoint of the daily high and low PRISM temperatures.

Climate Normals   We calculate climate summaries for each 2010 Census ZCTA using NOAA's 1980–2010 Climate Normals, which are produced for ground monitor stations across the United States. ZCTA Climate Normals, for a given climate element, are calculated as the inverse distance-weighted average of Normals at the nearest station and any other stations within a 20-mile radius of the ZCTA centroid. The primary climate element we use in the analysis is CDD. For a given year, CDD is calculated as the (non-negative) number of degrees that a day's average temperature exceeds 65°F, summed over all days in a year. We also use average temperature Normals, which we calculate as the midpoint between the maximum and minimum temperature Normals.

A.1.3   Climate Models Data

We calculate end-of-century climate change predictions using all 21 climate models for which daily scenarios are produced and distributed as part of the Coupled Model Intercomparison Project Phase 5 (CMIP5). Daily downscaled projections for each of these models come from the NASA Earth Exchange Global Daily Downscaled Projections (NEX-GDDP) dataset. The NEX-GDDP data include daily minimum and maximum temperature predictions on a 25km by 25km grid (0.25-degree spatial resolution) for the period 1950–2100 (projections end in 2099 for some models). Projections for each model are made under two greenhouse gas emissions scenarios: the Representative Concentration Pathway (RCP) 8.5 "business as usual" scenario, where emissions continue to rise throughout the 21st century; and the RCP 4.5 scenario, a mid-range projection under which emissions peak around 2,040 and then decline.

For each of the 21 NEX-GDDP climate models, we construct grid-point-specific projected distributions of average daily temperature for both the current period (1992–2013) and the end-of-century period (2080–2099). To do so, we take the projected daily minimum and maximum temperatures over a given period, construct projected daily average temperature using the midpoint of daily maximum and minimum temperatures, and then calculate the fraction of days in which the projected daily average temperature falls into 1°F bins ranging from −30°F to 120°F.

To summarize the projected temperature distributions of the 21 NEX-GDDP climate models, we construct two "meta" models that average over each of the 21 component models as follows. First, for a given grid point, emissions scenario, and time period (current or end-of-century), we pool the daily projections of all 21 models. We calculate the unweighted distribution of these pooled daily projections and call this the "unweighted meta-distribution" of the "unweighted meta-model." We also compute the weighted distribution of pooled daily

projections by weighting each daily projection by the model-specific weights employed by the Fourth National Climate Assessment that positively value model predictive skill but penalize codependency between models (Sanderson, Knutti and Caldwell, 2015; Sanderson and Wehner, 2017). We report these model weights in column 1 of appendix table B.2a. We call this weighted temperature distribution the "weighted meta-distribution" of the "weighted meta-model." Since the weighted meta-model is the primary model used in the paper, we also refer to these more concisely as the "meta-distribution" and the "meta-model."

A.2 Analysis Using PRISM Data

In this section, we present analogs to our main results where spatially interpolated temperature data from the PRISM Climate Group are used instead of the GHCN data. Although the PRISM data use a more sophisticated algorithm to assign temperatures to grid points (and then to ZIP codes), the algorithm it employs is less transparent than our simple distance weighting of the GHCN data. To the extent that the two methods differ, these differences tend to involve extreme temperatures, where the PRISM algorithm tends to assign less extreme values. In addition, while the GHCN data exist for the entire United States, including Alaska, Hawaii, and Puerto Rico, the PRISM data are limited to the contiguous United States. Because of the importance of extreme temperatures in our analysis and the fact that we do not know exactly why the PRISM algorithm moderates these days, we choose to use the distance-weighted data rather than the PRISM data. However, our results are qualitatively unchanged if PRISM data are used.

Appendix figure B.5 reproduces the main results of section 3 using PRISM weather data. Although the heterogeneous effects curves in the left panel are rotated slightly clockwise through the 60°F–65°F bin relative to the GHCN case (figure B.5a), the mortality results are qualitatively similar for both cases. The key reason for this is that, for both the GHCN and PRISM analyses, the homogeneous effects curve lies between the climate-specific effects curves for the warmest and coolest climate terciles, implying that using homogeneous effects will tend to overestimate the mortality impact of hot days in hot places and will underestimate their impact in cold places, with the opposite being true in the case of cold days. Numerical results corresponding to appendix figures B.5a and B.5b are presented in appendix tables B.1c and B.1d, respectively.

Appendix figure B.11 is a boxplot analogous to figure 5, using PRISM data instead of GHCN data. Although effect sizes are smaller, the same general patterns persist. In the homogeneous effects case (panel A), mortality effects increase as the regions get warmer, while in the heterogeneous effects case (panel B), mortality effects generally decrease as CDD increase. One exception is the coldest climates, where the effect of climate change is nearly zero. This could reflect that when PRISM data are used for estimating mortality effects, the implied mortality reduction from fewer very cold days is larger than when using GHCN data, which offsets much of the mortality increase from more very hot days.

Appendix table B.3 shows aggregate results for RCP 8.5 using PRISM data. Comparing it to the main results in table 1, which are based on GHCN data, the patterns are similar. Under homogeneous effects (column 5), the largest effects are once again found in the warmest third of ZIPs, while under heterogeneity with no adaptation (column 6), the effect on the warmest third of ZIPs is much smaller than in the other two. While the mortality effect

for the middle third of ZIP codes is larger under PRISM than GHCN, the standard error grows as well, suggesting that this increase may be driven by small changes in parts of the temperature distribution where mortality effects are large and imprecisely estimated (i.e., very hot days). All three terciles are expected to benefit from warming net of adaptation (column 7), although the coefficient is not statistically significant for the coolest third of ZIPs.

A.3   Analysis for the RCP 4.5 Emissions Scenario

As described in Van Vuuren et al. (2011), a Representative Concentration Pathway (RCP) is a comprehensive climate modeling scenario meant to capture possible climate change trajectories over the course of the century. The RCP 8.5 scenario we consider in our main analysis is a "business as usual" scenario where emissions continue to grow throughout the century. However, the climate models we consider also allow for consideration of the more moderate RCP 4.5 pathway, where emissions decline over the second half of the century and carbon dioxide concentrations stabilize around the year 2100.

The first four columns of table B.4 present summary statisics for the RCP 4.5 scenario for the United States overall and for each of the climate terciles. The RCP 4.5 scenario features more moderate warming, with an overall increase of 4.1°F, compared to the 8°F under RCP 8.5 reported in table 1. Each of the climate terciles also features an average temperature increase that is about half as large under RCP 4.5 as it is under RCP 8.5.

Figure B.10 presents a box plot for the RCP 4.5 scenario that can be compared to our main results for RCP 8.5 in figure 5. The qualitative patterns identified for the RCP 8.5 scenario persist in the RCP 4.5 scenario. Under homogeneous effects, the annual mortality change is increasing in CDD. As one might expect under a more modest warming scenario, the peak effect is about half as large as it is under RCP 8.5. The center and leftmost panels show each show effect sizes that decrease in CDD, again with generally smaller magnitudes than under RCP 8.5.

Columns 5–7 of table B.4 present aggregate results for the RCP 4.5 scenario analogous to the corresponding results for RCP 8.5 reported in table 1. The main qualitative result—that the warmest third of ZIPs experiences the largest mortality impact under homogeneous effects (column 5) but in the smallest effect under heterogeneous effects (columns 6 and 7)—continues to hold for RCP 4.5, although the magnitudes are muted due to the smaller amount of overall warming embodied in RCP 4.5.

The mortality results for all U.S. ZIP codes are smaller under RCP 4.5 for the homogenous effects (0.18%) and heterogeneous effects with no adaptation (0.28%) cases than they were under RCP 8.5, again consistent with less overall warming. For the heterogeneous effects with adaptation case, the overall mortality effect is essentially zero (−0.06%) under RCP 4.5, whereas it was negative (−0.53%) under RCP 8.5. This could be driven by the fact that less adaptation takes place when there is less warming, as is the case under RCP 4.5.

A.4   Regional Heterogneity and Air Conditioning Adoption

There are two possible categories of explanations for regional heterogeneity in the temperature-mortality relationship. The first is that the heterogeneity is substantially due to changes in

human physiology and behavior (i.e., adaptation). The second is that the regional differences we observe are due to characteristics that are correlated with current climate but not the results of human choices or physiology.

It is beyond the scope of this paper to identify each component of regional adaptation or to estimate how much regional heterogeneity is explained by each method of adaptation. However, in this section, we examine more closely one method of adaptation—residential AC—and the extent to which AC adoption can moderate the relationship between temperature and mortality. We find that differential AC adoption across climate regions is sufficient to explain their differences in mortality due to heat, but it cannot explain differential cold-related mortality. While we do not suggest that this should be interpreted as estimating the causal effect of AC, it suggests that the temperature-mortality relationship can be moderated by currently available technologies such as AC adoption.

Because we do not observe AC adoption at the ZIP code level, we impute a value for the ZIP code penetration rate by fitting a machine learning (LASSO) model of AC adoption based on housing unit characteristics including housing stock age, geography, and climate and using data from the Residential Energy Consumption Survey (RECS), the American Community Survey (ACS), and the 2010 Census. This process requires constructing a set of comparable housing characteristics in both the RECS and census data.

A.4.1 Data Sources for Air Conditioning Imputation

We begin by describing the housing characteristics we use and how we define them in terms of original RECS and census variables.

Residential Energy Consumption Survey (RECS) Data. Our data on AC are derived from the RECS, which is administered by the Energy Information Administration (EIA) and surveys a nationally representative sample of housing units in the United States across 50 states and the District of Columbia. The RECS collects information on energy consumption and energy-related characteristics of housing units, including AC. We use RECS data from survey years 1993, 1997, 2001, 2005, and 2009. We model whether a housing unit in the RECS data has AC as a function of housing-level characteristics including the housing unit type, the geographic location of the housing unit, and the climate for the location of the unit. Below we describe the specific variables used in this model and how these variables are defined in terms of the original RECS variables from each year of the survey.

1. *Air conditioning (AC).* An indicator variable for whether a household reports to have AC equipment at home. This corresponds to the RECS variable AIRCOND ("Do you have air conditioning equipment at home") in years 1993, 1997, 2001, and 2005. For year 2009, the AIRCOND survey question changed to whether AC equipment is "used." To obtain a consistent measure of AC ownership, for 2009, we instead rely on the variable DNTAC ("No air-conditioning equipment, or unused air-conditioning equipment"), which stratifies all households into three groups based on their report of AC ownership and usage status: (1) have AC equipment but do not use it, (2) have AC equipment and use it, and (3) do not have any AC equipment. We define a household unit to have AC equipment if it belongs to group (1) or (2).

2. *Year built.* A set of indicator variables (summing up to one for each household) identifying the decade when the housing unit was built (1939 or earlier, 1940 to 1949, ..., 1990 to 1999, 2000, or later). These variables are based on the RECS variable YEAR-MADE ("Year home built"), which reports the decadal interval when the home is built (mostly in early year) or the year the home is built. For each year, we group household units into decade built according to the categorization used by the 2007–2011 five-year ACS.

3. *Number of rooms.* A set of indicator variables (summing up to one for each household) identifying the number of rooms in the housing unit (one room, two rooms, ..., eight rooms, and nine or more rooms). For years 1993, 1997, and 2001, we count rooms by adding up RECS survey variables BEDROOMS ("Number of bedrooms") and OTH-ROOMS ("Number of other rooms"). We use the variable TOTROOMS ("Total number of rooms"), which is available for year 2005 and 2009. We then assign the number of rooms according to the categorization used by the 2007–2011 five-year ACS.

4. *Urban.* An indicator variable for whether the housing unit is in an urban area (i.e., nonrural area). This is based on the RECS variable UR (or URBRUR in early years). The RECS urban status information is obtained from interviewer observation (1993), household report (1997, 2001, 2005), and the Census Bureau's urban/rural geographic identifier (2009).

5. *Mobile.* An indicator variable for whether the housing unit is a mobile home. This variable is based on the RECS variable TYPEHUQ ("Type of home as report by respondent"). TYPEHUQ reports whether the housing unit is mobile, single-family detached, single-family attached, apartment in a building with two to four units, or apartment in a building with more than five units.

6. *Own.* An indicator variable for whether the housing unit is owned. This is based on the RECS variable KOWNRENT ("Housing unit owned or rented"). KOWNRENT reports whether the housing unit is owned by someone in the household, rented, or occupied without payment.

7. *CDD65.* A continuous measure of cooling degree days (CDD) of the survey year with a base temperature of 65°F (i.e., the total number of degrees the daily temperature exceeds 65°F from January to December of the survey year). We draw this information from the RECS variable CDD65 (CD65 in earlier years). RECS creates this variable using temperature monitoring data from the National Climate Data Center's weather stations. A housing unit is first matched to the closest weather station, and then CDD is computed using the station's daily temperature data from January to December of the survey year. To mask the household location, a "random error" was added to the CDD. RECS does not provide further information regarding the structure of the random error.

8. *Census region.* A set of categorical variables (summing up to one for each household) identifying the census region location of the housing unit. This variable corresponds to

the RECS variable REGIONC ("Census Region"), which includes Northeast, Midwest, South, and West Census Region.

9. *Census division.* A set of categorical variables (summing up to one for each household) identifying the census division location of the housing unit. This variable corresponds to the RECS variable DIVISION ("Census Division"). For years 1993, 1997, 2001, and 2005, DIVISION divides housing units into New England (CT, MA, ME, NH, RI, VT), Middle Atlantic (NJ, NY, PA), East North Central (IL, IN, MI, OH, WI), West North Central (AR, LA, OK, TX), South Atlantic (DC, DE, FL, GA, MD, NC, SC, VA, WV), East South Central (AL, KY, MS, TN), West South Central (AR, LA, OK, TX), Mountain (AZ, CO, ID, MT, NM, NV, UT, WY), and Pacific Census Division (AK, CA, HI, OR, WA). In 2009, the Mountain Census Region is further divided into the Mountain North Sub-Division (CO, ID, MT, UT, WY) and the Mountain South Sub-Division (AZ, NM, NV). We combine the two groups to the single Mountain Division to keep the division identifier coherent across years.

10. *Sampling weights.* The sampling weight variable NWEIGHT provided by the RECS. This variable is the sampling weight for the observation in each survey year, which is equal approximately to the inverse of the probability of selection into the sample. RECS applies a couple of adjustments to the weights, including (1) adjustments to interview nonresponse, (2) post-stratification to match total energy consumption by fuel types, and (3) benchmarking to ensure that the total RECS weights add up to the ACS's total number of occupied housing units.

Census Data. We use ZIP-code-level housing characteristics from the 2007–2011 five-year ACS and the 2010 Census to construct a set of housing characteristics comparable to that which was used to predict AC using the LASSO model fit to the RECS data, described above. We obtain census data provided by the Minnesota Population Center (2016) through the National Historical Geographic Information System NHGIS16, and the variable names we refer to below are from the NHGIS.

1. *Year built.* Eight variables, each measuring the fraction of housing units that were built in 1939 or earlier, 1940 to 1949, ..., 1990 to 1999, and 2000 or later. We create these variables from the ACS variable "Year Structure Built," which counts total number of housing units built in each of the decadal intervals listed above. We convert counts to fractions by dividing the total number of housing units in the ZIP code.

2. *Number of rooms.* Nine variables, each measuring the fraction of housing units that have one room, two rooms, ..., eight rooms, and nine or more rooms. These variables are based on the ACS variable "Rooms." We convert counts to fractions by dividing the total number of housing units in the ZIP code.

3. *Urban.* Fraction of urban population from 2010 Census data. We divide the urban population in the ZIP code by the total population.

4. *Mobile.* Fraction of housing units that are mobile homes. We base this on the ACS variable "Units in Structure." which provides the number of mobile homes in the ZIP code, and we divide counts by the total number of housing units in the ZIP code.

5. *Own.* Fraction of occupied housing units that are owned. We draw this information from the ACS variable "Tenure by Household Size." We divide the number of owner-occupied housing units by the total number of occupied housing units in the ZIP code.

6. *CDD65.* Cooling degree days for the ZIP code, obtained from NOAA Climate Normals over the period 1980–2010 using inverse distance weighting of all monitors within a 20-mile radius of the ZIP code centroid.

7. *Census region.* A set of categorical variables (summing up to one for each ZIP code) identifying the census region of the ZIP code centroid. We use the U.S. Census Bureau's standard definition of census regions.

8. *Census division.* A set of categorical variables (summing up to one for each ZIP code) identifying the census division of the ZIP code centroid. We use the U.S. Census Bureau's standard definition of census divisions.

A.4.2 Air Conditioning Imputation Procedure

We use the housing characteristics from the RECS and 2010 Census described above to estimate a model of AC as a function of the location and characteristics of housing units. Specifically, we estimate a housing-unit-level regression of whether the housing unit has AC equipment as a flexible function of CDD (a fourth-order polynomial) in the housing unit location, year built, number of rooms, urban location, mobile home status, and ownership status. We interact each of these housing characteristics with dummies for Census Region and Census Division. To avoid overfitting, we use LASSO penalized regression and select the penalty to minimize ten-fold cross-validated mean squared prediction error. We then apply this model to ZIP-code-level housing characteristics from the 2010 Census to compute predicted AC penetration for each U.S. ZIP code.

A potential cause of concern is that including local climate to predict local AC penetration could generate an artificial relationship between the mortality effects of temperature and AC adoption rates. While this could be an issue, empirically, AC adoption depends strongly on climate. As a result, omitting climate from the set of AC predictors introduces the possibility of systematic bias in the imputed AC measure that is correlated with climate. Because of this, our preferred imputation procedure includes local climate in the set of predictors. However, we also include results for an alternate imputation procedure that omits local climate variables.

A.4.3 Air Conditioning Results and Discussion

To estimate how temperature effects vary by AC penetration, we interact the imputed value of AC penetration (which is continuous between zero and one) with the temperature bins in equation 1. We also include in this regression Census Region by temperature bin fixed

effects. Appendix figure B.12a, panel A, presents these regression results for three-day mortality outcomes. The curve represents the regression coefficients on the interaction between the AC penetration variable and the specified temperature bin. The interaction effects are significantly negative for temperatures above 70°F. For example, the coefficient on the interaction between AC penetration and the 80°F–85°F temperature bin is around −5, which implies that each 10 percentage point increase in AC penetration corresponds to 0.5 fewer deaths per 100,000 individuals on an 80°F–85°F day. At hotter temperatures, the AC effect is even stronger: for example, the coefficient on the +95°F day bin implies about 1.8 fewer deaths per 100,000 for each 10 percentage point increase in AC penetration. By contrast, for temperatures below about 65°F, the interactions between AC and temperature tend to be quite small, indicating that the mortality effect of cold days is largely independent of the level of AC penetration.

Using these estimates as a linear estimate of the impact of AC adoption on mortality within each temperature bin, we calculate how much of the difference in heat sensitivity across regions can be explained by differences in AC penetration. Over the sample, AC penetration was 93.2% in the warmest ZIP codes, 82.1% in the middle third of ZIP codes, and 63.2% in the coolest. Panels B and C of appendix figure B.12a present counterfactual simulations, where we compute what the mortality curve would have been if the warmest ZIP codes had the AC penetration rates of the other two terciles, respectively. Thus, Panel B estimates what the temperature-mortality relationship would be in the warmest third of ZIP codes if the AC penetration rate in those ZIP codes were 30 percentage points lower than it actually is, as is the case in the coolest ZIP codes. The counterfactual warmest ZIP code curve closely tracks, and even rises, above the actual curve for the coolest ZIP codes at temperatures above 65°F–70°F, suggesting that differences in AC penetration can more than explain the differences in heat-related mortality between the warmest and coolest regions.[2]

At the same time, differences in AC penetration exacerbate the differences between the regions on cold days, consistent with AC as the mechanism driving the regional differences in heat-related mortality only. Panel C repeats this exercise, this time comparing a counterfactual where the warmest ZIP codes are adjusted for the approximately 11 percentage point difference in AC between the warmest and middle terciles. Once again, the counterfactual warmest tercile aligns closely with, but is slightly larger than, the middle tercile on hot days, again suggesting that differences in AC penetration account for a substantial portion of the estimated difference between the regions.[3]

These results extend the finding from Barreca et al. (2016) that increases in AC adoption over time can explain a substantial share of the reduction in heat-related mortality in the United States over the past century.[4] Our results show that in addition to explaining the reduction in heat-related mortality in the time-series, AC adoption can explain much of the cross-sectional differences in heat-related deaths observed across U.S. climate regions. These counterfactual exercises provide some support for the idea that the heterogeneity

---

[2]If the impact of AC adoption on heat sensitivity is concave, that could explain why our projections using a linear estimate are too large.

[3]Appendix figure B.12b reproduces the analysis using the alternative AC imputation procedure that excludes local climate variables. The results are very similar to those from the primary imputation procedure.

[4]Additionally, our results complement those of observational studies in the public health literature (e.g., Rogot, Sorlie and Backlund (1992)), which show that AC reduces the mortality impact of hot days.

in temperature effects across climate regions we observe is driven by adaptation, and in particular AC, rather than by immutable regional characteristics. Thus, we might expect places to engage in this and other types of adaptive behavior in response to warming.

Appendix B: Additional Figures and Tables

Figure B.1: Comparison of Medicare and Census Elderly Population and Mortality Rates
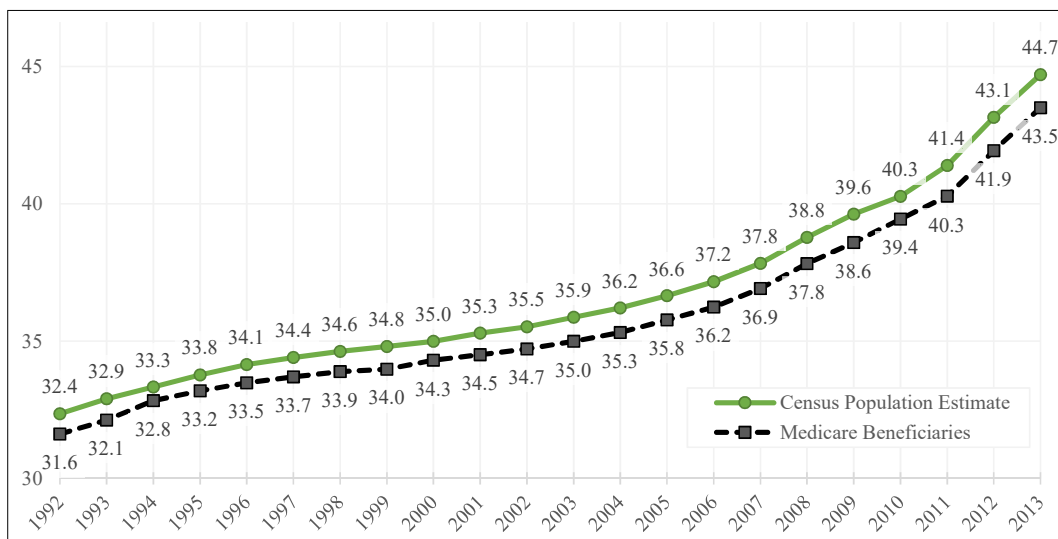
(a) Population (millions)
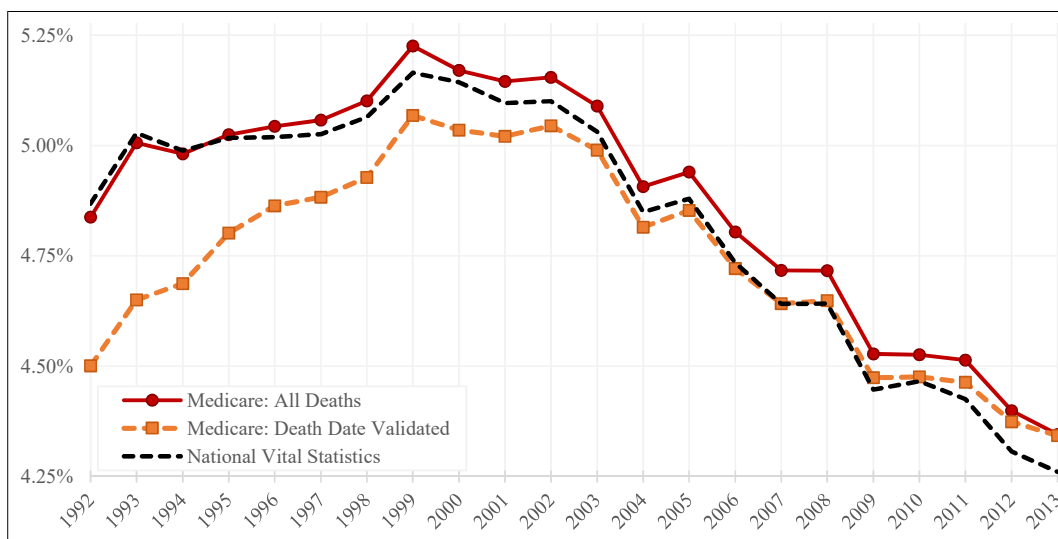
(b) Annual Mortality Rate

Panel (a): Census population estimates for the 50 United States and the District of Columbia come from the Compressed Mortality Files (CMF) 1979–1998 and 1999–2016. The population figures shown are April 1 Census counts in 2000 and 2010 and July 1 resident population estimates in other years. Medicare population counts include all beneficiaries in the annual Medicare enrollment file who were age 65 and over as of July 1 and had a U.S. ZIP code of residence in the 50 states or the District of Columbia.

Panel (b): National Vital Statistics mortality data come from the CMF described in Panel (a). National Vital Statistics mortality rates are calculated by dividing total CMF deaths among the 65 and over population in a given year by the Census population estimates shown in Panel (a). The dashed lines report annual mortality rates based on death dates recorded in the Medicare annual enrollment files. The figure reports both the total mortality rate in the Medicare sample ("Medicare: All Deaths"), as well as the mortality rate among the analytical sample used in the paper ("Medicare: Death Date Validated"), which excludes individuals who have a validated death that year but do not have a validated death *date* flag.

Figure B.2: U.S. Climate Normals: Cooling Degree Days
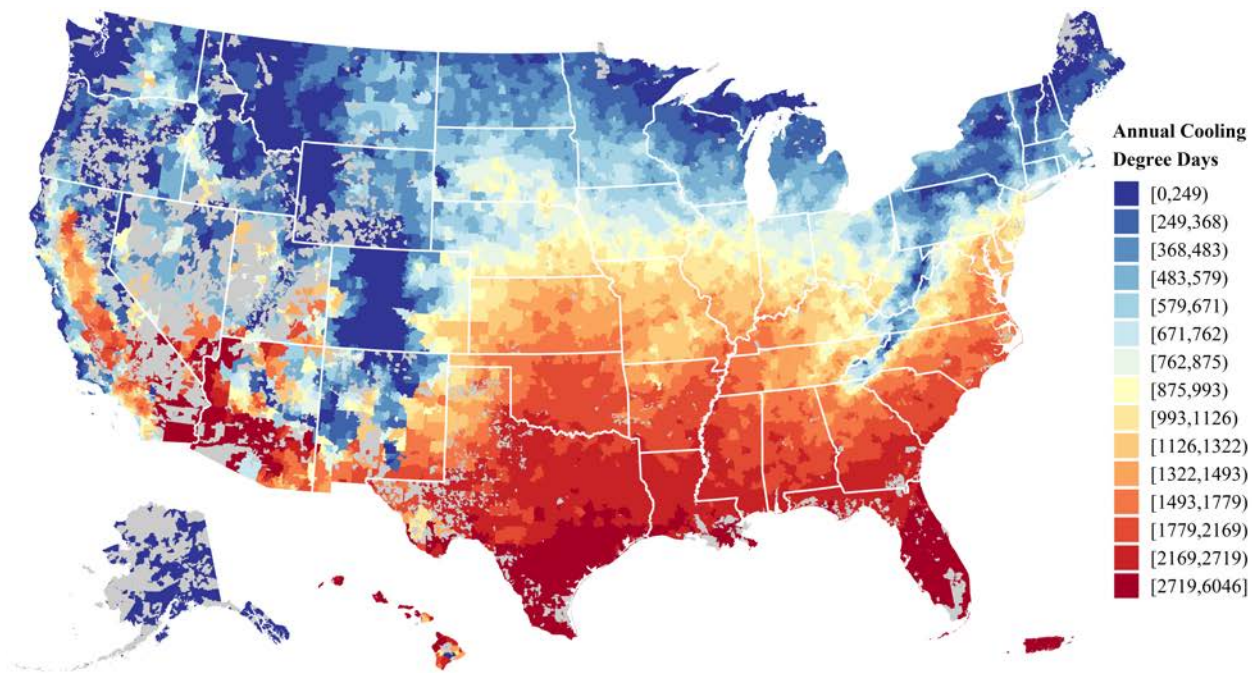
Notes: The figure shows the 1981–2010 cooling degree days (CDD) Climate Normals for the 2010 Census ZCTAs ($N = 33,120$). CDD Normals are available for 7,501 U.S. stations operated by the National Oceanic and Atmospheric Administration's National Weather Service. ZCTA Climate Normals are calculated as the inverse distance-weighted average of Normals at the nearest station and any other stations within a 20 mile radius of the ZCTA centroid. Gray regions represent parts of the U.S. that are not covered by a ZCTA.

Figure B.3: U.S. Daily Temperature Distribution (PRISM)
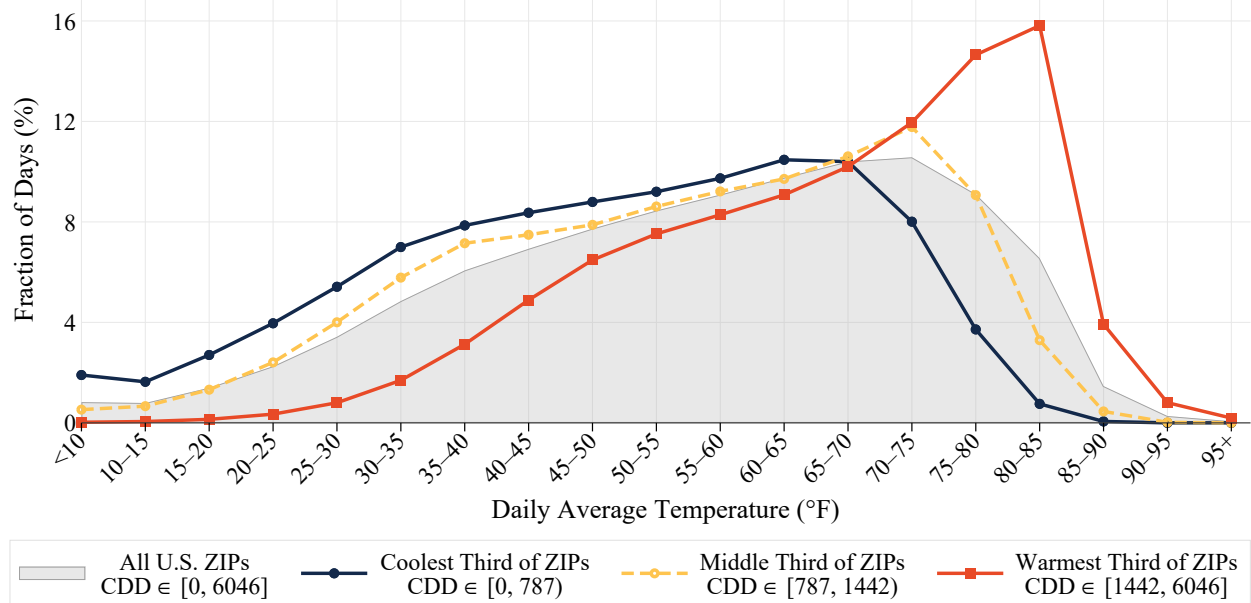
Notes: This figure summarizes the distribution of daily average temperature in the United States from 1992–2013. Distributions are reported separately for all U.S. ZIP codes and for the coolest, middle, and warmest population-weighted thirds of ZIP codes based on cooling degree days (CDD) Climate Normals. Daily temperature data come from the PRISM daily dataset and cover only the conterminous U.S. Appendix Tables B.1c–B.1d report numerical values of the points in this figure. For comparison to daily temperature for the entire U.S. based on GHCN land station monitor data, see Figure 1.

Figure B.4: Longer-Run Effects of Temperature on Mortality
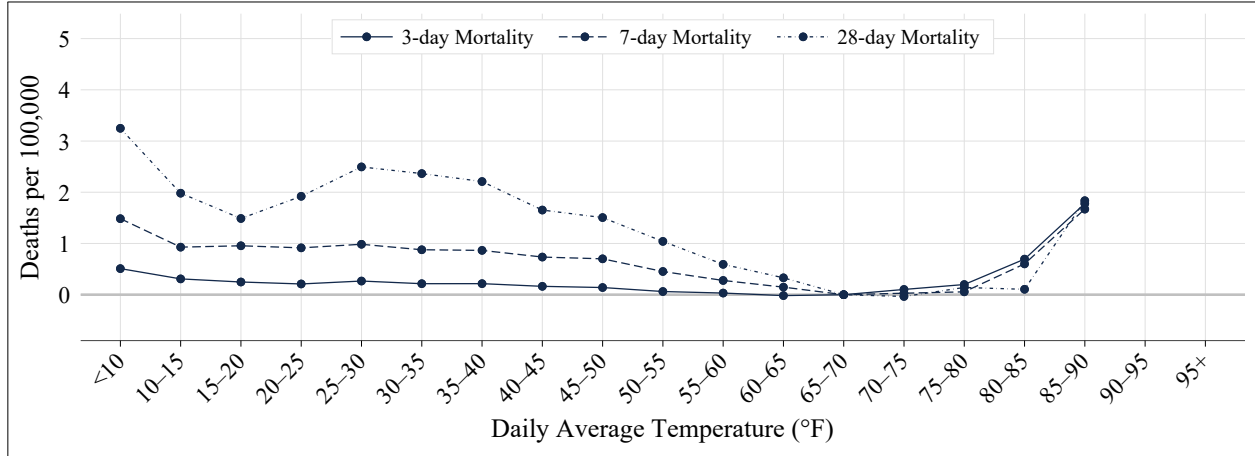
(a) Coolest Third of Regions
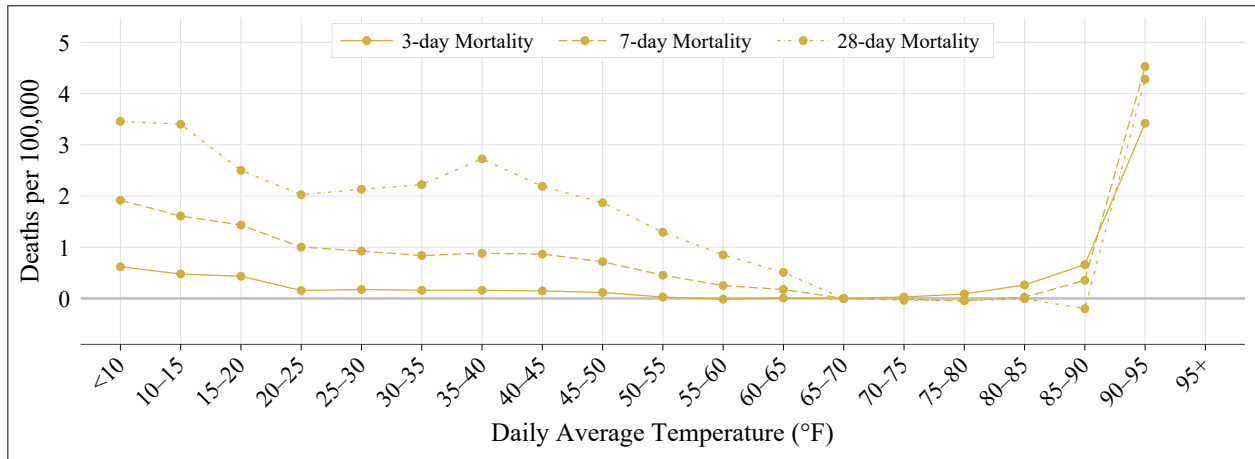
(b) Middle Third of Regions
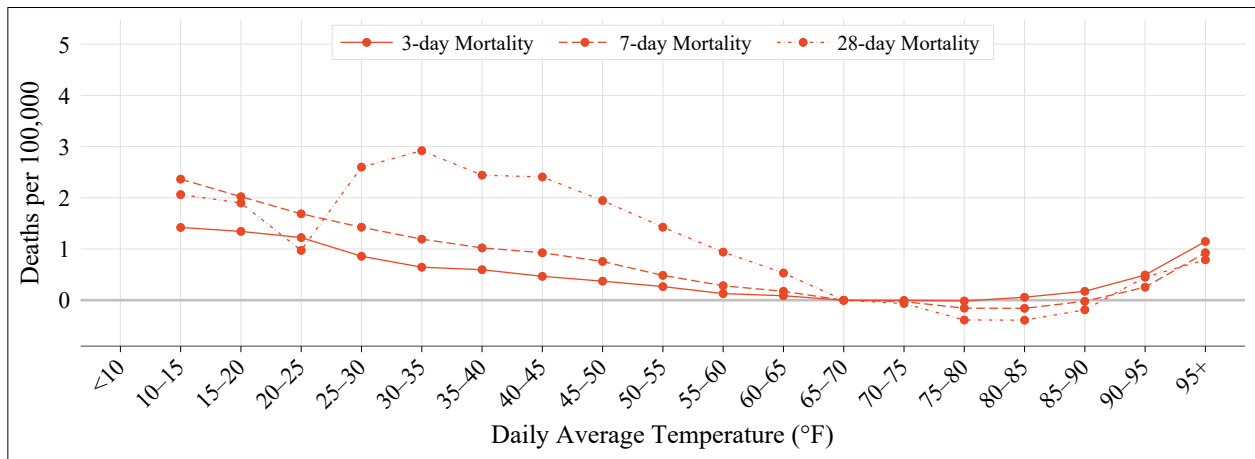
(c) Warmest Third of Regions

Notes: This figure presents coefficients from separate regressions for each of three outcome variables: 3-day, 7-day, and 28-day mortality. For all outcomes, the regression specification is that of Equation 1, but with temperature leads expanded to included average temperature in the 6 and 27 days following the event day.

Figure B.5: Effect of Temperature on Mortality (PRISM)

(a) Climate-Specific Temperature Effects

(b) Homogeneous Temperature Effects
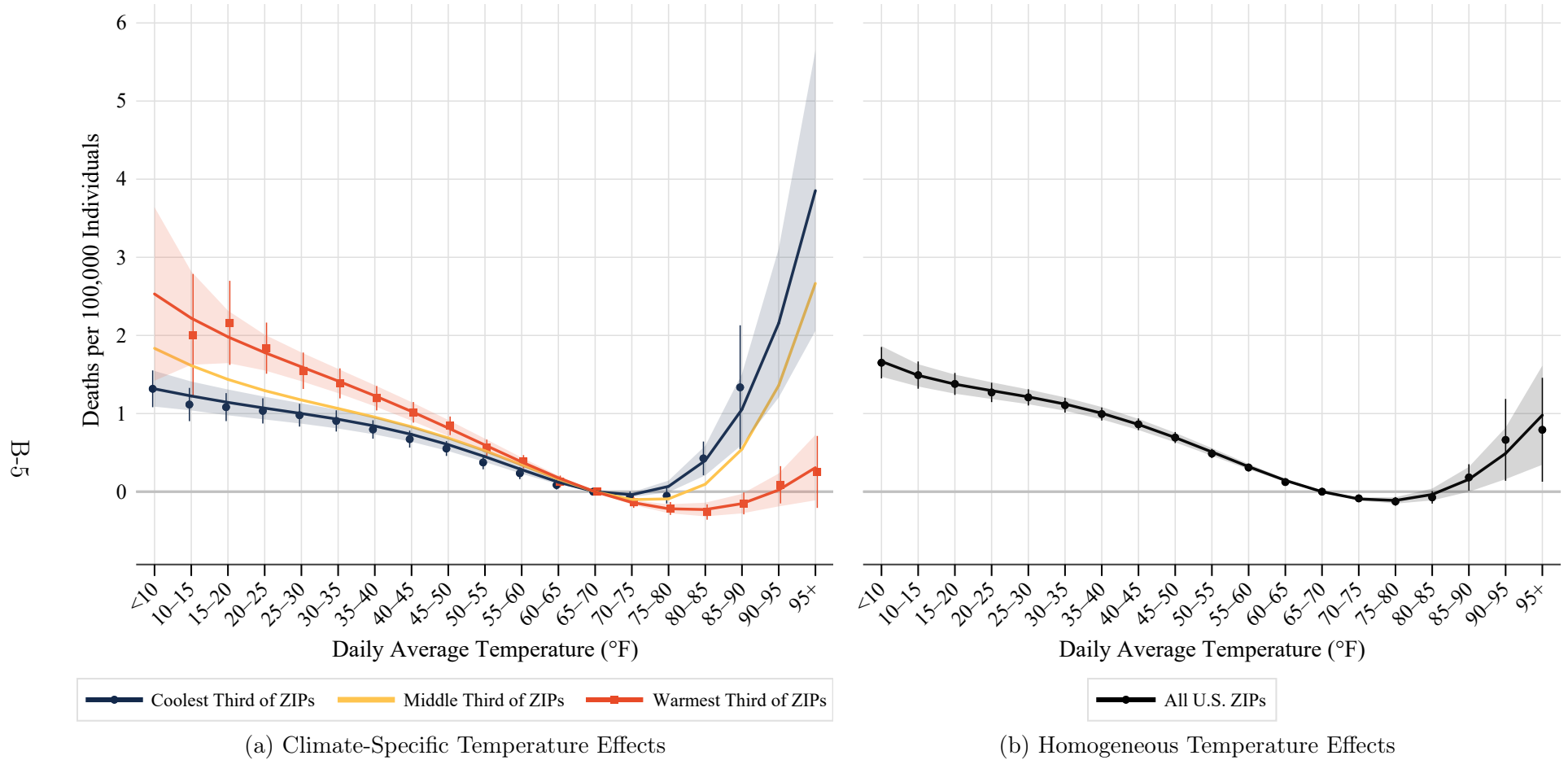
Notes: This figure is analogous to Figure 2 but plots estimated 3-day mortality effects of temperature as measured by PRISM data. In Panel (a), effects are allowed to differ by the coolest, middle, or warmest third of ZIP codes as defined in Figure 1. In Panel (b), effects are restricted to be common to all U.S. ZIP codes. Effects reflect excess mortality on a day with a given average temperature relative to a day with an average temperature of 65°F–70°F. Markers with whisker lines plot non-parametric temperature bin estimates and associated 95 percent confidence intervals. Markers are only shown for binned temperatures that occur with a frequency of at least one day per decade in the climate region. Solid lines and shaded regions plot semi-parametric (5th degree polynomial in the temperature bins) estimates and associated 95 percent confidence intervals. Confidence intervals are based on two-way clustered standard errors at the county and state×date levels. Numerical values for all point estimates and standard errors are reported Appendix Tables B.1c–B.1d.

Figure B.6: Predicted Climate Change, 2080–2099 versus current
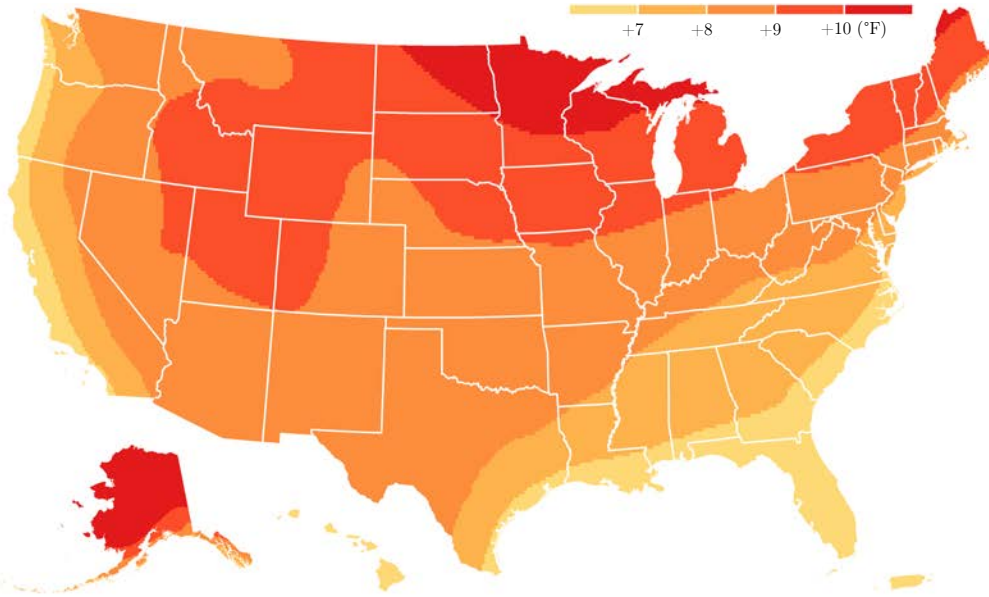
(a) Change in Average Temperature
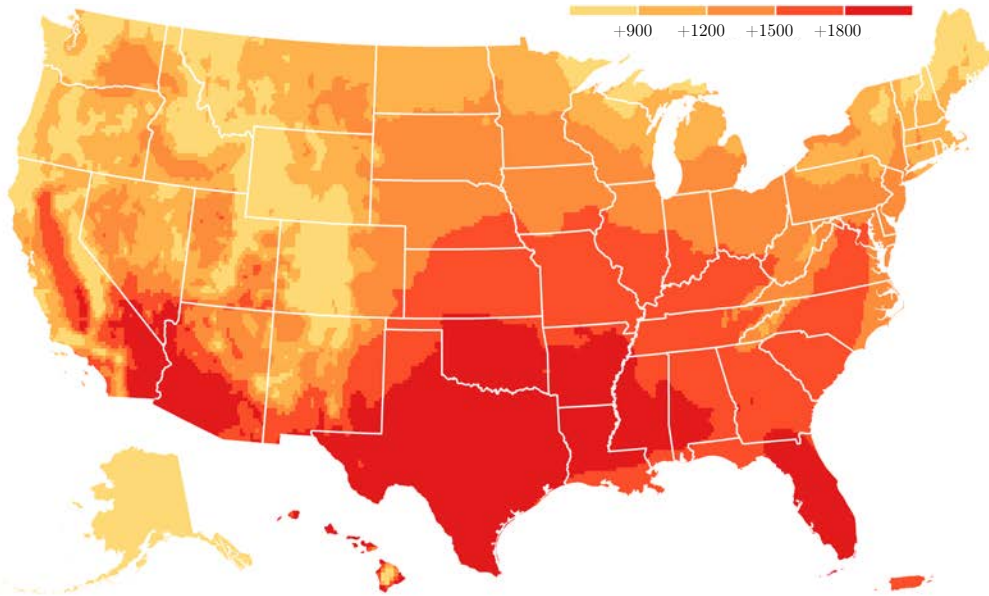
(b) Change in Annual Cooling Degree Days

Notes: The map shows projected end-of-century (2080–2099) changes in average temperature (panel (a))
and annual cooling degree days based on the meta-model, an average of the 21 NEX-GDDP climate models,
under the RCP8.5 emissions scenario. The map is shown at the resolution of the downscaled climate model
output, which is produced on a 25km by 25km grid (0.25 degree spatial resolution).

Figure B.7: Parametric versus Nonparametric Effects of Temperature
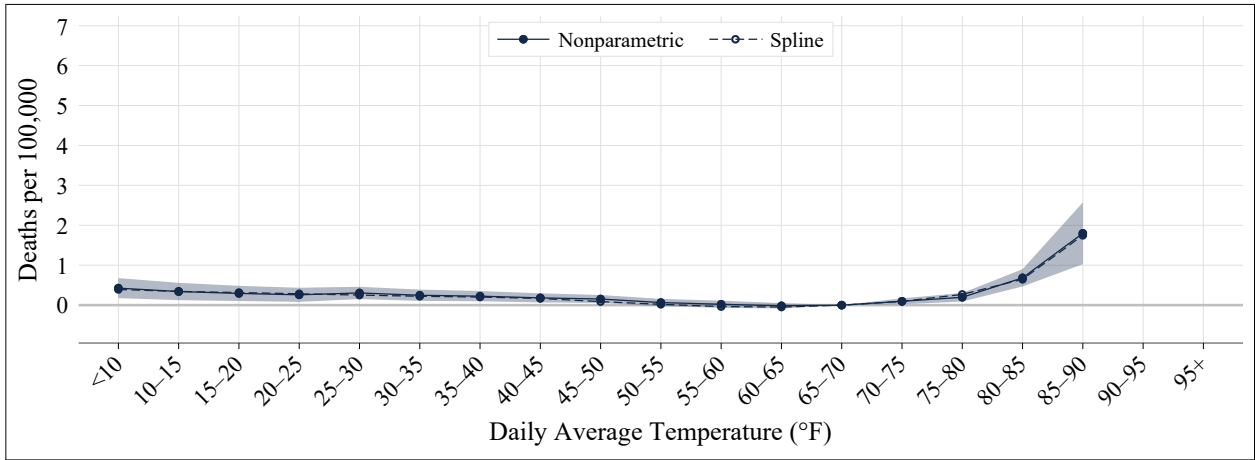
(a) Coolest Third of Regions
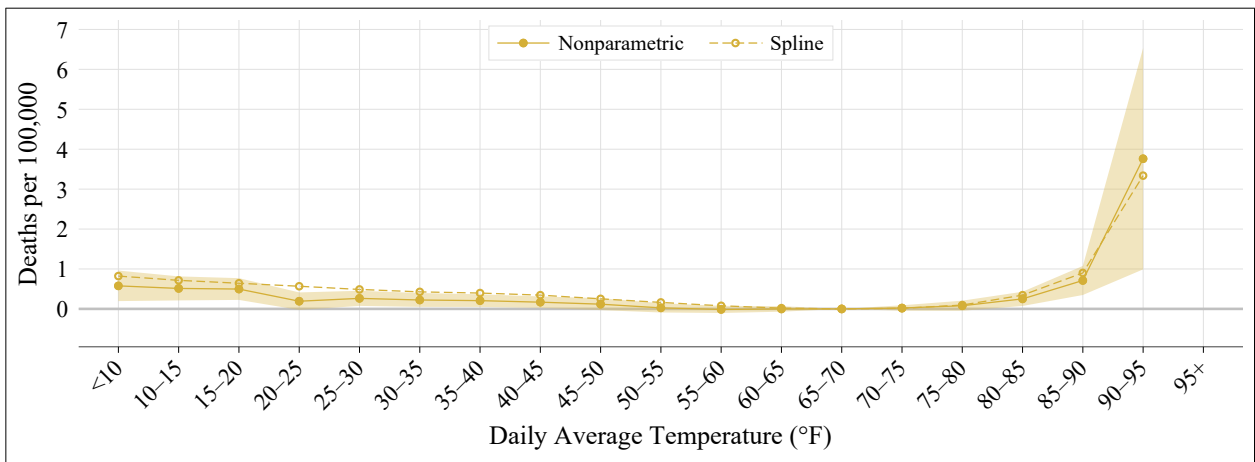
(b) Middle Third of Regions
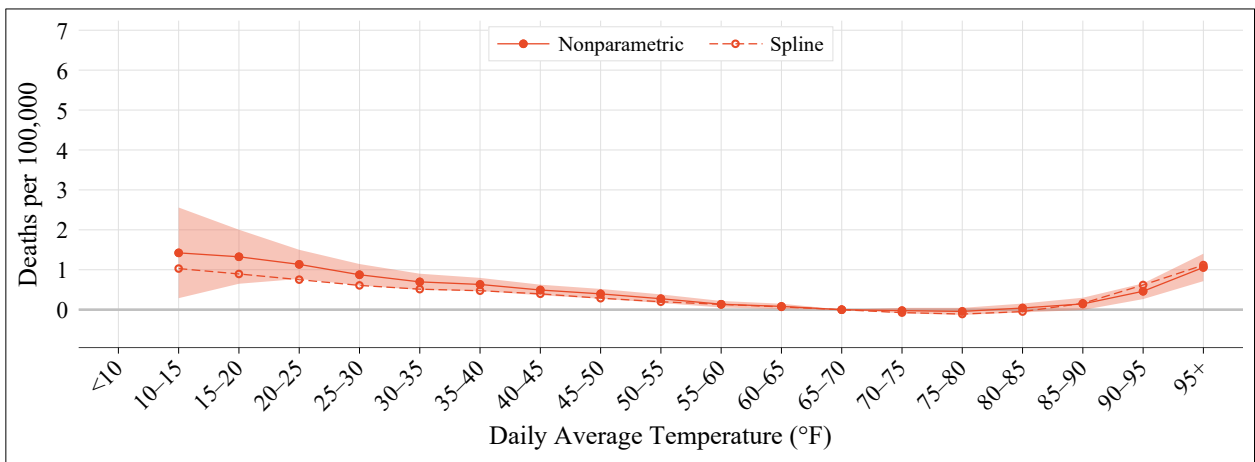
(c) Warmest Third of Regions

Notes: This figure summarizes how the estimated semi-parametric function of temperature and climate $f(t, CDD)$ performs relative to the nonparametric estimates of temperature effects by climate tercile reported in Figure 2a. The "spline" estimates plotted with hollow markers come from re-estimating Equation (1) but with the fitted mortality values $\hat{f}(t, CDD)$ as the outcome and controlling only for temperature bin indicators. For comparison, the nonparametric estimates and corresponding 95 percent confidence intervals are plotted with solid markers and shaded area, respectively.

Figure B.8: Estimated Temperature Effects for Select ZIP Codes
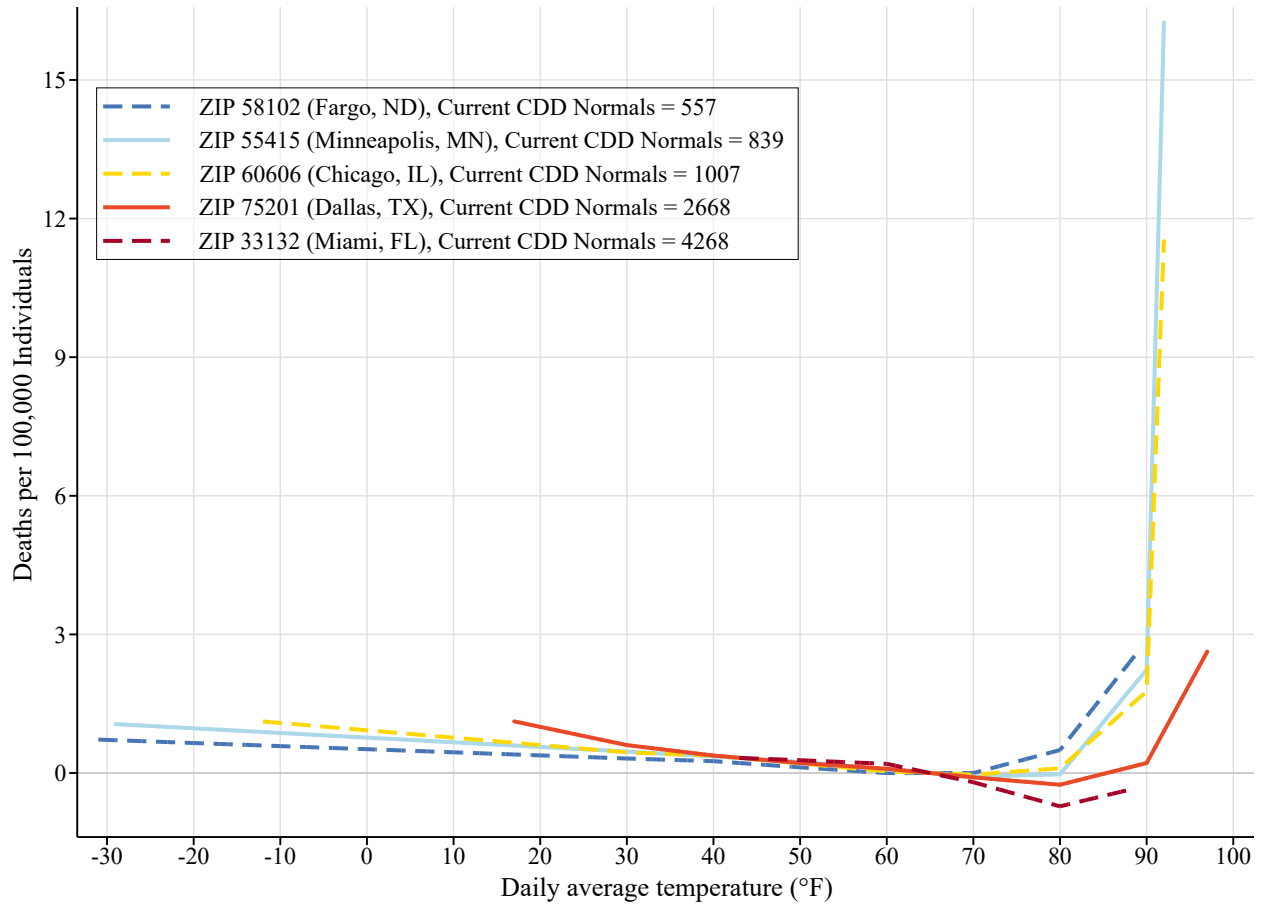
Notes: This figure illustrates estimates of the parametric spline $f(t, CDD)$ from Equation 3 by plotting the fitted temperature-mortality relationship for a selection of ZIP codes. For each ZIP code, $\hat{f}(t, CDD)$ is evaluated at the ZIP code's current CDD Normal and at all temperatures in the support of realized average daily temperatures for the ZIP code in the sample period 1992–2013.

Figure B.9a: Weighted Meta Model: End-of-Century Climate Change Effects (RCP 8.5)

(a) Homogeneous Effects, No Adaptation

(b) Current Climate Effects, No Adaptation

(c) Current Climate Effects, Future Adaptation

Notes: The figure summarizes annual mortality effects of end-of-century (2080–2099) climate change relative to the current period (1992–2013) under the RCP 8.5 emissions scenario, as predicted by the weighted-meta-NEX-GDDP model. Observations are at the ZIP code level and are grouped by current climate (CDD). Box and whisker plots summarize the distribution of climate change effects across ZIP codes in each climate range. Boxes stretch from the 25th percentile (lower hinge) to the 75th percentile (upper hinge). The median is plotted as a line across the box. Whiskers stretch from the 5th percentile to the 95th percentile. Statistics are weighted by the elderly Medicare population in each ZIP code.

Figure B.9b: Unweighted Meta Model: End-of-Century Climate Change Effects (RCP 8.5)
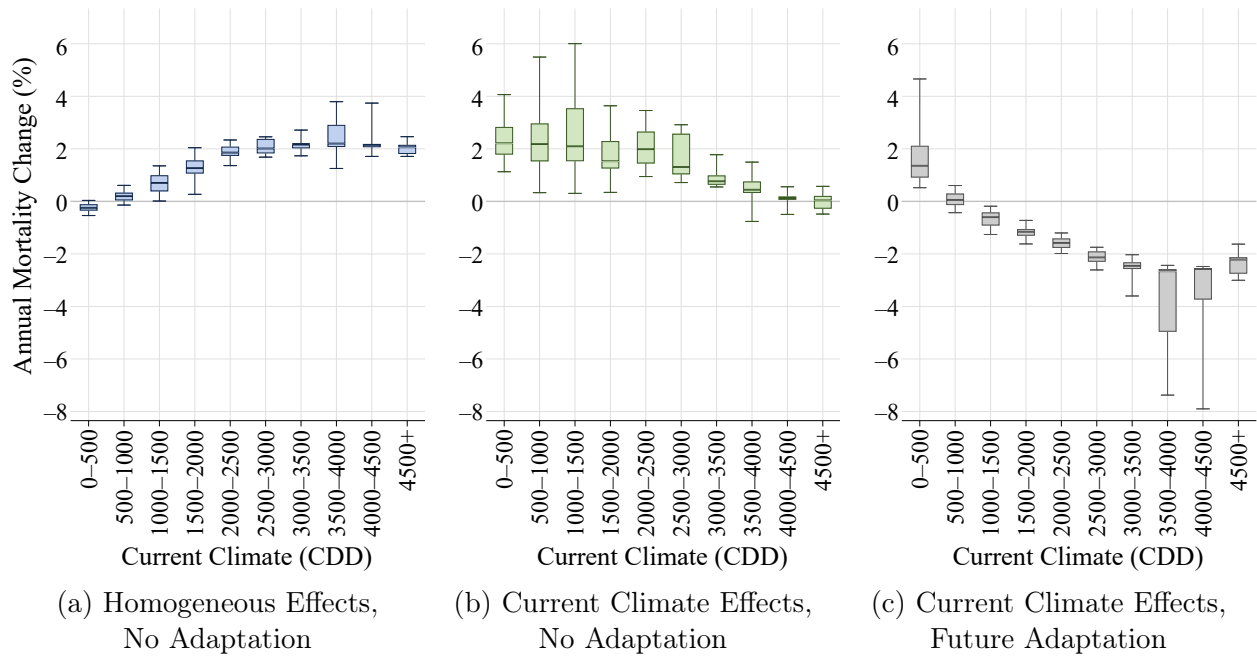
(a) Homogeneous Effects,
No Adaptation

(b) Current Climate Effects,
No Adaptation

(c) Current Climate Effects,
Future Adaptation

Notes: The figure summarizes annual mortality effects of end-of-century (2080–2099) climate change relative to the current period (1992–2013) under the RCP 8.5 emissions scenario, as predicted by the meta-NEX-GDDP model. Box and whisker plots summarize ZIP code-level effects by current climate. Additional notes in Appendix Figure B.9a.

Figure B.9c: ACCESS1-0: End-of-Century Climate Change Effects (RCP 8.5)

(a) Homogeneous Effects,
No Adaptation

(b) Current Climate Effects,
No Adaptation

(c) Current Climate Effects,
Future Adaptation

Notes: The figure summarizes annual mortality effects of end-of-century (2080–2099) climate change relative to the current period (1992–2013) under the RCP 8.5 emissions scenario, as predicted by the ACCESS1-0 model. Box and whisker plots summarize ZIP code-level effects by current climate. Additional notes in Appendix Figure B.9a.

Figure B.9d: BNU-ESM: End-of-Century Climate Change Effects (RCP 8.5)

(a) Homogeneous Effects,
No Adaptation

(b) Current Climate Effects,
No Adaptation

(c) Current Climate Effects,
Future Adaptation

Notes: The figure summarizes annual mortality effects of end-of-century (2080–2099) climate change relative to the current period (1992–2013) under the RCP 8.5 emissions scenario, as predicted by the BNU-ESM model. Box and whisker plots summarize ZIP code-level effects by current climate. Additional notes in Appendix Figure B.9a.

Figure B.9e: CCSM4: End-of-Century Climate Change Effects (RCP 8.5)

(a) Homogeneous Effects,
No Adaptation

(b) Current Climate Effects,
No Adaptation

(c) Current Climate Effects,
Future Adaptation

Notes: The figure summarizes annual mortality effects of end-of-century (2080–2099) climate change relative to the current period (1992–2013) under the RCP 8.5 emissions scenario, as predicted by the CCSM4 model. Box and whisker plots summarize ZIP code-level effects by current climate. Additional notes in Appendix Figure B.9a.

Figure B.9f: CESM1-BGC: End-of-Century Climate Change Effects (RCP 8.5)

(a) Homogeneous Effects, No Adaptation

(b) Current Climate Effects, No Adaptation

(c) Current Climate Effects, Future Adaptation

Notes: The figure summarizes annual mortality effects of end-of-century (2080–2099) climate change relative to the current period (1992–2013) under the RCP 8.5 emissions scenario, as predicted by the CESM1-BGC model. Box and whisker plots summarize ZIP code-level effects by current climate. Additional notes in Appendix Figure B.9a.

Figure B.9g: CNRM-CM5: End-of-Century Climate Change Effects (RCP 8.5)

(a) Homogeneous Effects, No Adaptation

(b) Current Climate Effects, No Adaptation

(c) Current Climate Effects, Future Adaptation

Notes: The figure summarizes annual mortality effects of end-of-century (2080–2099) climate change relative to the current period (1992–2013) under the RCP 8.5 emissions scenario, as predicted by the CNRM-CM5 model. Box and whisker plots summarize ZIP code-level effects by current climate. Additional notes in Appendix Figure B.9a.

Figure B.9h: CSIRO-Mk3-6-0: End-of-Century Climate Change Effects (RCP 8.5)

(a) Homogeneous Effects, No Adaptation

(b) Current Climate Effects, No Adaptation

(c) Current Climate Effects, Future Adaptation

Notes: The figure summarizes annual mortality effects of end-of-century (2080–2099) climate change relative to the current period (1992–2013) under the RCP 8.5 emissions scenario, as predicted by the CSIRO-Mk3-6-0 model. Box and whisker plots summarize ZIP code-level effects by current climate. Additional notes in Appendix Figure B.9a.

Figure B.9i: CanESM2: End-of-Century Climate Change Effects (RCP 8.5)

(a) Homogeneous Effects, No Adaptation

(b) Current Climate Effects, No Adaptation

(c) Current Climate Effects, Future Adaptation

Notes: The figure summarizes annual mortality effects of end-of-century (2080–2099) climate change relative to the current period (1992–2013) under the RCP 8.5 emissions scenario, as predicted by the CanESM2 model. Box and whisker plots summarize ZIP code-level effects by current climate. Additional notes in Appendix Figure B.9a.

Figure B.9j: GFDL-CM3: End-of-Century Climate Change Effects (RCP 8.5)

(a) Homogeneous Effects,
No Adaptation

(b) Current Climate Effects,
No Adaptation

(c) Current Climate Effects,
Future Adaptation

Notes: The figure summarizes annual mortality effects of end-of-century (2080–2099) climate change relative to the current period (1992–2013) under the RCP 8.5 emissions scenario, as predicted by the GFDL-CM3 model. Box and whisker plots summarize ZIP code-level effects by current climate. Additional notes in Appendix Figure B.9a.

Figure B.9k: GFDL-ESM2G: End-of-Century Climate Change Effects (RCP 8.5)

(a) Homogeneous Effects,
No Adaptation

(b) Current Climate Effects,
No Adaptation

(c) Current Climate Effects,
Future Adaptation

Notes: The figure summarizes annual mortality effects of end-of-century (2080–2099) climate change relative to the current period (1992–2013) under the RCP 8.5 emissions scenario, as predicted by the GFDL-ESM2G model. Box and whisker plots summarize ZIP code-level effects by current climate. Additional notes in Appendix Figure B.9a.

Figure B.9l: GFDL-ESM2M: End-of-Century Climate Change Effects (RCP 8.5)

(a) Homogeneous Effects, No Adaptation

(b) Current Climate Effects, No Adaptation

(c) Current Climate Effects, Future Adaptation

Notes: The figure summarizes annual mortality effects of end-of-century (2080–2099) climate change relative to the current period (1992–2013) under the RCP 8.5 emissions scenario, as predicted by the GFDL-ESM2M model. Box and whisker plots summarize ZIP code-level effects by current climate. Additional notes in Appendix Figure B.9a.

Figure B.9m: IPSL-CM5A-LR: End-of-Century Climate Change Effects (RCP 8.5)

(a) Homogeneous Effects, No Adaptation

(b) Current Climate Effects, No Adaptation

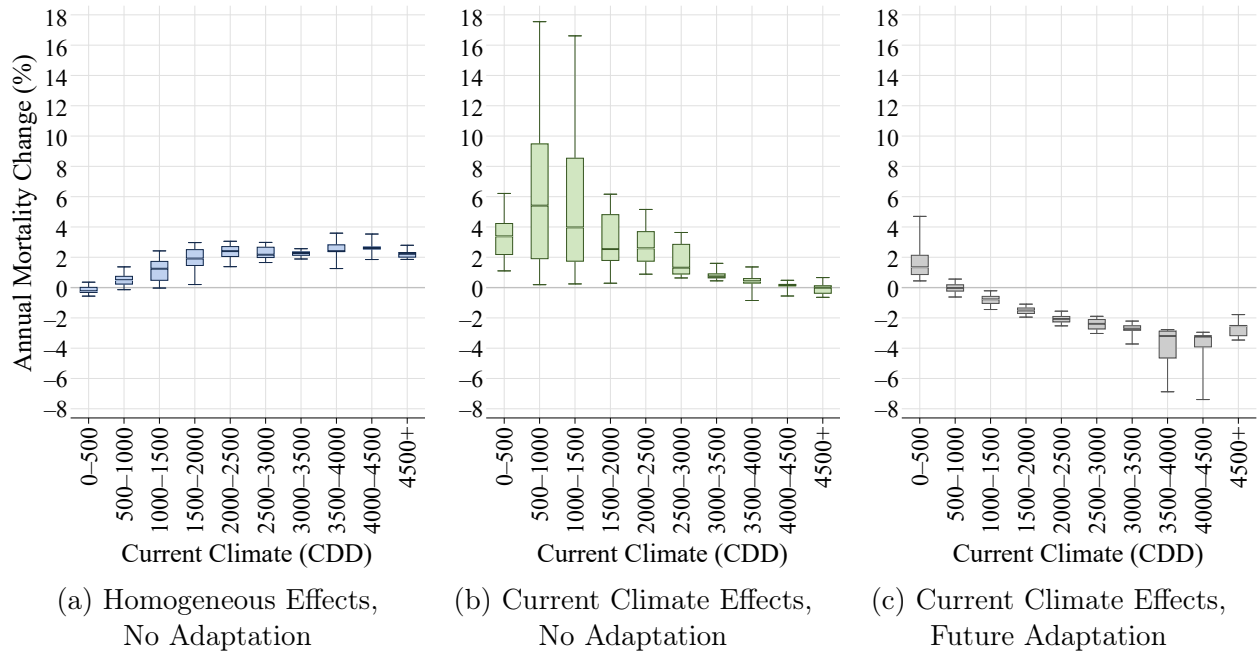(c) Current Climate Effects, Future Adaptation

Notes: The figure summarizes annual mortality effects of end-of-century (2080–2099) climate change relative to the current period (1992–2013) under the RCP 8.5 emissions scenario, as predicted by the IPSL-CM5A-LR model. Box and whisker plots summarize ZIP code-level effects by current climate. Additional notes in Appendix Figure B.9a.

B-15

Figure B.9n: IPSL-CM5A-MR: End-of-Century Climate Change Effects (RCP 8.5)

(a) Homogeneous Effects, No Adaptation

(b) Current Climate Effects, No Adaptation

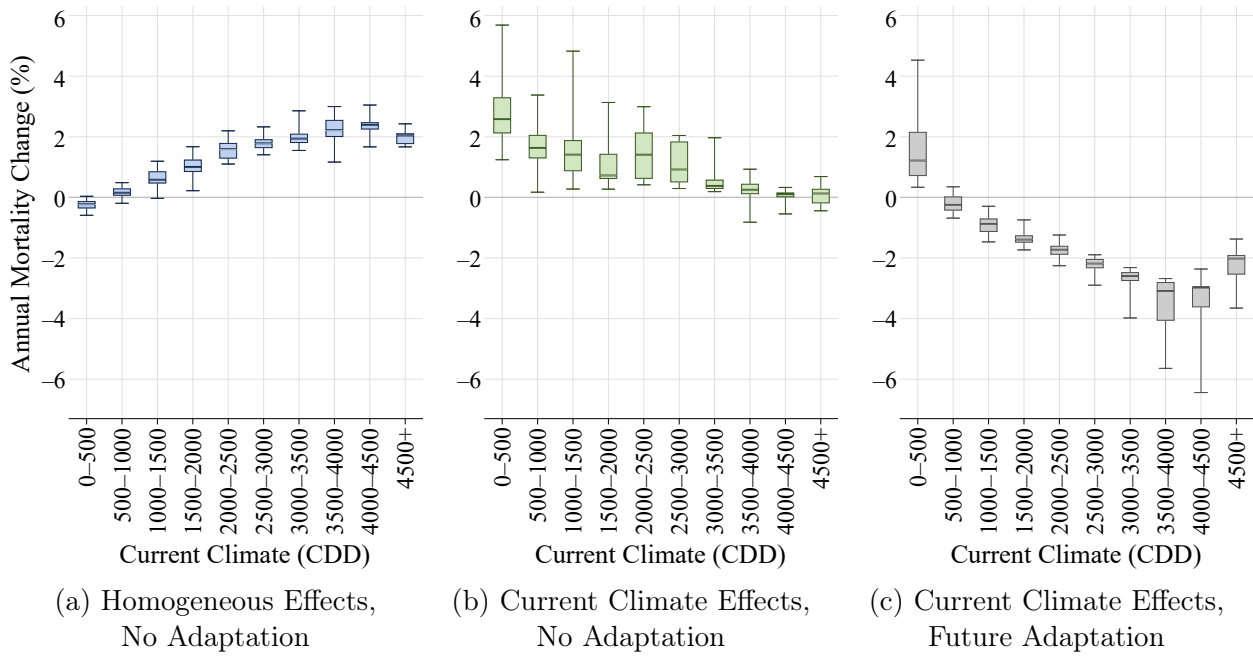(c) Current Climate Effects, Future Adaptation

Notes: The figure summarizes annual mortality effects of end-of-century (2080–2099) climate change relative to the current period (1992–2013) under the RCP 8.5 emissions scenario, as predicted by the IPSL-CM5A-MR model. Box and whisker plots summarize ZIP code-level effects by current climate. Additional notes in Appendix Figure B.9a.

Figure B.9o: MIROC-ESM: End-of-Century Climate Change Effects (RCP 8.5)

(a) Homogeneous Effects, No Adaptation

(b) Current Climate Effects, No Adaptation

(c) Current Climate Effects, Future Adaptation

Notes: The figure summarizes annual mortality effects of end-of-century (2080–2099) climate change relative to the current period (1992–2013) under the RCP 8.5 emissions scenario, as predicted by the MIROC-ESM model. Box and whisker plots summarize ZIP code-level effects by current climate. Additional notes in Appendix Figure B.9a.

Figure B.9p: MIROC-ESM-CHEM: End-of-Century Climate Change Effects (RCP 8.5)

(a) Homogeneous Effects,
No Adaptation

(b) Current Climate Effects,
No Adaptation
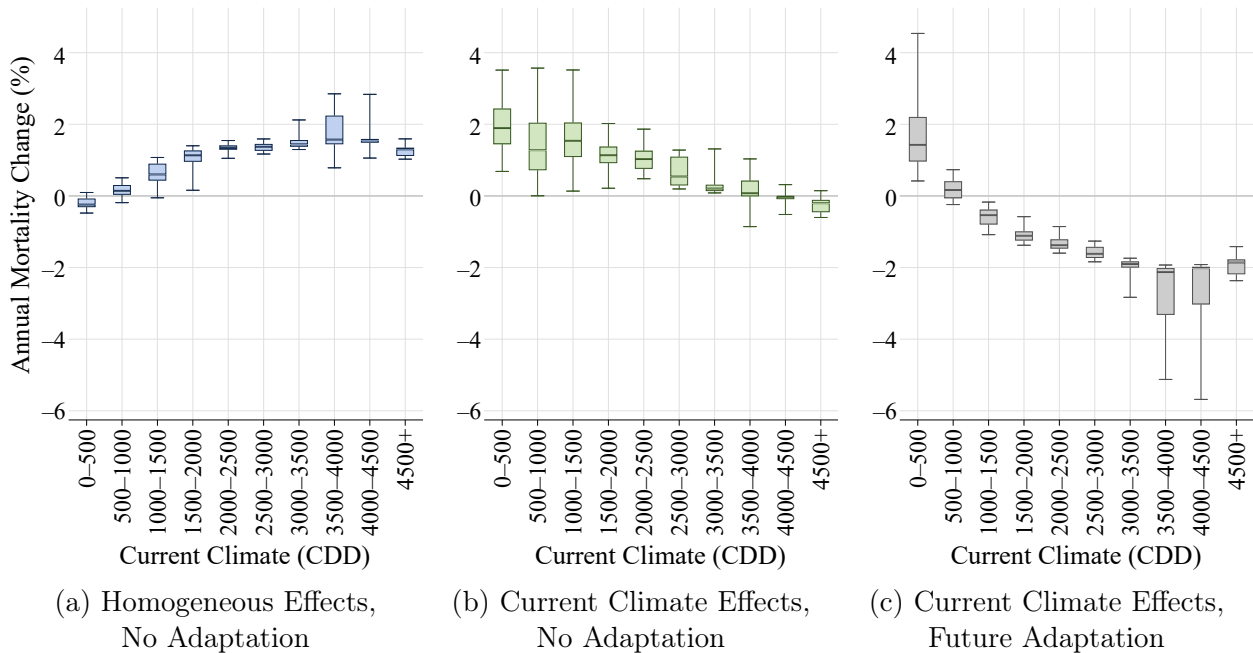
(c) Current Climate Effects,
Future Adaptation

Notes: The figure summarizes annual mortality effects of end-of-century (2080–2099) climate change relative to the current period (1992–2013) under the RCP 8.5 emissions scenario, as predicted by the MIROC-ESM-CHEM model. Box and whisker plots summarize ZIP code-level effects by current climate. Additional notes in Appendix Figure B.9a.

Figure B.9q: MIROC5: End-of-Century Climate Change Effects (RCP 8.5)
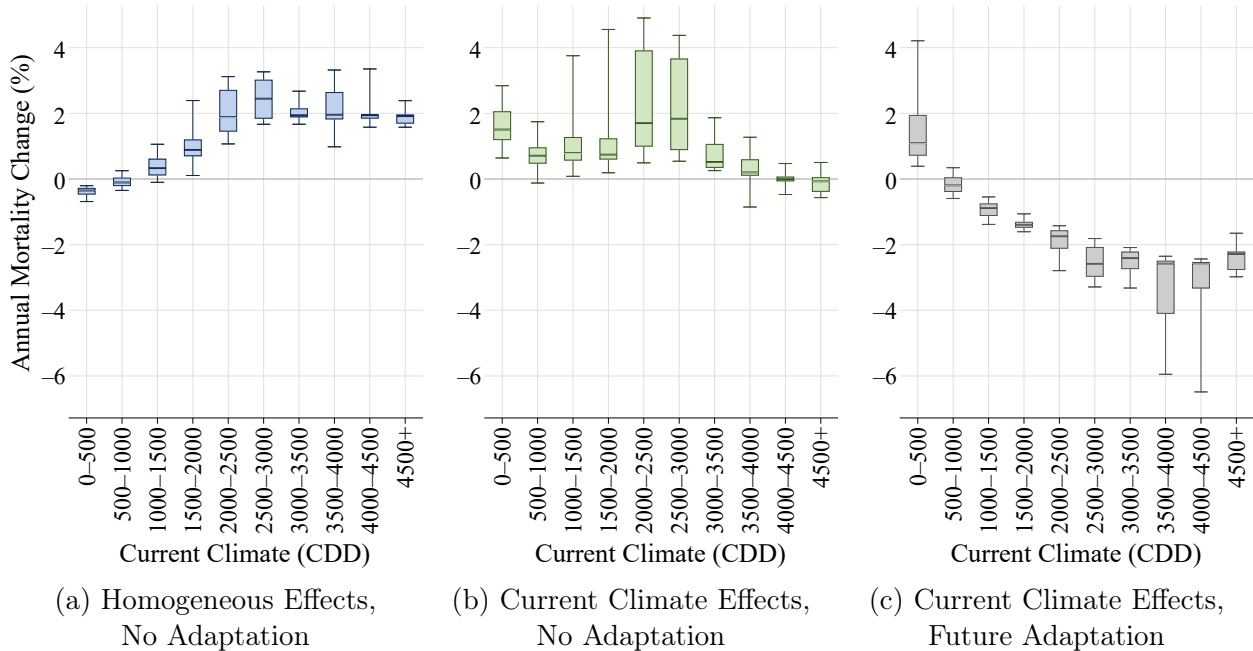
(a) Homogeneous Effects,
No Adaptation

(b) Current Climate Effects,
No Adaptation
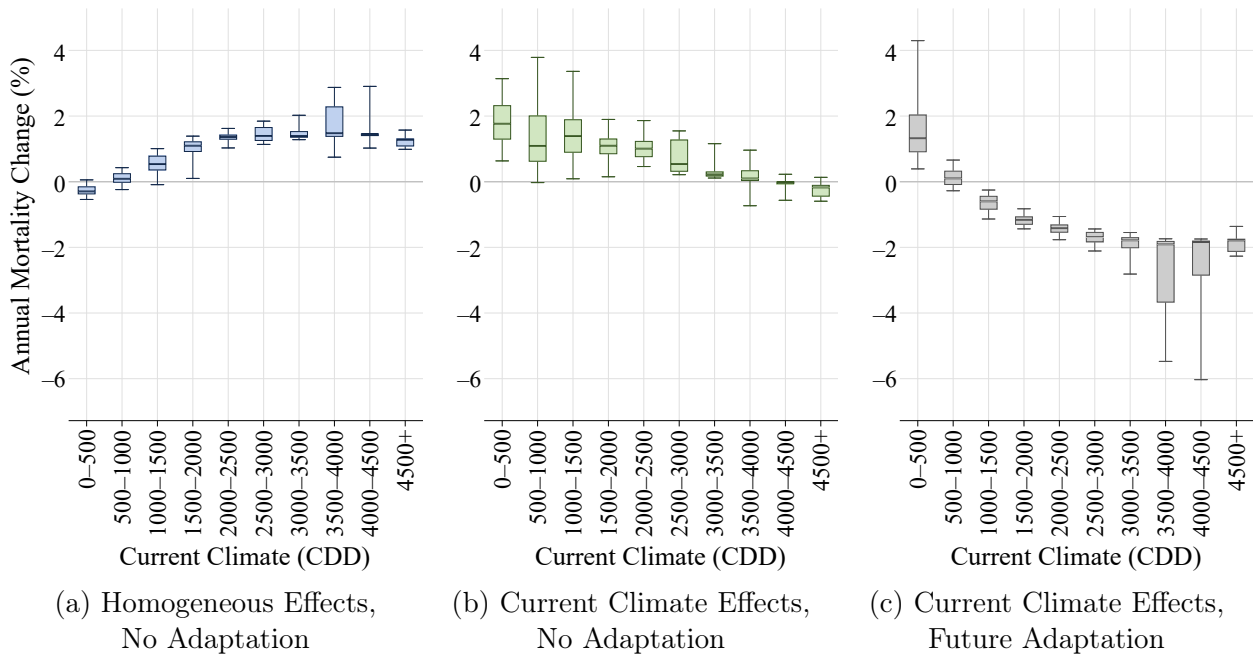
(c) Current Climate Effects,
Future Adaptation

Notes: The figure summarizes annual mortality effects of end-of-century (2080–2099) climate change relative to the current period (1992–2013) under the RCP 8.5 emissions scenario, as predicted by the MIROC5 model. Box and whisker plots summarize ZIP code-level effects by current climate. Additional notes in Appendix Figure B.9a.

Figure B.9r: MPI-ESM-LR: End-of-Century Climate Change Effects (RCP 8.5)
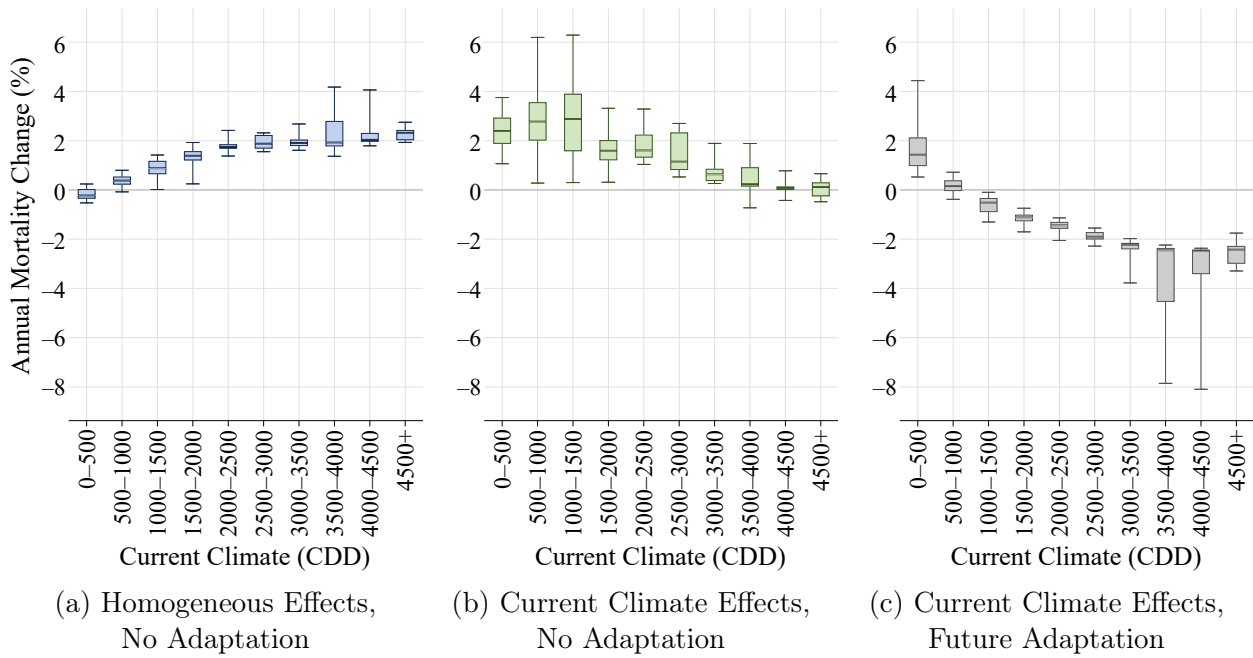
(a) Homogeneous Effects, No Adaptation

(b) Current Climate Effects, No Adaptation

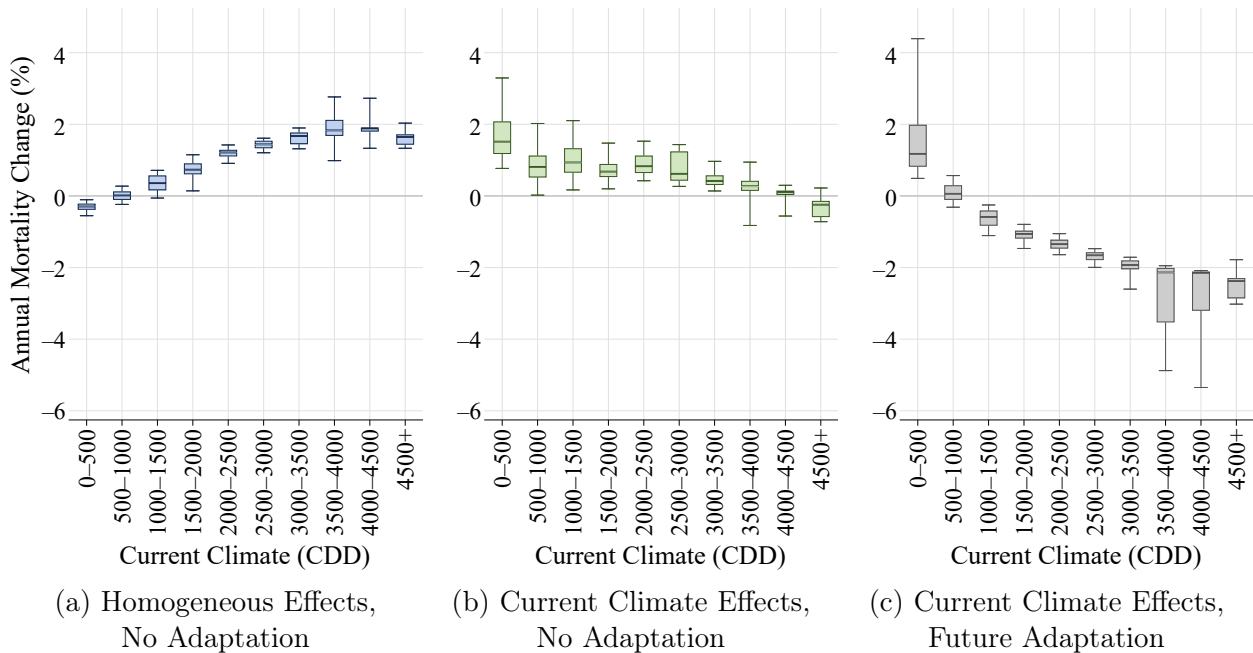(c) Current Climate Effects, Future Adaptation

Notes: The figure summarizes annual mortality effects of end-of-century (2080–2099) climate change relative to the current period (1992–2013) under the RCP 8.5 emissions scenario, as predicted by the MPI-ESM-LR model. Box and whisker plots summarize ZIP code-level effects by current climate. Additional notes in Appendix Figure B.9a.

Figure B.9s: MPI-ESM-MR: End-of-Century Climate Change Effects (RCP 8.5)
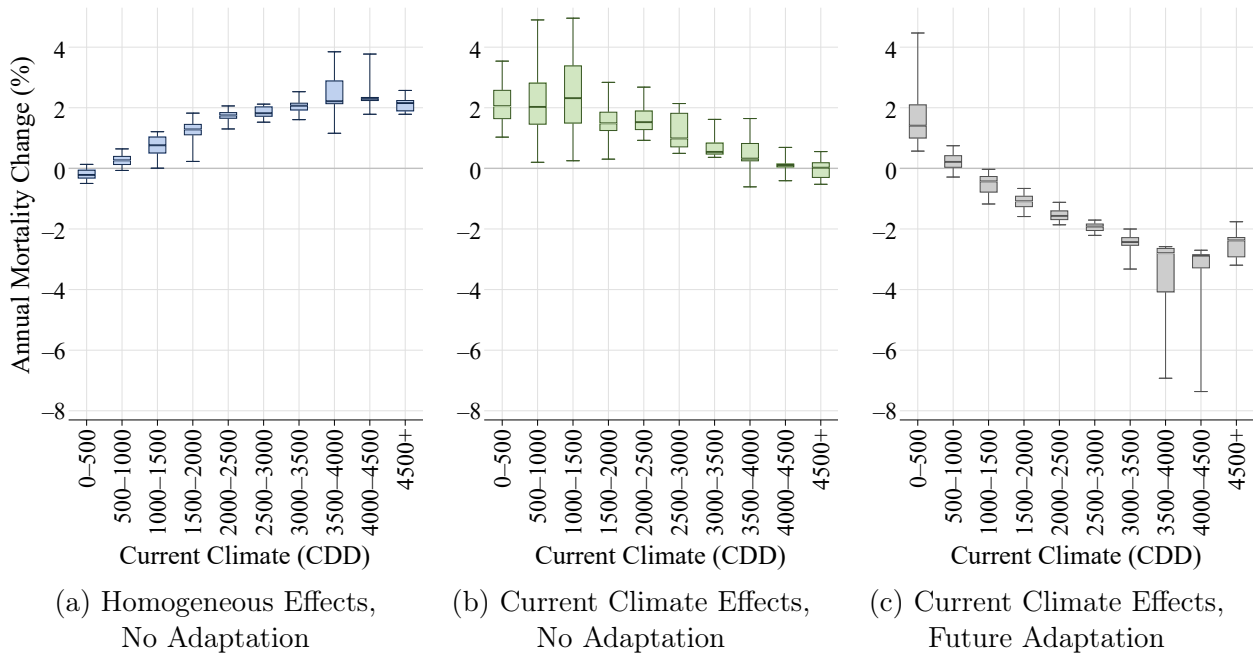
(a) Homogeneous Effects, No Adaptation

(b) Current Climate Effects, No Adaptation

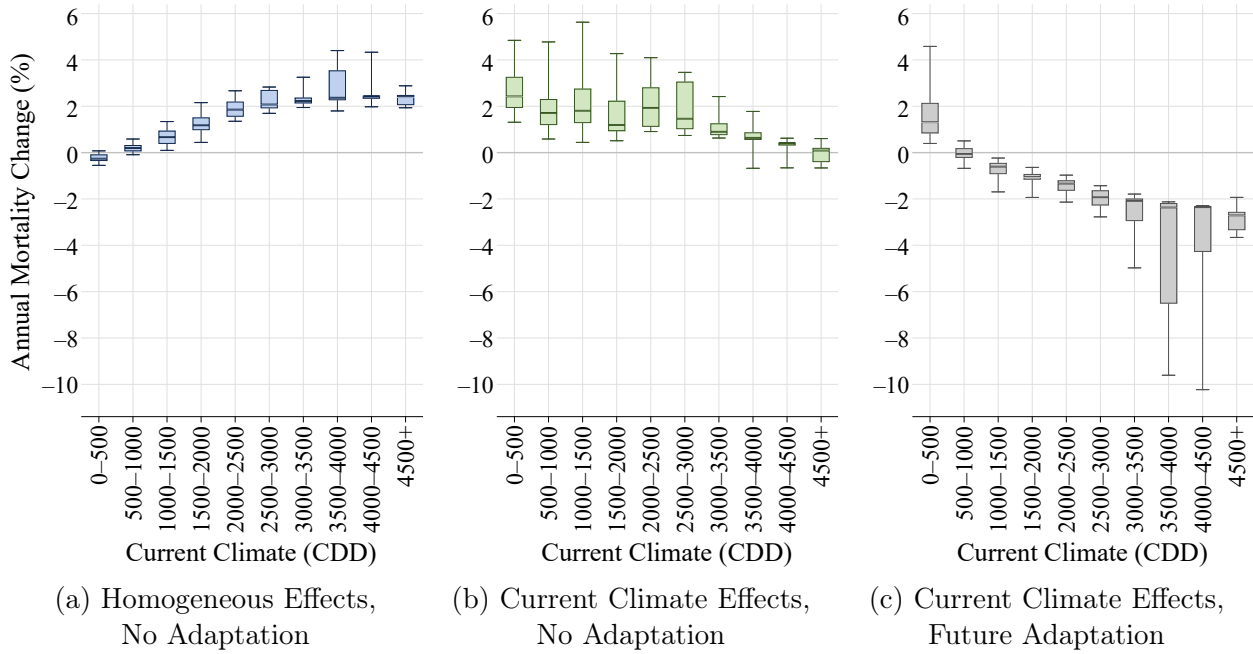(c) Current Climate Effects, Future Adaptation

Notes: The figure summarizes annual mortality effects of end-of-century (2080–2099) climate change relative to the current period (1992–2013) under the RCP 8.5 emissions scenario, as predicted by the MPI-ESM-MR model. Box and whisker plots summarize ZIP code-level effects by current climate. Additional notes in Appendix Figure B.9a.

Figure B.9t: MRI-CGCM3: End-of-Century Climate Change Effects (RCP 8.5)
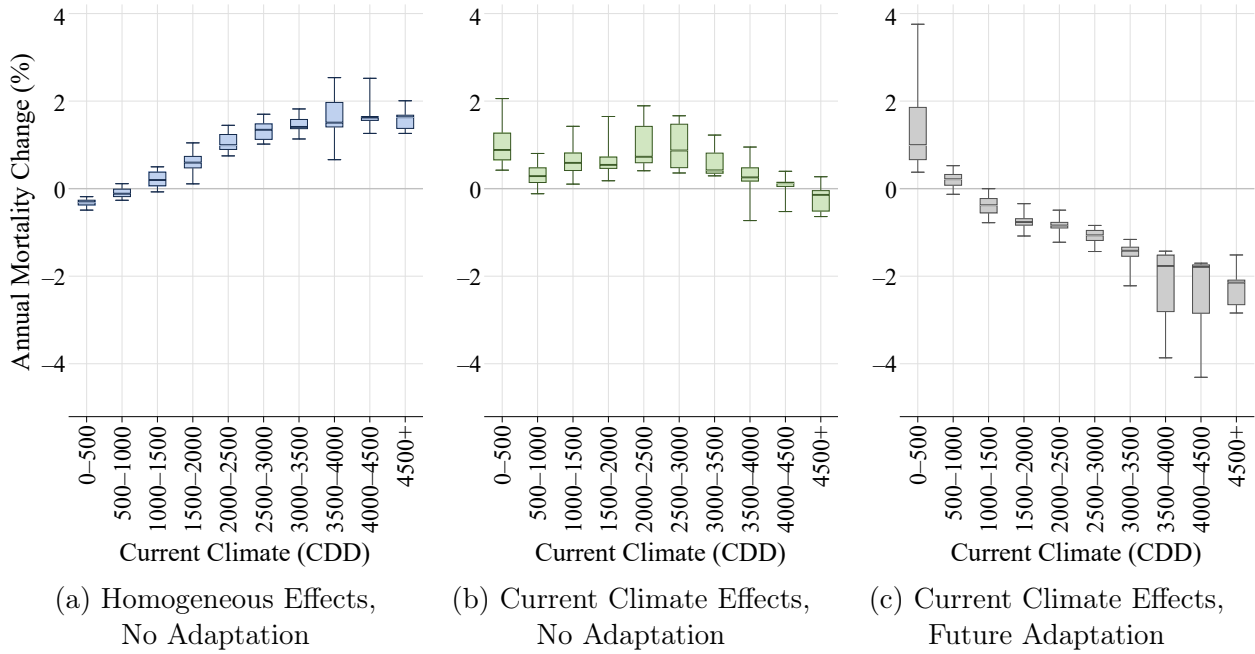
(a) Homogeneous Effects,
No Adaptation

(b) Current Climate Effects,
No Adaptation

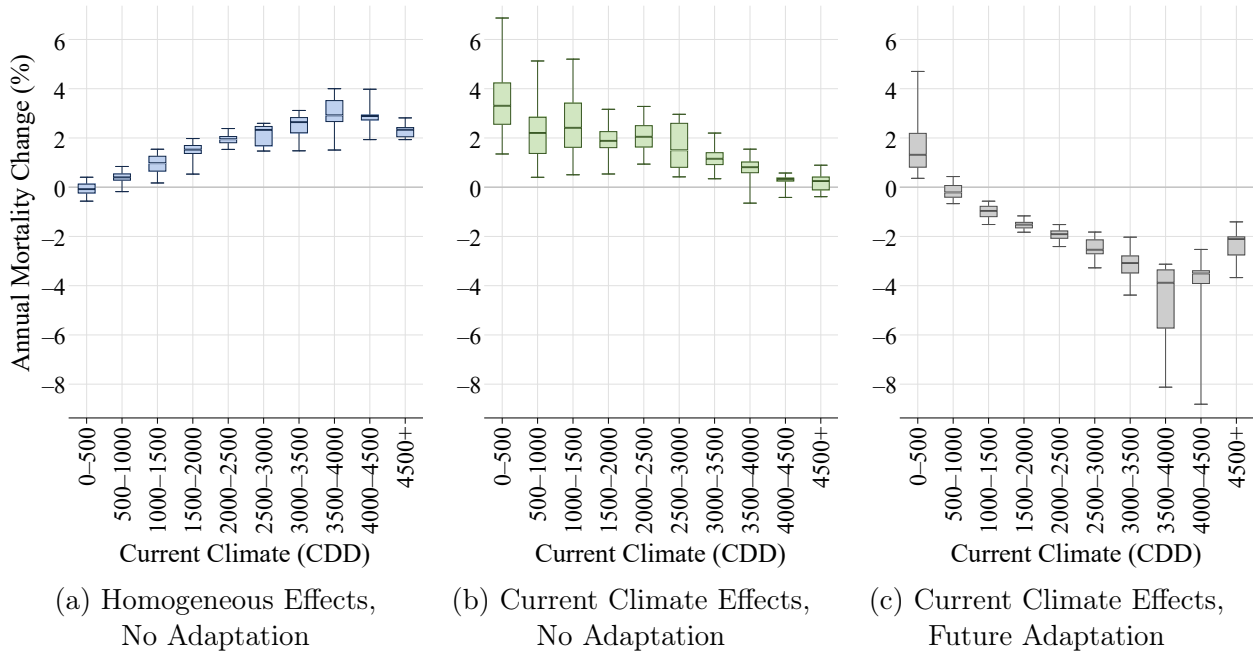(c) Current Climate Effects,
Future Adaptation

Notes: The figure summarizes annual mortality effects of end-of-century (2080–2099) climate change relative to the current period (1992–2013) under the RCP 8.5 emissions scenario, as predicted by the MRI-CGCM3 model. Box and whisker plots summarize ZIP code-level effects by current climate. Additional notes in Appendix Figure B.9a.

Figure B.9u: NorESM1-M: End-of-Century Climate Change Effects (RCP 8.5)
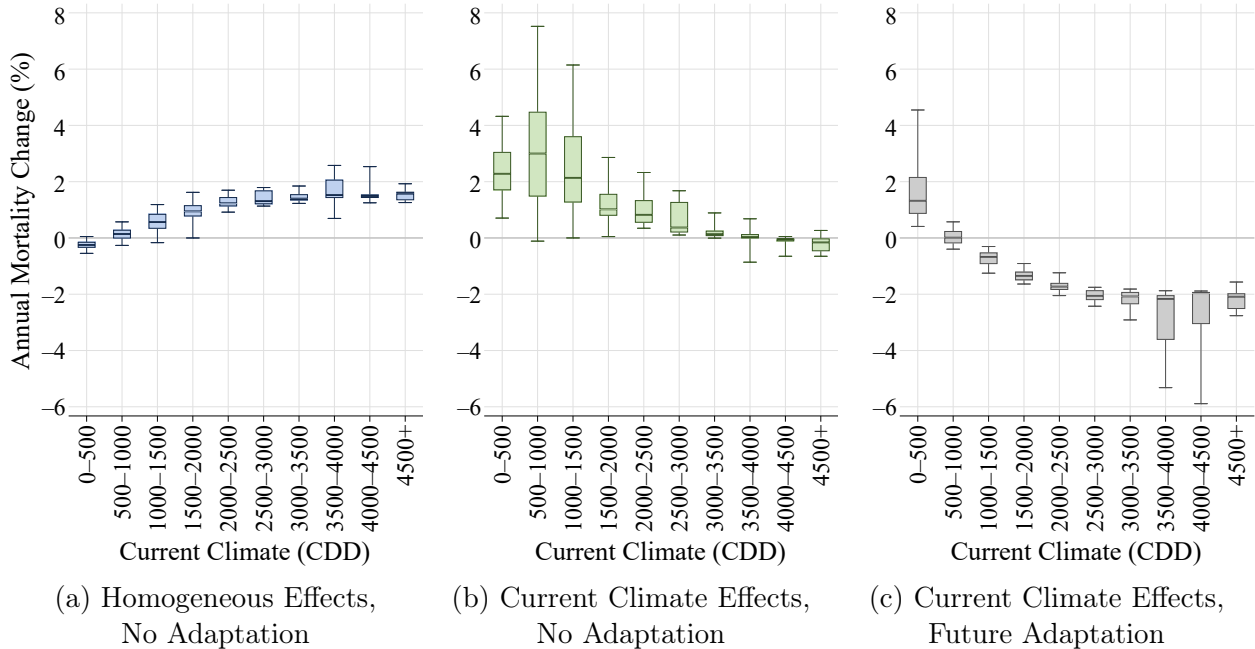
(a) Homogeneous Effects,
No Adaptation

(b) Current Climate Effects,
No Adaptation

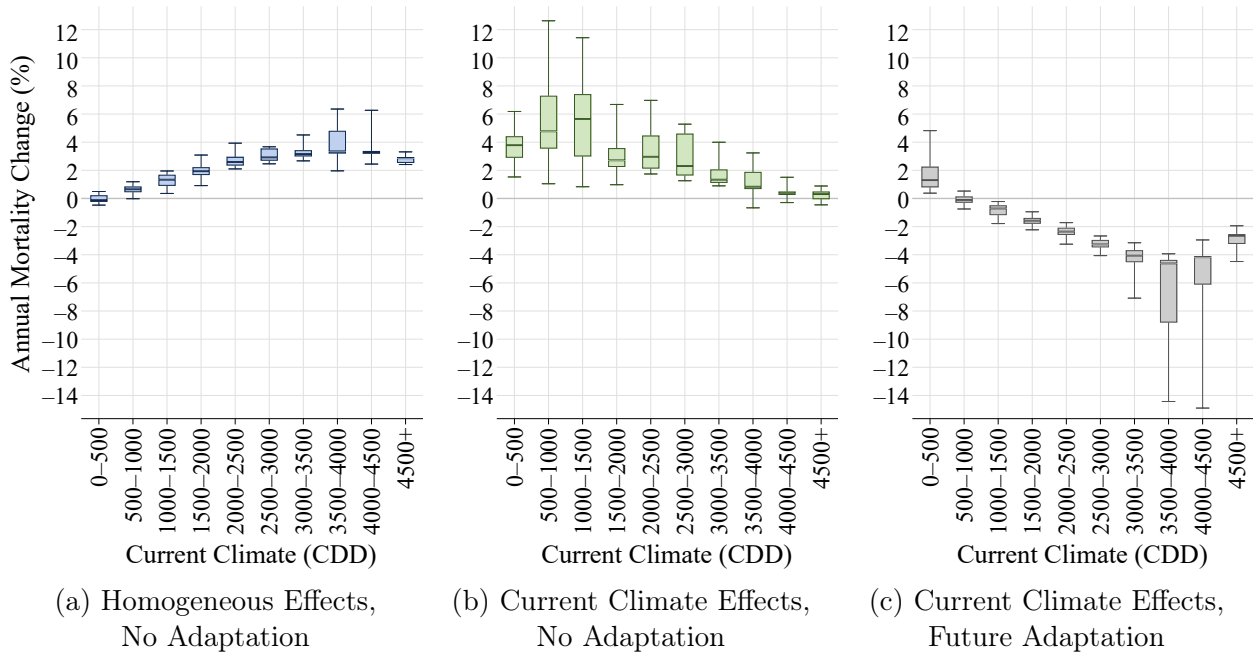(c) Current Climate Effects,
Future Adaptation

Notes: The figure summarizes annual mortality effects of end-of-century (2080–2099) climate change relative to the current period (1992–2013) under the RCP 8.5 emissions scenario, as predicted by the NorESM1-M model. Box and whisker plots summarize ZIP code-level effects by current climate. Additional notes in Appendix Figure B.9a.

Figure B.9v: bcc-csm1-1: End-of-Century Climate Change Effects (RCP 8.5)
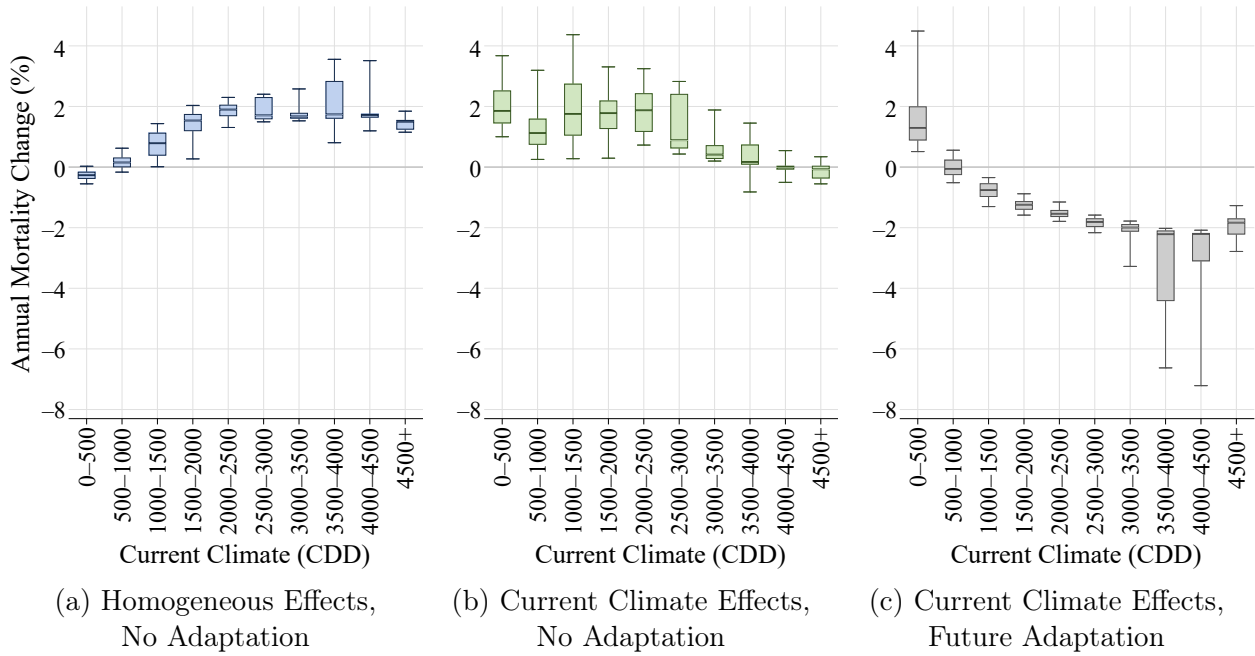
(a) Homogeneous Effects,
No Adaptation

(b) Current Climate Effects,
No Adaptation

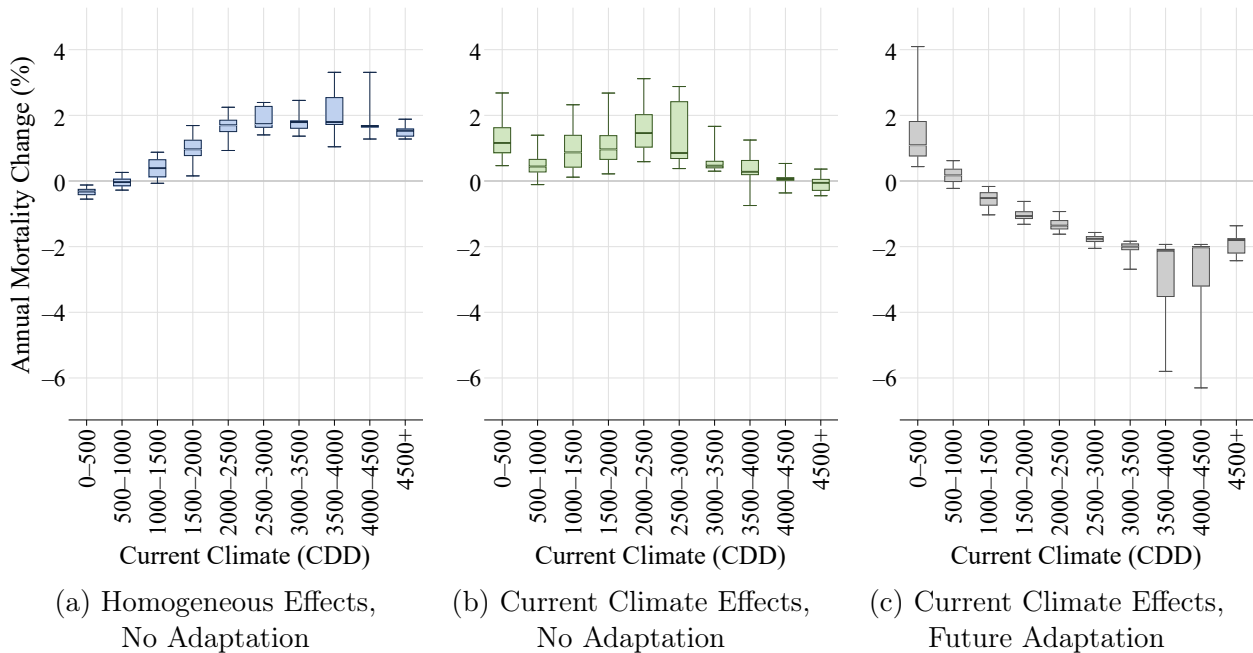(c) Current Climate Effects,
Future Adaptation

Notes: The figure summarizes annual mortality effects of end-of-century (2080–2099) climate change relative to the current period (1992–2013) under the RCP 8.5 emissions scenario, as predicted by the bcc-csm1-1 model. Box and whisker plots summarize ZIP code-level effects by current climate. Additional notes in Appendix Figure B.9a.

Figure B.9w: inmcm4: End-of-Century Climate Change Effects (RCP 8.5)
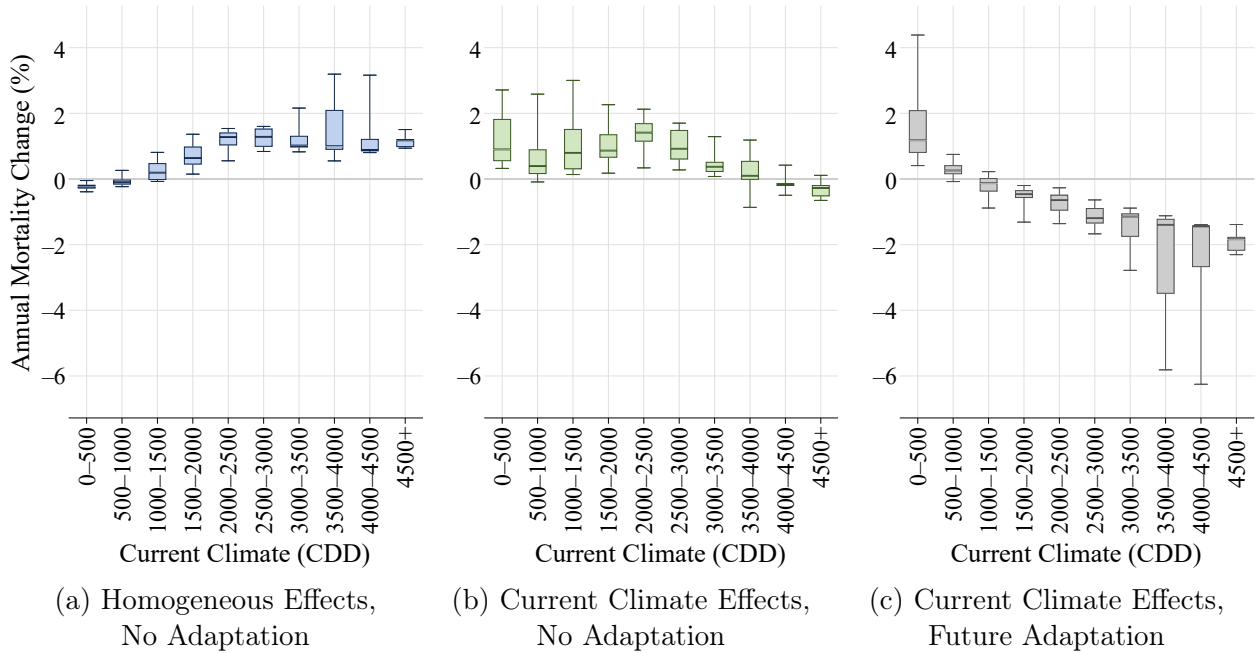
(a) Homogeneous Effects,
No Adaptation

(b) Current Climate Effects,
No Adaptation

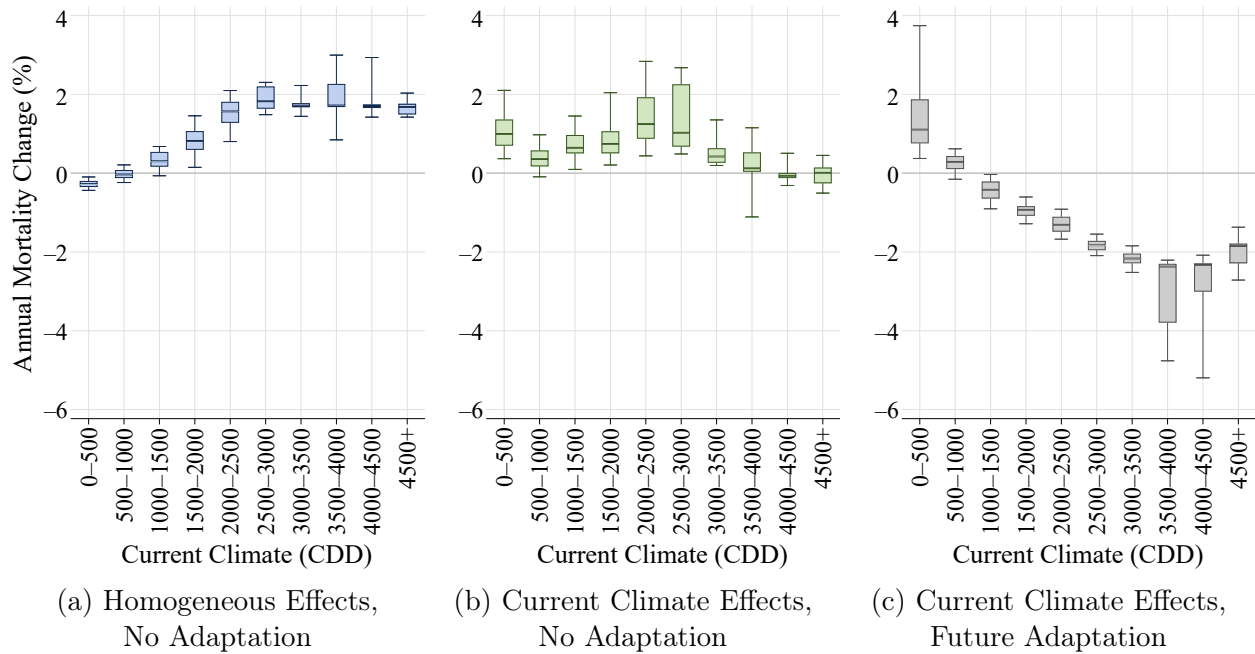(c) Current Climate Effects,
Future Adaptation

Notes: The figure summarizes annual mortality effects of end-of-century (2080–2099) climate change relative to the current period (1992–2013) under the RCP 8.5 emissions scenario, as predicted by the inmcm4 model. Box and whisker plots summarize ZIP code-level effects by current climate. Additional notes in Appendix Figure B.9a.

Figure B.10: Weighted Meta Model: End-of-Century Climate Change Effects (RCP 4.5)
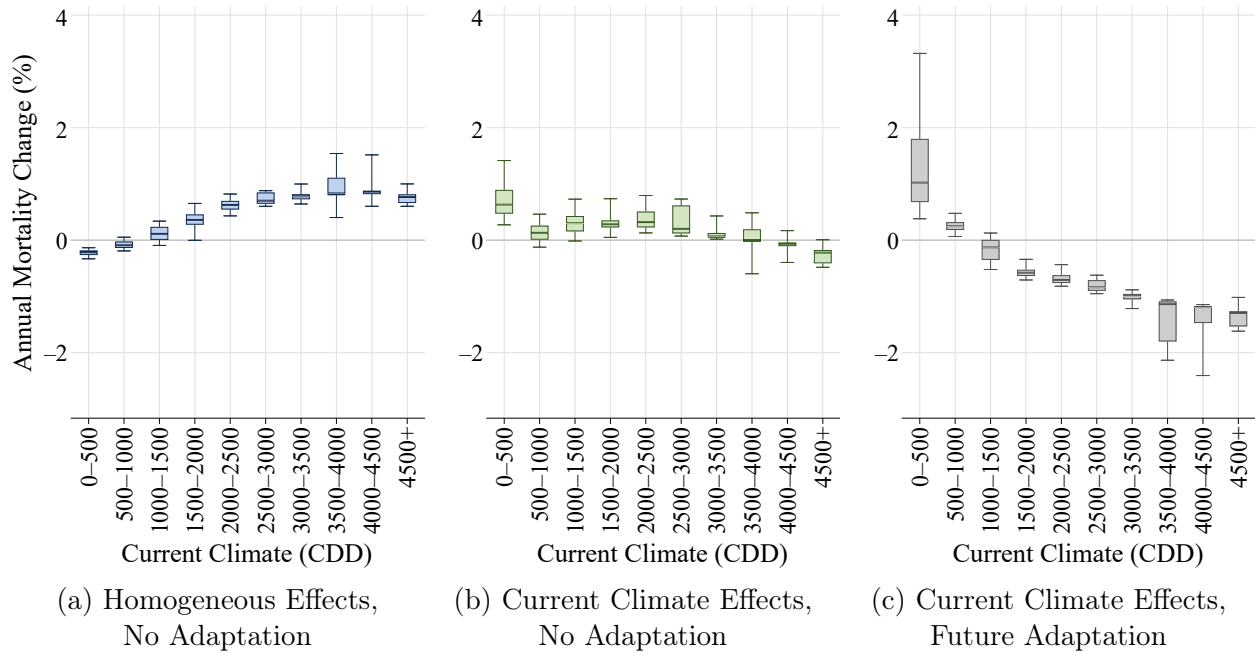
(a) Homogeneous Effects, No Adaptation

(b) Current Climate Effects, No Adaptation

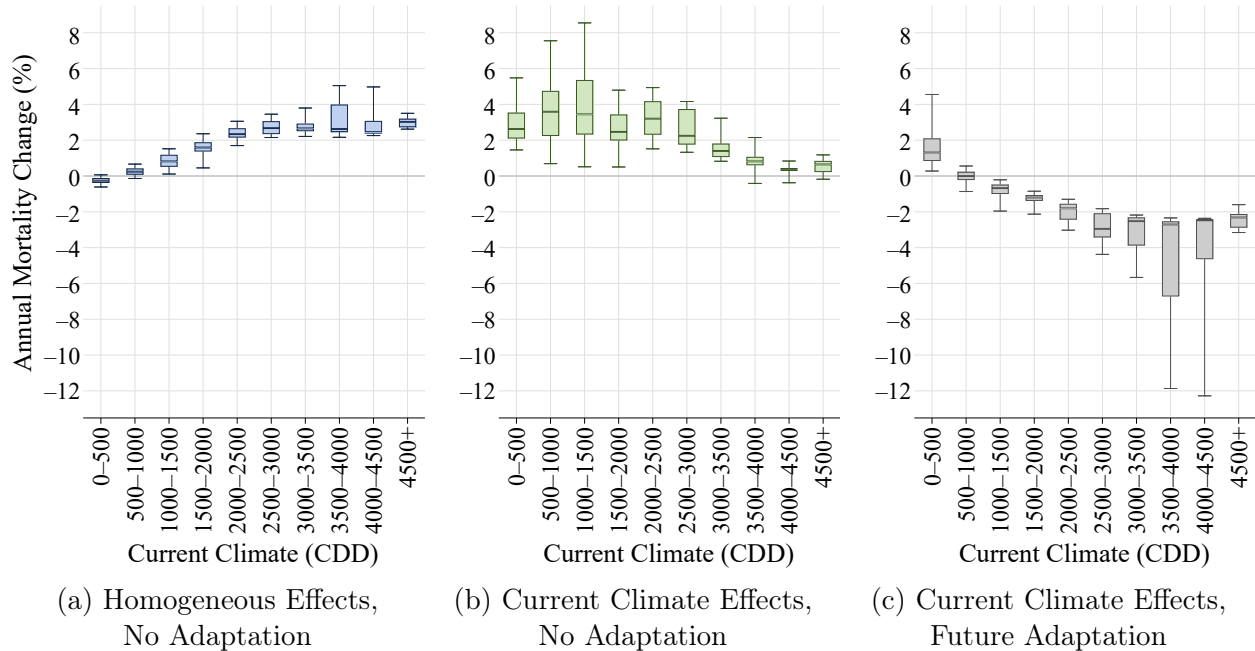(c) Current Climate Effects, Future Adaptation

Notes: The figure summarizes annual mortality effects of end-of-century (2080–2099) climate change relative to the current period (1992–2013) under the RCP 4.5 emissions scenario, as predicted by the weighted-meta-NEX-GDDP model. Observations are at the ZIP code level and are grouped by current climate (CDD). Box and whisker plots summarize the distribution of climate change effects across ZIP codes in each climate range. Boxes stretch from the 25th percentile (lower hinge) to the 75th percentile (upper hinge). The median is plotted as a line across the box. Whiskers stretch from the 5th percentile to the 95th percentile. Statistics are weighted by the elderly Medicare population in each ZIP code. Appendix Table B.4 summarizes these climate change impacts, aggregated to climate terciles and to the United States as a whole.

Figure B.11: Weighted Meta Model: End-of-Century Climate Change Effects (RCP 8.5, PRISM)

(a) Homogeneous Effects,   (b) Current Climate Effects,   (c) Current Climate Effects,
    No Adaptation   No Adaptation   Future Adaptation
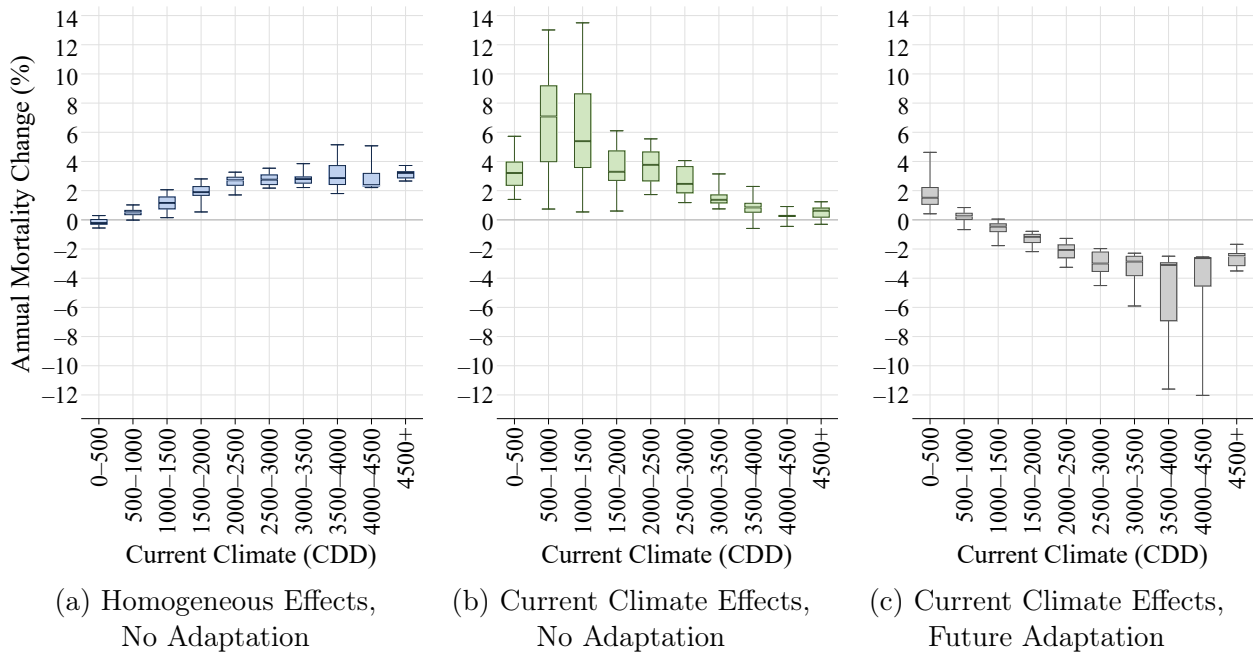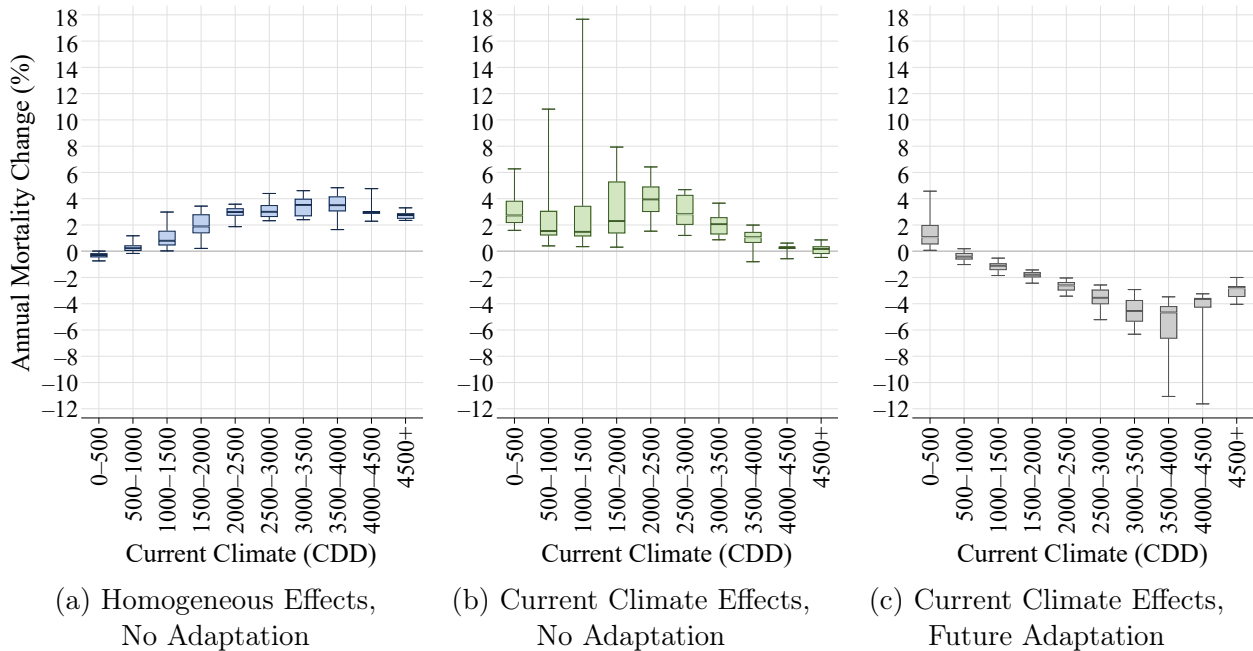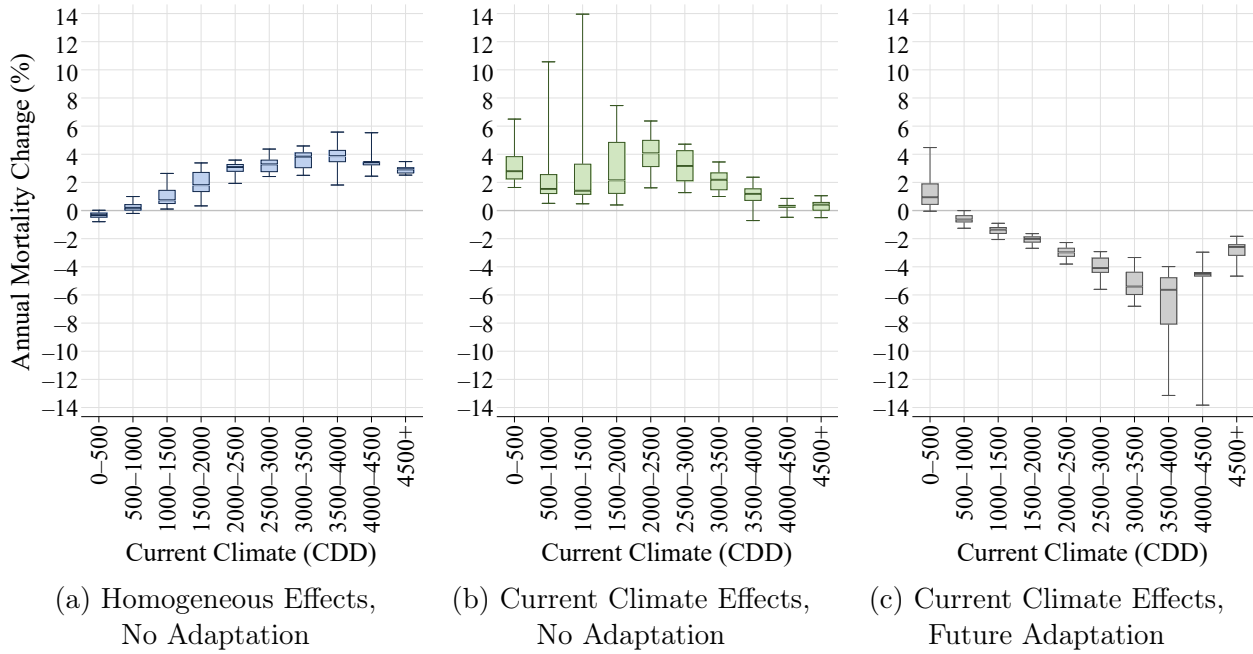
Notes: The figure summarizes annual mortality effects of end-of-century (2080–2099) climate change relative to the current period (1992–2013) under the RCP 8.5 emissions scenario, as predicted by the weighted-meta-NEX-GDDP model. Observations are at the ZIP code level and are grouped by current climate (CDD). Box and whisker plots summarize the distribution of climate change effects across ZIP codes in each climate range. Boxes stretch from the 25th percentile (lower hinge) to the 75th percentile (upper hinge). The median is plotted as a line across the box. Whiskers stretch from the 5th percentile to the 95th percentile. Statistics are weighted by the elderly Medicare population in each ZIP code. Appendix Table B.3 summarizes these climate change impacts, aggregated to climate terciles and to the United States as a whole.

Figure B.12a: Differential Effects of Temperature by Air Conditioning (AC) Penetration, Primary AC Imputation

(a) Estimation

(b) Counterfactual 1

(c) Counterfactual 2
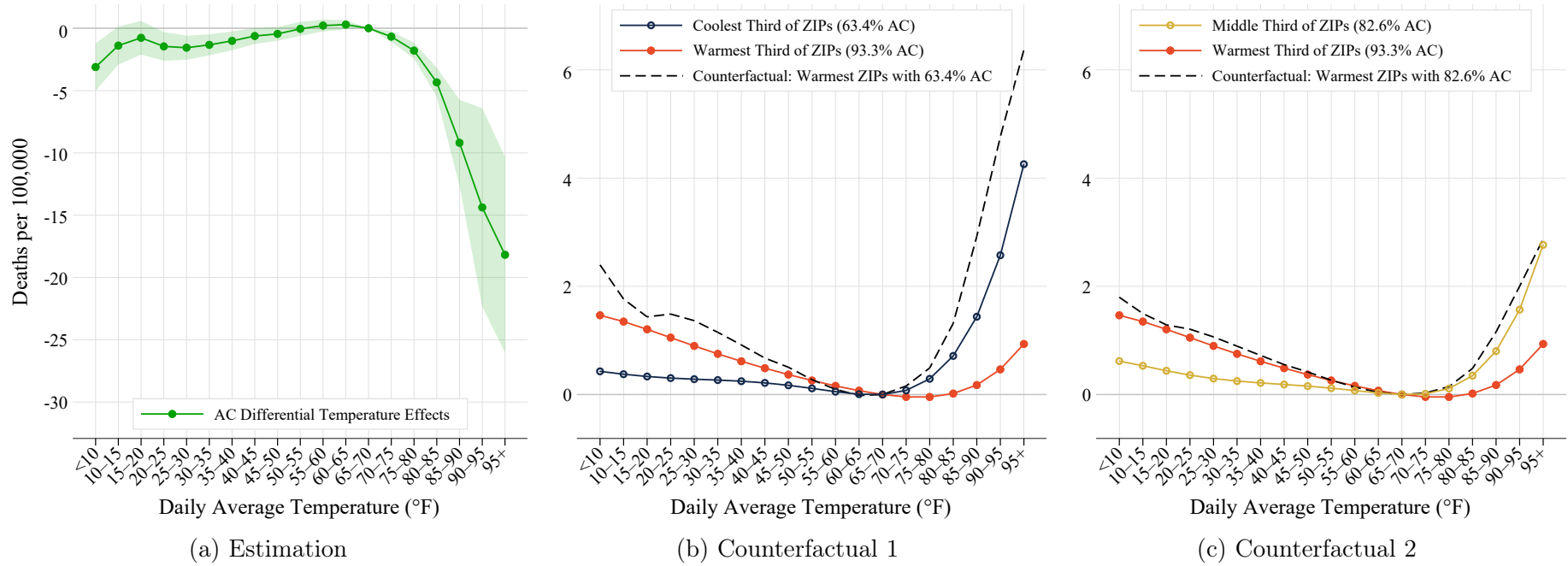
Notes: Panel (a) reports estimates of how the mortality effects of temperature vary with regional AC penetration. The estimates come from estimating a version of Equation 1 where daily average temperature bins are interacted with ZIP code-level AC penetration instead of with climate tercile indicators and separate temperature controls for each Census Region are added. The shaded region reports 95 percent confidence intervals based on two-way clustered standard errors at the county and state×date levels. Panels (b) and (c) present the implied counterfactual mortality effects of temperature in the warmest third of ZIP codes if exposed to the lower AC penetration rates in the coolest and middle third of ZIP codes, respectively.

Figure B.12b: Differential Effects of Temperature by Air Conditioning (AC) Penetration, Alternate AC Imputation

(a) Estimation (b) Counterfactual 1 (c) Counterfactual 2
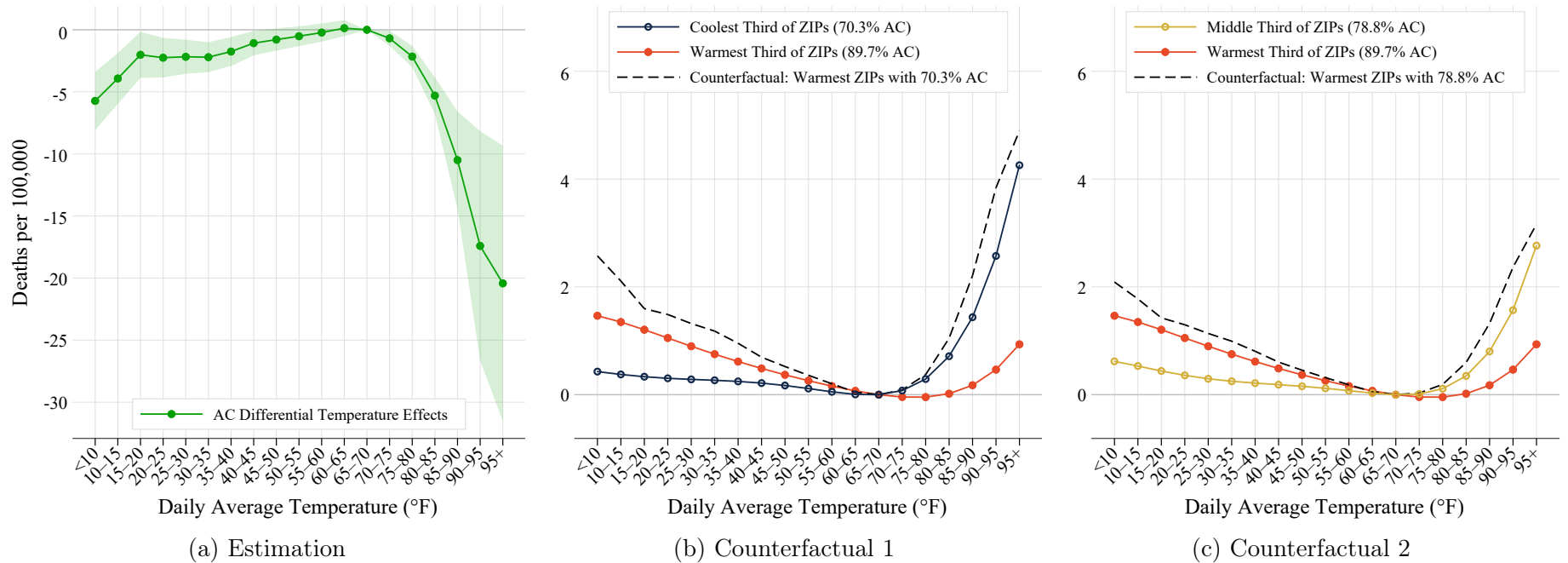
Notes: This figure shows results from replicating the AC heterogeneity analysis presented in Appendix Figure B.12a except that the AC penetration imputation procedure described in Appendix section A.4.2 was modified to exclude any climate variables. Panel (a) reports estimates of how the mortality effect of each temperature bin varies with regional AC penetration. The estimates come from estimating a version of Equation 1 where daily average temperature bins are interacted with ZIP code-level AC penetration instead of with climate tercile indicators and separate temperature controls for each Census Region are added. The shaded region reports 95 percent confidence intervals based on two-way clustered standard errors at the county and state×date levels. Panels (b) and (c) present the implied counterfactual mortality effects of temperature in the warmest third of ZIP codes if exposed to the lower AC penetration rates in the coolest and middle third of ZIP codes, respectively.

Table B.1a: Heterogeneous Effects of Temperature on Mortality (GHCN)

	(1)	(2)	(3)	(4)	(5)	(6)	(7)	(8)	(9)	(10)
			Non-parametric temperature bin estimation				Semi-parametric polynomial estimation			
	Freq. (%)	3-day mort.	Coef.	Std. Err	Std. Err	Std. Err	Coef.	Std. Err	Std. Err	Std. Err
Coolest Third of ZIPs ×										
$tavg \in [-\infty, 10)$	1.72	44.0	0.43***	0.11	0.19	0.13	0.43***	0.10	0.17	0.12
$tavg \in [10, 15)$	1.52	44.2	0.34***	0.09	0.11	0.11	0.38***	0.08	0.12	0.10
$tavg \in [15, 20)$	2.53	44.0	0.29***	0.08	0.11	0.10	0.33***	0.08	0.10	0.09
$tavg \in [20, 25)$	3.88	43.7	0.26***	0.08	0.12	0.09	0.30***	0.07	0.10	0.08
$tavg \in [25, 30)$	5.33	43.3	0.31***	0.07	0.11	0.08	0.28***	0.06	0.09	0.07
$tavg \in [30, 35)$	6.96	42.6	0.25***	0.07	0.09	0.07	0.27***	0.06	0.08	0.07
$tavg \in [35, 40)$	7.78	41.8	0.23***	0.06	0.08	0.07	0.25***	0.05	0.08	0.06
$tavg \in [40, 45)$	8.33	40.9	0.18***	0.06	0.08	0.06	0.22***	0.05	0.07	0.05
$tavg \in [45, 50)$	8.85	39.9	0.15***	0.05	0.07	0.05	0.17***	0.04	0.06	0.04
$tavg \in [50, 55)$	9.30	38.7	0.07	0.04	0.07	0.05	0.11***	0.04	0.06	0.04
$tavg \in [55, 60)$	9.83	37.3	0.02	0.04	0.06	0.05	0.05*	0.03	0.04	0.03
$tavg \in [60, 65)$	10.50	36.2	−0.02	0.03	0.03	0.03	0.01	0.02	0.02	0.02
$tavg \in [65, 70)$	10.61	35.8	0.00	0.00	0.00	0.00	0.00	0.00	0.00	0.00
$tavg \in [70, 75)$	8.11	36.1	0.10**	0.04	0.05	0.04	0.08***	0.02	0.03	0.02
$tavg \in [75, 80)$	3.87	36.4	0.20***	0.05	0.07	0.05	0.29***	0.04	0.08	0.04
$tavg \in [80, 85)$	0.81	37.0	0.68***	0.11	0.20	0.11	0.71***	0.09	0.19	0.10
$tavg \in [85, 90)$	0.06	37.7	1.80***	0.34	0.64	0.39	1.44***	0.21	0.38	0.24
$tavg \in [90, 95)$	< 0.002	48.8	11.78***	4.26	4.73	4.42	2.57***	0.43	0.72	0.49
$tavg \in [95, \infty]$	< 0.002	43.6	14.08	16.94	18.34	17.40	4.26***	0.81	1.27	0.92
Middle Third of ZIPs ×										
$tavg \in [-\infty, 10)$	0.45	46.9	0.58***	0.16	0.20	0.19	0.62***	0.15	0.21	0.19
$tavg \in [10, 15)$	0.58	46.4	0.51***	0.13	0.15	0.15	0.53***	0.10	0.13	0.12
$tavg \in [15, 20)$	1.18	45.9	0.50***	0.12	0.13	0.14	0.44***	0.08	0.10	0.10
$tavg \in [20, 25)$	2.26	45.2	0.19*	0.10	0.10	0.11	0.36***	0.08	0.09	0.09
$tavg \in [25, 30)$	3.80	44.5	0.26***	0.09	0.10	0.10	0.30***	0.08	0.09	0.09
$tavg \in [30, 35)$	5.63	43.9	0.22**	0.08	0.10	0.09	0.25***	0.08	0.10	0.08
$tavg \in [35, 40)$	7.09	43.1	0.21**	0.07	0.08	0.08	0.21***	0.08	0.10	0.08
$tavg \in [40, 45)$	7.52	42.2	0.17**	0.07	0.09	0.07	0.19**	0.07	0.10	0.07
$tavg \in [45, 50)$	7.81	41.0	0.12	0.07	0.08	0.08	0.16**	0.06	0.09	0.07
$tavg \in [50, 55)$	8.62	39.9	0.03	0.06	0.05	0.06	0.12**	0.05	0.08	0.06
$tavg \in [55, 60)$	9.40	38.9	−0.01	0.04	0.05	0.05	0.07*	0.04	0.06	0.04
$tavg \in [60, 65)$	9.78	37.7	−0.00	0.03	0.03	0.03	0.03	0.02	0.03	0.02
$tavg \in [65, 70)$	10.70	36.5	0.00	0.00	0.00	0.00	0.00	0.00	0.00	0.00
$tavg \in [70, 75)$	11.84	36.0	0.02	0.03	0.05	0.03	0.01	0.02	0.03	0.02
$tavg \in [75, 80)$	9.30	36.1	0.08	0.06	0.09	0.06	0.11**	0.05	0.06	0.05
$tavg \in [80, 85)$	3.45	36.2	0.25***	0.09	0.12	0.09	0.35***	0.10	0.11	0.10
$tavg \in [85, 90)$	0.54	36.8	0.71***	0.18	0.17	0.19	0.80***	0.22	0.21	0.23
$tavg \in [90, 95)$	0.03	39.7	3.76***	1.40	1.56	1.41	1.57***	0.45	0.41	0.46
$tavg \in [95, \infty]$	< 0.002	41.2	1.03	5.21	4.10	5.12	2.77***	0.83	0.77	0.86
Warmest Third of ZIPs ×										
$tavg \in [-\infty, 10)$	0.02	51.7	1.13	0.88	1.27	0.94	1.46**	0.66	0.91	0.71
$tavg \in [10, 15)$	0.04	50.5	1.42**	0.55	0.37	0.58	1.35***	0.36	0.49	0.39
$tavg \in [15, 20)$	0.11	50.1	1.33***	0.33	0.43	0.35	1.21***	0.19	0.26	0.22
$tavg \in [20, 25)$	0.28	49.2	1.14***	0.17	0.18	0.19	1.05***	0.12	0.15	0.14
$tavg \in [25, 30)$	0.68	48.0	0.88***	0.12	0.12	0.14	0.90***	0.08	0.11	0.10
$tavg \in [30, 35)$	1.45	47.1	0.70***	0.09	0.10	0.10	0.75***	0.07	0.10	0.08
$tavg \in [35, 40)$	2.77	46.0	0.63***	0.07	0.09	0.08	0.61***	0.06	0.09	0.07
$tavg \in [40, 45)$	4.48	45.0	0.49***	0.06	0.10	0.07	0.49***	0.05	0.08	0.06
$tavg \in [45, 50)$	6.00	43.8	0.40***	0.06	0.07	0.06	0.37***	0.05	0.07	0.05
$tavg \in [50, 55)$	7.11	42.7	0.27***	0.05	0.07	0.06	0.26***	0.04	0.06	0.04
$tavg \in [55, 60)$	8.02	41.6	0.14***	0.04	0.05	0.04	0.16***	0.03	0.04	0.03
$tavg \in [60, 65)$	8.74	40.5	0.08**	0.03	0.04	0.03	0.07***	0.01	0.02	0.01
$tavg \in [65, 70)$	10.04	39.4	0.00	0.00	0.00	0.00	0.00	0.00	0.00	0.00
$tavg \in [70, 75)$	12.63	38.0	−0.02	0.03	0.03	0.04	−0.04***	0.01	0.02	0.01
$tavg \in [75, 80)$	16.19	36.8	−0.04	0.04	0.04	0.05	−0.05	0.03	0.05	0.03
$tavg \in [80, 85)$	15.96	36.4	0.04	0.06	0.07	0.06	0.02	0.05	0.08	0.05
$tavg \in [85, 90)$	4.30	36.2	0.15*	0.08	0.11	0.08	0.18**	0.07	0.11	0.07
$tavg \in [90, 95)$	0.92	35.0	0.46***	0.10	0.10	0.10	0.46***	0.09	0.15	0.09
$tavg \in [95, \infty]$	0.25	35.0	1.06***	0.17	0.25	0.18	0.93***	0.15	0.23	0.15
Dependent variable			3-day mort.	3-day mort.	3-day mort.	3-day mort.	3-day mort.	3-day mort.	3-day mort.	3-day mort.
Dep. var. mean			39.40	39.40	39.40	39.40	39.40	39.40	39.40	39.40
Observations	250, 247, 311	250, 247, 311	250, 247, 311	250, 247, 311	250, 247, 311	250, 247, 311	250, 247, 311	250, 247, 311	250, 247, 311	250, 247, 311
First cluster level			county	county	state	county	county	county	state	county
Second cluster level			state × date			state × date	state × date			state × date
Weather source	GHCN	GHCN	GHCN	GHCN	GHCN	GHCN	GHCN	GHCN	GHCN	GHCN

Notes: This table provides sample summary statistics and estimated 3-day mortality effects of temperature as measured by GHCN data. An observation is a ZIP code day. Columns (1) and (2) summarize the sample distributions of realized temperature and 3-day mortality across each of 19 temperature bins. Columns (3)–(10) report results from estimating Equation 1. Columns (3)–(6) report non-parametric temperature bin estimates and standard errors under various levels of clustering. Columns (7)–(10) report semi-parametric (5th order polynomial in the temperature bin) estimates and associated standard errors. Figure 2a plots a selection of these estimates.

B-25

Table B.1b: Homogeneous Effects of Temperature on Mortality (GHCN)

	(1)	(2)	(3)	(4)	(5)	(6)	(7)	(8)	(9)	(10)
			Non-parametric temperature bin estimation				Semi-parametric polynomial estimation			
	Freq. (%)	3-day mort.	Coef.	Std. Err	Std. Err	Std. Err	Coef.	Std. Err	Std. Err	Std. Err
All U.S. ZIPs										
$tavg \in [-\infty, 10)$	0.73	44.6	0.65***	0.09	0.15	0.11	0.66***	0.08	0.14	0.11
$tavg \in [10, 15)$	0.72	44.9	0.57***	0.07	0.10	0.09	0.56***	0.06	0.10	0.08
$tavg \in [15, 20)$	1.28	44.8	0.54***	0.06	0.09	0.08	0.50***	0.05	0.08	0.07
$tavg \in [20, 25)$	2.14	44.5	0.41***	0.06	0.09	0.07	0.46***	0.05	0.08	0.06
$tavg \in [25, 30)$	3.27	44.1	0.45***	0.05	0.08	0.06	0.43***	0.05	0.08	0.05
$tavg \in [30, 35)$	4.68	43.6	0.39***	0.05	0.07	0.05	0.40***	0.04	0.07	0.05
$tavg \in [35, 40)$	5.88	43.0	0.36***	0.04	0.07	0.05	0.35***	0.04	0.07	0.05
$tavg \in [40, 45)$	6.77	42.2	0.30***	0.04	0.07	0.04	0.30***	0.04	0.07	0.04
$tavg \in [45, 50)$	7.55	41.3	0.24***	0.04	0.06	0.04	0.23***	0.03	0.06	0.04
$tavg \in [50, 55)$	8.34	40.3	0.14***	0.03	0.05	0.03	0.16***	0.03	0.05	0.03
$tavg \in [55, 60)$	9.08	39.1	0.06**	0.03	0.04	0.03	0.09***	0.02	0.04	0.02
$tavg \in [60, 65)$	9.67	38.0	0.03	0.02	0.03	0.02	0.03***	0.01	0.02	0.01
$tavg \in [65, 70)$	10.45	37.2	0.00	0.00	0.00	0.00	0.00	0.00	0.00	0.00
$tavg \in [70, 75)$	10.86	36.8	0.03*	0.02	0.03	0.02	0.01	0.01	0.03	0.01
$tavg \in [75, 80)$	9.79	36.5	0.07**	0.04	0.06	0.04	0.08***	0.03	0.06	0.03
$tavg \in [80, 85)$	6.75	36.4	0.23***	0.05	0.10	0.05	0.24***	0.05	0.09	0.05
$tavg \in [85, 90)$	1.64	36.3	0.44***	0.08	0.15	0.08	0.49***	0.08	0.14	0.08
$tavg \in [90, 95)$	0.32	35.2	1.02***	0.23	0.29	0.23	0.87***	0.13	0.21	0.13
$tavg \in [95, \infty]$	0.08	35.0	1.59***	0.27	0.40	0.27	1.41***	0.22	0.33	0.23
Dependent variable			3-day mort.	3-day mort.	3-day mort.	3-day mort.	3-day mort.	3-day mort.	3-day mort.	3-day mort.
Dep. var. mean			39.40	39.40	39.40	39.40	39.40	39.40	39.40	39.40
Observations	250, 247, 311	250, 247, 311	250, 247, 311	250, 247, 311	250, 247, 311	250, 247, 311	250, 247, 311	250, 247, 311	250, 247, 311	250, 247, 311
First cluster level			county	county	state	county	county	county	state	county
Second cluster level			state × date			state × date	state × date			state × date
Weather source	GHCN	GHCN	GHCN	GHCN	GHCN	GHCN	GHCN	GHCN	GHCN	GHCN

Notes: This table provides sample summary statistics and estimated 3-day mortality effects of temperature as measured by GHCN data. An observation is a ZIP code day. Columns (1) and (2) summarize the sample distributions of realized temperature and 3-day mortality across each of 19 temperature bins. Columns (3)–(10) report results from estimating Equation 1, but with temperature effects constrained to be the same across all regions. Columns (3)–(6) report non-parametric temperature bin estimates and standard errors under various levels of clustering. Columns (7)–(10) report semi-parametric (5th order polynomial in the temperature bin) estimates and associated standard errors. Figure 2b plots a selection of these estimates.

Table B.1c: Heterogeneous Effects of Temperature on Mortality (PRISM)

	(1)	(2)	(3)	(4)	(5)	(6)	(7)	(8)	(9)	(10)
			Non-parametric temperature bin estimation				Semi-parametric polynomial estimation			
	Freq. (%)	3-day mort.	Coef.	Std. Err	Std. Err	Std. Err	Coef.	Std. Err	Std. Err	Std. Err
Coolest Third of ZIPs ×										
$tavg \in [-\infty, 10)$	1.91	44.3	1.32***	0.10	0.14	0.12	1.32***	0.09	0.15	0.12
$tavg \in [10, 15)$	1.63	44.4	1.12***	0.09	0.11	0.11	1.22***	0.08	0.11	0.09
$tavg \in [15, 20)$	2.70	44.2	1.08***	0.08	0.08	0.09	1.14***	0.07	0.09	0.08
$tavg \in [20, 25)$	3.96	43.8	1.03***	0.07	0.08	0.08	1.07***	0.06	0.08	0.07
$tavg \in [25, 30)$	5.42	43.3	0.98***	0.06	0.09	0.07	1.00***	0.06	0.08	0.07
$tavg \in [30, 35)$	7.00	42.6	0.91***	0.06	0.07	0.07	0.93***	0.05	0.07	0.06
$tavg \in [35, 40)$	7.86	41.8	0.80***	0.06	0.06	0.06	0.84***	0.05	0.06	0.06
$tavg \in [40, 45)$	8.37	40.8	0.67***	0.05	0.05	0.06	0.73***	0.04	0.05	0.05
$tavg \in [45, 50)$	8.80	39.8	0.55***	0.05	0.04	0.05	0.60***	0.04	0.05	0.04
$tavg \in [50, 55)$	9.20	38.6	0.37***	0.04	0.04	0.04	0.45***	0.03	0.04	0.04
$tavg \in [55, 60)$	9.74	37.3	0.24***	0.04	0.04	0.04	0.28***	0.02	0.03	0.03
$tavg \in [60, 65)$	10.47	36.2	0.09***	0.03	0.02	0.03	0.12***	0.01	0.02	0.01
$tavg \in [65, 70)$	10.40	35.8	0.00	0.00	0.00	0.00	0.00	0.00	0.00	0.00
$tavg \in [70, 75)$	8.01	36.0	−0.07*	0.03	0.03	0.04	−0.04**	0.01	0.02	0.02
$tavg \in [75, 80)$	3.72	36.3	−0.05	0.05	0.07	0.05	0.07*	0.04	0.06	0.04
$tavg \in [80, 85)$	0.76	36.9	0.43***	0.10	0.15	0.11	0.40***	0.09	0.15	0.10
$tavg \in [85, 90)$	0.06	37.2	1.34***	0.37	0.55	0.40	1.05***	0.20	0.34	0.23
$tavg \in [90, 95)$	< 0.002	49.8	13.09***	4.04	4.48	4.66	2.16***	0.42	0.69	0.49
$tavg \in [95, \infty]$	< 0.002	109.9	31.48***	4.16	4.17	4.24	3.85***	0.80	1.25	0.92
Middle Third of ZIPs ×										
$tavg \in [-\infty, 10)$	0.53	46.9	1.77***	0.16	0.15	0.19	1.83***	0.15	0.16	0.19
$tavg \in [10, 15)$	0.67	46.6	1.73***	0.12	0.13	0.15	1.61***	0.09	0.10	0.11
$tavg \in [15, 20)$	1.32	45.8	1.39***	0.10	0.09	0.12	1.44***	0.07	0.09	0.09
$tavg \in [20, 25)$	2.41	45.2	1.20***	0.08	0.08	0.10	1.29***	0.07	0.08	0.08
$tavg \in [25, 30)$	4.00	44.5	1.15***	0.07	0.08	0.08	1.17***	0.06	0.08	0.07
$tavg \in [30, 35)$	5.78	43.9	1.04***	0.06	0.06	0.07	1.06***	0.06	0.08	0.07
$tavg \in [35, 40)$	7.15	43.0	0.96***	0.06	0.08	0.07	0.95***	0.06	0.08	0.07
$tavg \in [40, 45)$	7.49	42.1	0.85***	0.06	0.07	0.06	0.83***	0.06	0.07	0.06
$tavg \in [45, 50)$	7.88	40.9	0.63***	0.06	0.07	0.06	0.69***	0.05	0.07	0.06
$tavg \in [50, 55)$	8.61	39.9	0.47***	0.05	0.04	0.05	0.52***	0.05	0.06	0.05
$tavg \in [55, 60)$	9.22	38.9	0.28***	0.04	0.04	0.04	0.34***	0.03	0.04	0.04
$tavg \in [60, 65)$	9.71	37.6	0.14***	0.04	0.03	0.04	0.16***	0.02	0.02	0.02
$tavg \in [65, 70)$	10.61	36.5	0.00	0.00	0.00	0.00	0.00	0.00	0.00	0.00
$tavg \in [70, 75)$	11.78	36.0	−0.07**	0.03	0.02	0.03	−0.10***	0.02	0.02	0.02
$tavg \in [75, 80)$	9.07	36.0	−0.11***	0.04	0.04	0.04	−0.09***	0.03	0.03	0.03
$tavg \in [80, 85)$	3.29	36.1	−0.00	0.06	0.06	0.06	0.10	0.08	0.07	0.08
$tavg \in [85, 90)$	0.46	36.8	0.60***	0.22	0.19	0.22	0.54**	0.21	0.18	0.22
$tavg \in [90, 95)$	0.02	39.5	3.89**	1.84	2.20	1.96	1.36***	0.47	0.41	0.49
$tavg \in [95, \infty]$	< 0.002	31.7	−8.76**	5.25	4.53	4.07	2.67***	0.92	0.81	0.97
Warmest Third of ZIPs ×										
$tavg \in [-\infty, 10)$	0.03	51.5	2.40***	0.64	0.95	0.77	2.53***	0.49	0.69	0.57
$tavg \in [10, 15)$	0.05	50.5	2.00***	0.36	0.30	0.40	2.22***	0.26	0.35	0.30
$tavg \in [15, 20)$	0.14	50.0	2.16***	0.25	0.28	0.27	1.98***	0.14	0.17	0.17
$tavg \in [20, 25)$	0.35	49.1	1.84***	0.14	0.13	0.17	1.78***	0.09	0.10	0.12
$tavg \in [25, 30)$	0.80	48.0	1.55***	0.10	0.09	0.12	1.60***	0.07	0.09	0.09
$tavg \in [30, 35)$	1.69	47.1	1.39***	0.08	0.09	0.10	1.42***	0.06	0.08	0.08
$tavg \in [35, 40)$	3.13	46.0	1.20***	0.07	0.09	0.08	1.23***	0.05	0.07	0.07
$tavg \in [40, 45)$	4.89	44.9	1.02***	0.06	0.06	0.07	1.03***	0.05	0.07	0.06
$tavg \in [45, 50)$	6.49	43.8	0.84***	0.05	0.07	0.06	0.82***	0.04	0.06	0.05
$tavg \in [50, 55)$	7.52	42.6	0.56***	0.05	0.06	0.05	0.60***	0.04	0.05	0.04
$tavg \in [55, 60)$	8.28	41.6	0.38***	0.04	0.04	0.04	0.38***	0.03	0.04	0.03
$tavg \in [60, 65)$	9.08	40.5	0.13***	0.04	0.04	0.04	0.18***	0.01	0.02	0.01
$tavg \in [65, 70)$	10.20	39.4	0.00	0.00	0.00	0.00	0.00	0.00	0.00	0.00
$tavg \in [70, 75)$	11.96	38.3	−0.14***	0.03	0.05	0.04	−0.14***	0.01	0.02	0.01
$tavg \in [75, 80)$	14.65	37.4	−0.22***	0.04	0.06	0.04	−0.22***	0.03	0.05	0.03
$tavg \in [80, 85)$	15.82	36.5	−0.26***	0.05	0.06	0.05	−0.23***	0.04	0.07	0.04
$tavg \in [85, 90)$	3.93	36.3	−0.15**	0.07	0.10	0.07	−0.15**	0.06	0.08	0.06
$tavg \in [90, 95)$	0.80	35.1	0.09	0.12	0.14	0.12	0.02	0.10	0.12	0.11
$tavg \in [95, \infty]$	0.19	35.5	0.25	0.23	0.24	0.23	0.31	0.21	0.23	0.21
Dependent variable			3-day mort.	3-day mort.	3-day mort.	3-day mort.	3-day mort.	3-day mort.	3-day mort.	3-day mort.
Dep. var. mean			39.54	39.54	39.54	39.54	39.54	39.54	39.54	39.54
Observations	259, 433, 198	259, 433, 198	259, 433, 198	259, 433, 198	259, 433, 198	259, 433, 198	259, 433, 198	259, 433, 198	259, 433, 198	259, 433, 198
First cluster level			county	county	state	county	county	county	state	county
Second cluster level			state × date			state × date	state × date			state × date
Weather source	PRISM	PRISM	prism	prism	prism	prism	prism	prism	prism	prism

Notes: This table provides sample summary statistics and estimated 3-day mortality effects of temperature as measured by PRISM data. An observation is a ZIP code day. Columns (1) and (2) summarize the sample distributions of realized temperature and 3-day mortality across each of 19 temperature bins. Columns (3)–(10) report results from estimating Equation 1. Columns (3)–(6) report non-parametric temperature bin estimates and standard errors under various levels of clustering. Columns (7)–(10) report semi-parametric (5th order polynomial in the temperature bin) estimates and associated standard errors. Figure B.5a plots a selection of these estimates.

Table B.1d: Homogeneous Effects of Temperature on Mortality (PRISM)

	(1)	(2)	(3)	(4)	(5)	(6)	(7)	(8)	(9)	(10)
			Non-parametric temperature bin estimation				Semi-parametric polynomial estimation			
	Freq. (%)	3-day mort.	Coef.	Std. Err	Std. Err	Std. Err	Coef.	Std. Err	Std. Err	Std. Err
All U.S. ZIPs										
$tavg \in [-\infty, 10)$	0.83	44.9	1.65***	0.08	0.12	0.10	1.67***	0.07	0.12	0.10
$tavg \in [10, 15)$	0.79	45.1	1.49***	0.07	0.09	0.09	1.49***	0.05	0.08	0.07
$tavg \in [15, 20)$	1.40	44.9	1.38***	0.05	0.07	0.07	1.38***	0.04	0.06	0.06
$tavg \in [20, 25)$	2.25	44.6	1.27***	0.05	0.06	0.06	1.29***	0.04	0.06	0.05
$tavg \in [25, 30)$	3.43	44.1	1.21***	0.04	0.06	0.05	1.21***	0.04	0.06	0.05
$tavg \in [30, 35)$	4.85	43.7	1.11***	0.04	0.06	0.05	1.12***	0.04	0.06	0.04
$tavg \in [35, 40)$	6.07	43.0	0.99***	0.04	0.06	0.04	1.00***	0.03	0.06	0.04
$tavg \in [40, 45)$	6.93	42.3	0.86***	0.03	0.05	0.04	0.86***	0.03	0.05	0.04
$tavg \in [45, 50)$	7.73	41.3	0.69***	0.03	0.05	0.04	0.69***	0.03	0.04	0.03
$tavg \in [50, 55)$	8.45	40.2	0.49***	0.03	0.03	0.03	0.51***	0.02	0.04	0.03
$tavg \in [55, 60)$	9.08	39.1	0.31***	0.02	0.03	0.03	0.32***	0.02	0.03	0.02
$tavg \in [60, 65)$	9.76	38.0	0.12***	0.02	0.02	0.02	0.14***	0.01	0.02	0.01
$tavg \in [65, 70)$	10.40	37.2	0.00	0.00	0.00	0.00	0.00	0.00	0.00	0.00
$tavg \in [70, 75)$	10.57	36.9	−0.09***	0.02	0.02	0.02	−0.09***	0.01	0.02	0.01
$tavg \in [75, 80)$	9.11	36.8	−0.13***	0.03	0.04	0.03	−0.11***	0.02	0.04	0.02
$tavg \in [80, 85)$	6.56	36.5	−0.07*	0.04	0.06	0.04	−0.04	0.04	0.07	0.04
$tavg \in [85, 90)$	1.46	36.3	0.18**	0.08	0.14	0.09	0.16*	0.08	0.12	0.08
$tavg \in [90, 95)$	0.27	35.3	0.66**	0.26	0.33	0.27	0.49***	0.16	0.22	0.17
$tavg \in [95, \infty]$	0.06	35.5	0.79**	0.33	0.39	0.34	0.98***	0.31	0.40	0.32
Dependent variable			3-day mort.	3-day mort.	3-day mort.	3-day mort.	3-day mort.	3-day mort.	3-day mort.	3-day mort.
Dep. var. mean			39.54	39.54	39.54	39.54	39.54	39.54	39.54	39.54
Observations	259, 433, 198	259, 433, 198	259, 433, 198	259, 433, 198	259, 433, 198	259, 433, 198	259, 433, 198	259, 433, 198	259, 433, 198	259, 433, 198
First cluster level			county	county	state	county	county	county	state	county
Second cluster level			state × date			state × date	state × date			state × date
Weather source	PRISM	PRISM	prism	prism	prism	prism	prism	prism	prism	prism

Notes: This table provides sample summary statistics and estimated 3-day mortality effects of temperature as measured by PRISM data. An observation is a ZIP code day. Columns (1) and (2) summarize the sample distributions of realized temperature and 3-day mortality across each of 19 temperature bins. Columns (3)–(10) report results from estimating Equation 1, but with temperature effects constrained to be the same across all regions. Columns (3)–(6) report non-parametric temperature bin estimates and standard errors under various levels of clustering. Columns (7)–(10) report semi-parametric (5th order polynomial in the temperature bin) estimates and associated standard errors. Figure B.5b plots a selection of these estimates.

Table B.2a: End-of-Century Climate Change Effects (RCP 8.5): All U.S. ZIPs

	(1)	(2)	(3)	(4)	(5)	(6)	(7)	(8)
						Annual Mortality Change (%)		
		Avg. Temp. (°F)		Annual CDD		Homogeneous Effects	Climate Heterogeneity	
	Model Weight	Current	Future	Current	Future	No Adaptation	No Adaptation	Future Adaptation
Average of NEX-GDDP Models								
Meta-model, weighted average		57.1	65.1	1413	2864	0.76***	2.15***	-0.53*
						(0.18)	(0.47)	(0.32)
Meta-model, unweighted average		57.1	65.3	1413	2897	0.79***	2.12***	-0.57*
						(0.18)	(0.45)	(0.33)
NEX-GDDP Models								
ACCESS1-0	1.02	57.1	66.7	1413	3215	1.12***	4.47***	-0.74*
						(0.23)	(1.24)	(0.45)
BNU-ESM	0.68	57.1	66.2	1413	2979	0.69***	1.62***	-0.76**
						(0.18)	(0.27)	(0.35)
CCSM4	0.68	57.1	64.1	1413	2707	0.59***	1.34***	-0.38
						(0.15)	(0.25)	(0.28)
CESM1-BGC	0.64	57.1	64.4	1413	2681	0.55***	1.25***	-0.44
						(0.14)	(0.24)	(0.27)
CNRM-CM5	1.01	57.1	64.4	1413	2613	0.46***	0.92***	-0.45*
						(0.14)	(0.17)	(0.25)
CSIRO-Mk3-6-0	0.74	57.1	65.5	1413	2941	0.83***	2.01***	-0.65*
						(0.19)	(0.37)	(0.34)
CanESM2	0.63	57.1	66.1	1413	3193	1.00***	2.30***	-0.88**
						(0.21)	(0.37)	(0.44)
GFDL-CM3	0.95	57.1	67.1	1413	3413	1.40***	4.44***	-1.07**
						(0.27)	(1.05)	(0.53)
GFDL-ESM2G	0.44	57.1	63.7	1413	2599	0.54***	0.87***	-0.43
						(0.14)	(0.14)	(0.26)
GFDL-ESM2M	0.43	57.1	63.0	1413	2497	0.50***	0.69***	-0.37
						(0.12)	(0.12)	(0.24)
IPSL-CM5A-LR	0.72	57.1	66.3	1413	3099	1.00***	3.18***	-0.81**
						(0.22)	(0.75)	(0.39)
IPSL-CM5A-MR	0.82	57.1	66.2	1413	3174	1.21***	4.86***	-0.70*
						(0.24)	(1.38)	(0.41)
MIROC-ESM	0.15	57.1	67.7	1413	3370	1.20***	3.14***	-1.28**
						(0.26)	(0.58)	(0.52)
MIROC-ESM-CHEM	0.17	57.1	68.5	1413	3464	1.21***	2.91***	-1.57***
						(0.27)	(0.50)	(0.55)
MIROC5	1.11	57.1	65.7	1413	2839	0.58***	1.13***	-0.78**
						(0.17)	(0.20)	(0.32)
MPI-ESM-LR	0.49	57.1	64.9	1413	2925	0.88***	2.32***	-0.49
						(0.18)	(0.49)	(0.35)
MPI-ESM-MR	0.52	57.1	64.6	1413	2845	0.80***	1.93***	-0.46
						(0.17)	(0.38)	(0.33)
MRI-CGCM3	0.68	57.1	62.7	1413	2344	0.34***	0.58***	-0.24
						(0.10)	(0.11)	(0.19)
NorESM1-M	0.88	57.1	65.5	1413	2795	0.56***	2.21***	-0.55*
						(0.16)	(0.63)	(0.29)
bcc-csm1-1	0.55	57.1	65.2	1413	2881	0.75***	1.54***	-0.58*
						(0.17)	(0.24)	(0.33)
inmcm4	1.08	57.1	62.3	1413	2255	0.35***	0.88***	-0.13
						(0.10)	(0.18)	(0.16)

Notes: The table summarizes ZIP code-level climate change impacts, aggregated to the United States as a whole, under all 21 NEX-GDDP climate models and two meta-models. The climate model is given by the row label. The results for the weighted meta-model—the first listed in the table—are the same as those reported for "All U.S. ZIPs" in Table 1.

Table B.2b: End-of-Century Climate Change Effects (RCP 8.5): Coolest Third of ZIPs

	(1)	(2)	(3)	(4)	(5)	(6)	(7)	(8)
						Annual Mortality Change (%)		
		Avg. Temp. (°F)		Annual CDD		Homogeneous Effects	Climate Heterogeneity	
	Model Weight	Current	Future	Current	Future	No Adaptation	No Adaptation	Future Adaptation
Average of NEX-GDDP Models								
Meta-model, weighted average		49.4	58.1	525	1661	-0.03 (0.12)	2.25*** (0.50)	0.84** (0.35)
Meta-model, unweighted average		49.4	58.2	525	1683	-0.03 (0.12)	2.18*** (0.45)	0.82** (0.35)
NEX-GDDP Models								
ACCESS1-0	1.02	49.4	59.9	525	1979	0.17 (0.16)	4.65*** (1.37)	0.74** (0.36)
BNU-ESM	0.68	49.4	59.7	525	1869	-0.05 (0.14)	2.15*** (0.34)	0.61* (0.34)
CCSM4	0.68	49.4	57.0	525	1563	-0.03 (0.10)	1.64*** (0.30)	0.90** (0.36)
CESM1-BGC	0.64	49.4	57.3	525	1513	-0.08 (0.10)	1.52*** (0.29)	0.82** (0.35)
CNRM-CM5	1.01	49.4	57.4	525	1466	-0.16 (0.10)	1.14*** (0.19)	0.77** (0.36)
CSIRO-Mk3-6-0	0.74	49.4	58.6	525	1772	-0.02 (0.13)	2.15*** (0.39)	0.72** (0.35)
CanESM2	0.63	49.4	59.3	525	2036	0.15 (0.15)	2.74*** (0.46)	0.68* (0.37)
GFDL-CM3	0.95	49.4	60.0	525	2136	0.30* (0.17)	4.32*** (1.02)	0.70* (0.38)
GFDL-ESM2G	0.44	49.4	56.4	525	1342	-0.19** (0.09)	0.77*** (0.14)	0.77** (0.35)
GFDL-ESM2M	0.43	49.4	55.2	525	1226	-0.16** (0.07)	0.63*** (0.11)	0.79** (0.33)
IPSL-CM5A-LR	0.72	49.4	59.3	525	1836	-0.02 (0.13)	3.03*** (0.74)	0.74** (0.35)
IPSL-CM5A-MR	0.82	49.4	58.8	525	1878	0.17 (0.14)	4.87*** (1.57)	0.95*** (0.36)
MIROC-ESM	0.15	49.4	61.0	525	2057	-0.03 (0.16)	2.53*** (0.41)	0.41 (0.35)
MIROC-ESM-CHEM	0.17	49.4	61.8	525	2107	-0.08 (0.17)	2.48*** (0.40)	0.26 (0.34)
MIROC5	1.11	49.4	58.7	525	1584	-0.25** (0.11)	1.07*** (0.20)	0.58* (0.33)
MPI-ESM-LR	0.49	49.4	57.8	525	1736	0.10 (0.12)	2.45*** (0.49)	0.88** (0.35)
MPI-ESM-MR	0.52	49.4	57.3	525	1622	0.03 (0.11)	1.98*** (0.36)	0.90** (0.36)
MRI-CGCM3	0.68	49.4	55.6	525	1198	-0.22*** (0.07)	0.55*** (0.11)	0.71** (0.33)
NorESM1-M	0.88	49.4	58.6	525	1661	-0.06 (0.12)	2.75*** (0.78)	0.77** (0.34)
bcc-csm1-1	0.55	49.4	58.0	525	1662	-0.07 (0.12)	1.47*** (0.22)	0.73** (0.34)
inmcm4	1.08	49.4	54.8	525	1105	-0.16** (0.06)	0.81*** (0.18)	0.83*** (0.28)

Notes: The table summarizes ZIP code-level climate change impacts, aggregated to the coolest U.S. climate tercile, under all 21 NEX-GDDP climate models and two meta-models. The climate model is given by the row label. The results for the weighted meta-model—the first listed in the table—are the same as those reported for "Coolest third of ZIPs" in Table 1.

Table B.2c: End-of-Century Climate Change Effects (RCP 8.5): Middle Third of ZIPs

	(1)	(2)	(3)	(4)	(5)	(6)	(7)	(8)
						Annual Mortality Change (%)		
		Avg. Temp. (°F)		Annual CDD		Homogeneous Effects	Climate Heterogeneity	
	Model Weight	Current	Future	Current	Future	No Adaptation	No Adaptation	Future Adaptation
Average of NEX-GDDP Models								
Meta-model, weighted average		55.2	63.5	1079	2491	0.54***	2.89***	-0.41
						(0.16)	(0.93)	(0.35)
Meta-model, unweighted average		55.2	63.6	1079	2519	0.55***	2.82***	-0.45
						(0.16)	(0.89)	(0.36)
NEX-GDDP Models								
ACCESS1-0	1.02	55.2	65.1	1079	2887	0.98***	6.85***	-0.57
						(0.22)	(2.40)	(0.49)
BNU-ESM	0.68	55.2	64.6	1079	2591	0.49***	1.83***	-0.71*
						(0.17)	(0.51)	(0.37)
CCSM4	0.68	55.2	62.5	1079	2376	0.46***	1.66***	-0.35
						(0.14)	(0.46)	(0.33)
CESM1-BGC	0.64	55.2	62.7	1079	2337	0.39***	1.52***	-0.41
						(0.13)	(0.44)	(0.31)
CNRM-CM5	1.01	55.2	62.7	1079	2231	0.26**	1.05***	-0.42
						(0.12)	(0.32)	(0.26)
CSIRO-Mk3-6-0	0.74	55.2	63.8	1079	2544	0.55***	2.44***	-0.55
						(0.16)	(0.73)	(0.36)
CanESM2	0.63	55.2	64.4	1079	2825	0.77***	2.66***	-0.75
						(0.19)	(0.70)	(0.48)
GFDL-CM3	0.95	55.2	65.4	1079	3008	1.10***	6.52***	-0.61
						(0.24)	(2.18)	(0.53)
GFDL-ESM2G	0.44	55.2	61.9	1079	2202	0.27**	0.87***	-0.33
						(0.11)	(0.25)	(0.27)
GFDL-ESM2M	0.43	55.2	61.1	1079	2069	0.22**	0.63***	-0.21
						(0.10)	(0.19)	(0.23)
IPSL-CM5A-LR	0.72	55.2	64.7	1079	2708	0.67***	4.37***	-0.60
						(0.18)	(1.51)	(0.40)
IPSL-CM5A-MR	0.82	55.2	64.4	1079	2802	0.96***	7.19***	-0.37
						(0.21)	(2.59)	(0.45)
MIROC-ESM	0.15	55.2	65.9	1079	2948	0.84***	4.25***	-0.93*
						(0.22)	(1.28)	(0.51)
MIROC-ESM-CHEM	0.17	55.2	66.8	1079	3035	0.79***	3.61***	-1.18**
						(0.23)	(1.05)	(0.51)
MIROC5	1.11	55.2	64.1	1079	2444	0.25*	1.07***	-0.71**
						(0.14)	(0.34)	(0.34)
MPI-ESM-LR	0.49	55.2	63.2	1079	2588	0.72***	3.27***	-0.38
						(0.17)	(1.00)	(0.40)
MPI-ESM-MR	0.52	55.2	62.8	1079	2456	0.60***	2.68***	-0.30
						(0.15)	(0.81)	(0.36)
MRI-CGCM3	0.68	55.2	61.0	1079	1967	0.12	0.56***	-0.19
						(0.09)	(0.20)	(0.20)
NorESM1-M	0.88	55.2	64.0	1079	2455	0.44***	3.19***	-0.49
						(0.16)	(1.14)	(0.34)
bcc-csm1-1	0.55	55.2	63.7	1079	2563	0.58***	1.90***	-0.56
						(0.16)	(0.49)	(0.38)
inmcm4	1.08	55.2	60.5	1079	1870	0.15*	1.03***	-0.03
						(0.08)	(0.36)	(0.17)

Notes: The table summarizes ZIP code-level climate change impacts, aggregated to the middle U.S. climate tercile, under all 21 NEX-GDDP climate models and two meta-models. The climate model is given by the row label. The results for the weighted meta-model—the first listed in the table—are the same as those reported for "Middle third of ZIPs" in Table 1.

Table B.2d: End-of-Century Climate Change Effects (RCP 8.5): Warmest Third of ZIPs

	(1)	(2)	(3)	(4)	(5)	(6)	(7)	(8)
						Annual Mortality Change (%)		
		Avg. Temp. (°F)		Annual CDD		Homogeneous Effects	Climate Heterogeneity	
	Model Weight	Current	Future	Current	Future	No Adaptation	No Adaptation	Future Adaptation
Average of NEX-GDDP Models								
Meta-model, weighted average		66.5	73.6	2600	4397	1.75***	1.33***	-1.97***
						(0.28)	(0.31)	(0.67)
Meta-model, unweighted average		66.5	73.8	2600	4443	1.81***	1.40***	-2.04***
						(0.29)	(0.32)	(0.69)
NEX-GDDP Models								
ACCESS1-0	1.02	66.5	74.7	2600	4736	2.18***	1.99***	-2.35***
						(0.34)	(0.45)	(0.84)
BNU-ESM	0.68	66.5	74.0	2600	4435	1.60***	0.91***	-2.14***
						(0.26)	(0.25)	(0.69)
CCSM4	0.68	66.5	72.7	2600	4143	1.32***	0.73***	-1.64***
						(0.22)	(0.19)	(0.56)
CESM1-BGC	0.64	66.5	73.0	2600	4152	1.31***	0.72***	-1.69***
						(0.22)	(0.20)	(0.57)
CNRM-CM5	1.01	66.5	72.9	2600	4102	1.25***	0.60***	-1.68***
						(0.21)	(0.19)	(0.55)
CSIRO-Mk3-6-0	0.74	66.5	73.8	2600	4463	1.93***	1.45***	-2.06***
						(0.31)	(0.32)	(0.73)
CanESM2	0.63	66.5	74.4	2600	4677	2.06***	1.52***	-2.52***
						(0.33)	(0.33)	(0.81)
GFDL-CM3	0.95	66.5	75.6	2600	5048	2.77***	2.52***	-3.24***
						(0.44)	(0.54)	(1.04)
GFDL-ESM2G	0.44	66.5	72.7	2600	4208	1.51***	0.97***	-1.69***
						(0.24)	(0.22)	(0.60)
GFDL-ESM2M	0.43	66.5	72.4	2600	4149	1.40***	0.80***	-1.67***
						(0.22)	(0.20)	(0.58)
IPSL-CM5A-LR	0.72	66.5	74.9	2600	4708	2.31***	2.18***	-2.53***
						(0.38)	(0.48)	(0.83)
IPSL-CM5A-MR	0.82	66.5	75.0	2600	4794	2.48***	2.59***	-2.62***
						(0.40)	(0.58)	(0.87)
MIROC-ESM	0.15	66.5	75.9	2600	5058	2.74***	2.65***	-3.25***
						(0.44)	(0.58)	(1.04)
MIROC-ESM-CHEM	0.17	66.5	76.6	2600	5200	2.86***	2.64***	-3.72***
						(0.46)	(0.58)	(1.13)
MIROC5	1.11	66.5	74.0	2600	4445	1.72***	1.25***	-2.16***
						(0.28)	(0.30)	(0.70)
MPI-ESM-LR	0.49	66.5	73.4	2600	4407	1.77***	1.27***	-1.94***
						(0.28)	(0.28)	(0.69)
MPI-ESM-MR	0.52	66.5	73.4	2600	4413	1.74***	1.15***	-1.95***
						(0.27)	(0.26)	(0.70)
MRI-CGCM3	0.68	66.5	71.4	2600	3823	1.09***	0.62***	-1.22***
						(0.18)	(0.16)	(0.44)
NorESM1-M	0.88	66.5	73.6	2600	4227	1.27***	0.73***	-1.90***
						(0.22)	(0.22)	(0.58)
bcc-csm1-1	0.55	66.5	73.6	2600	4376	1.71***	1.25***	-1.86***
						(0.27)	(0.28)	(0.66)
inmcm4	1.08	66.5	71.3	2600	3746	1.05***	0.79***	-1.15***
						(0.18)	(0.20)	(0.38)

Notes: The table summarizes ZIP code-level climate change impacts, aggregated to the warmest U.S. climate tercile, under all 21 NEX-GDDP climate models and two meta-models. The climate model is given by the row label. The results for the weighted meta-model—the first listed in the table—are the same as those reported for "Warmest third of ZIPs" in Table 1.

Table B.3: End-of-Century Climate Change Effects (RCP 8.5, PRISM)

	(1)	(2)	(3)	(4)	(5)	(6)	(7)
					Annual Mortality Change (%)		
	Avg. Temp. (°F)		Annual CDD		Homogeneous Effects	Climate Heterogeneity	
	Current	Future	Current	Future	No Adaptation	No Adaptation	Future Adaptation
Coolest third of ZIPs	49.5	58.1	526	1666	-1.38*** (0.09)	1.32** (0.64)	-0.48 (0.36)
Middle third of ZIPs	55.2	63.5	1079	2491	-0.80*** (0.15)	3.80** (1.80)	-1.47*** (0.32)
Warmest third of ZIPs	66.0	73.3	2526	4323	0.54 (0.34)	0.38 (0.36)	-3.13*** (0.67)
All U.S. ZIPs	56.9	64.9	1372	2820	-0.55*** (0.18)	1.84** (0.79)	-1.69*** (0.30)

Notes: The table summarizes ZIP code-level climate change impacts, aggregated to climate terciles and to the United States as a whole. The table is the same as Table 1, except that the current distributions of temperature and estimated temperature-mortality relationships for ZIP codes are based off PRISM data, rather than GHCN data. Columns (1)–(4) summarize the current climate of each region as well as the end-of-century (2080–2099) climate projected by the meta-model under the RCP 8.5 greenhouse gas emissions scenario. Columns (5)–(7) are based on the ZIP code-level annual mortality effects summarized in Appendix Figure B.11. Column (5) reports climate effects under the assumption of homogeneous temperature effects. Column (6) reports "business as usual" climate effects that allow for heterogeneous temperature effects based on current climate but do not allow for future adaptation. Column (7) reports climate effects that incorporate both current heterogeneity and future adaptation.

Table B.4: End-of-Century Climate Change Effects (RCP 4.5, GHCN)

	(1)	(2)	(3)	(4)	(5)	(6)	(7)
					Annual Mortality Change (%)		
	Avg. Temp. (°F)		Annual CDD		Homogeneous Effects	Climate Heterogeneity	
	Current	Future	Current	Future	No Adaptation	No Adaptation	Future Adaptation
Coolest third of ZIPs	49.4	53.9	525	1007	-0.16***	0.36***	0.68***
					(0.05)	(0.08)	(0.26)
Middle third of ZIPs	55.2	59.4	1079	1708	0.06	0.25**	0.01
					(0.06)	(0.11)	(0.16)
Warmest third of ZIPs	66.5	70.0	2600	3429	0.62***	0.23**	-0.85***
					(0.11)	(0.09)	(0.28)
All U.S. ZIPs	57.1	61.2	1413	2061	0.18**	0.28***	-0.06
					(0.07)	(0.06)	(0.13)

Notes: The table summarizes ZIP code-level climate change impacts, aggregated to climate terciles and to the United States as a whole. Columns (1)–(4) summarize the current climate of each region as well as the end-of-century (2080–2099) climate projected by the meta-model under the RCP 4.5 greenhouse gas emissions scenario. Columns (5)–(7) are based on the ZIP code-level annual mortality effects summarized in Appendix Figure B.10. Column (5) reports climate effects under the assumption of homogeneous temperature effects. Column (6) reports "business as usual" climate effects that allow for heterogeneous temperature effects based on current climate but do not allow for future adaptation. Column (7) reports climate effects that incorporate both current heterogeneity and future adaptation.